NBSIR 73-318

MASS QUANTITY GAUGING BY RF MODE ANALYSIS

R.S. Collier
Doyle Ellerbruch
J.E. Cruz
Robert W. Stokes
Philip E. Luft
R. Gordon Peterson
A.E. Hiester

Cryogenics Division
Institute for Basic Standards
National Bureau of Standards
Boulder, Colorado 80302

June 1973

Interim Report

Prepared for
National Aeronautics and Space Administration
Johnson Space Center
Houston, Texas 77058

NBSIR 73-318

Mass Quantity Gauging by RF Mode Analysis

R.S. Collier
Doyle Ellerbruch
J.E. Cruz
Robert W. Stokes
Philip E. Luft
R. Gordon Peterson
A.E. Hiester

Cryogenics Division
Institute for Basic Standards
National Bureau of Standards
Boulder, Colorado 80302

June 1973

Interim Report

Prepared for
National Aeronautics and Space Administration
Johnson Space Center
Houston, Texas 77058

U.S. DEPARTMENT OF COMMERCE, Frederick B. Dent, Secretary
NATIONAL BUREAU OF STANDARDS, Richard W. Roberts, Director

Issued February 1973

FOREWORD

Background - The RF technique is a gauging method which samples all parts of the inside of a tank. The response is characteristic of the total mass of fluid within a tank; this is one of the advantages of the RF system over the standard capacitance system which is essentially a local measurement of fluid density. Another advantage of the RF system is the simplicity of the hardware involved; a small grounded antenna about the size of a paper clip is sufficient to communicate with the inside of the tank.

Preliminary theoretical and experimental results on the RF gauging idea were obtained by NBS in connection with a NASA sponsored contract on slush hydrogen gauging. These results may be found in NBS Report 9793 dated June 1, 1971, on "Instrumentation for Hydrogen Slush Storage Containers."

Purpose - The purpose of this report is to summarize work done under purchase order T-1738B from the NASA Johnson Space Center Houston, Texas, to the National Bureau of Standards, Cryogenics Division, Boulder, Colorado. Items covered include:

1) Phase I - Preliminary studies of the radio frequency (RF) mass quantity gauging system for two phase and supercritical fluids; and construction of experimental system for detailed feasibility studies.

2) Phase II - Experimental evaluation of the system for supercritical nitrogen and hydrogen. (Oxygen is also included in Phase II; the results will be reported separately upon the completion of the oxygen testing.)

PRECEDING PAGE BLANK NOT FILMED

Objective - The primary objective of this work is to design and develop a breadboard system to verify that the radio frequency resonant cavity mode analysis technique is conceptually sound for the fluid mass quantity gauging of the Space Shuttle Orbiter PRSD (Power Reactant Storage and Distribution) subsystem tankage, i. e., supercritically stored hydrogen and oxygen, in all gravity fields. The secondary program objective is to analytically determine the applicability of the concept to the quantity gauging of Shuttle Orbiter propulsion systems tankage. (i. e. sub-critical fluids).

End Product - The end product of this contractual effort is to be a breadboard RF mass quantity gauging system capable of gauging supercritically stored hydrogen and oxygen to an accuracy of one percent of total tank quantity in any gravity environment. This should also include the gauging of subcritical hydrogen and oxygen representative of fill and drain operations on the PRSD tanks.

Acknowledgements - The authors wish to acknowledge D. B. Mann, Chief of the Cryogenic Metrology Section, Peter V. Tryon and John F. LaBecque of the NBS Statistical Engineering Laboratory, and Dan S. Trent, the NASA, JSC technical monitor, for assistance and encouragement in planning this program. The authors also appreciate the assistance of Larry Lowe, Bill German, Bob Gray, Tim Hipsher, Ed Rogers, Brian Nakagawa, and Jeannette Garing.

CONTENTS

ABSTRACT

This is a summary report of work done to date on NASA (Johnson Space Center) purchase order T-1738B concerning Radio Frequency (RF) Mass Quantity Gauging. Experimental apparatus has been designed and tested which measures the resonant frequencies of a tank in the "time domain." These frequencies correspond to the total mass of fluid within the tank. Experimental results are discussed for nitrogen and hydrogen in normal gravity both in the supercritical state and also in the two phase (liquid-gas) region. Theoretical discussions for more general cases are given.

Key Words: Gauging; hydrogen; nitrogen; radio frequency; total mass.

INTRODUCTION

When a small antenna is placed in a closed metal cavity, the electromagnetic field pattern which the antenna generates inside the cavity depends on the excitation frequency and the shape of the cavity. At certain frequencies, f_n (called resonant frequencies), the field patterns are standing waves (called resonant modes). These modes are easily detected at the antenna since the impedance match of the antenna to the cavity is more efficient at the resonant frequencies.

The presence of a dielectric fluid within the cavity will change the resonant frequencies. The resonant frequencies will decrease with an increasing amount of fluid because the presence of the fluid slows down the propagation of the electromagnetic wave. This presents the possibility of gauging the amount of fluid by measuring the resonant frequencies.

If the density of fluid is uniform throughout the cavity,

$$f_n = \frac{f_{on}}{\sqrt{\epsilon}} \tag{1}$$

where f_{on} is the resonant frequency of the empty cavity for the nth mode and ϵ is the dielectric constant of the fluid. For many nonpolar fluids of interest (including hydrogen and oxygen), the dielectric constant depends only on the density of the fluid. In this case there is a unique relationship between each resonant frequency and the total mass within the cavity; and only one mode is necessary to determine the total mass.

If the density of the fluid is not uniform throughout the cavity (either because of a two phase liquid-gas interface or a single phase fluid with temperature gradients) the resonant frequencies depend on the amount of fluid mass in the cavity and also somewhat on where the dense portions of the fluid are located within the cavity (fluid geometry effects). Since the geometry of each standing wave is different (the modes are linearly independent functions of the space variables), it is possible to partially compensate for the fluid geometry effects by comparing two or more modes. This process of comparison is called Mass Quantity Gauging by RF Mode Analysis.

The purpose of this present work is to develop an experimental system which will

(1) Provide a breadboard total mass gauge for measuring uniform density fluids; developing the accuracy and data reduction of the time domain technique for measuring a single resonant frequency, and

(2) Determine the feasibility of RF Mode Analysis for nonuniform fluids; to measure the total mass with sufficient accuracy for dynamic Normal-g and Zero-g fluid geometries.

This report will emphasize item (1) above under the heading Uniform Density Fluids and also give some preliminary discussion and results of item (2) above under the heading Nonuniform Density Fluids.

EXPERIMENTAL SYSTEM

The experimental system consists of (1) an electronic signal conditioner and data acquisition system which measures the resonant frequencies in the time domain and (2) an 18 inch diameter spherical cryogenic storage tank (experimental vessel) designed for testing nitrogen and hydrogen, in both the two-phase and supercritical states; it is expected that after further testing that the tank will also be suitable for oxygen. The total fluid mass is determined by weighing with a calibrated load cell; there are a number of thermocouples and resistance thermometers attached to the sphere to measure temperature gradients in the fluid. There are several antenna locations for measuring the effect of antenna orientation with respect to a non-homogeneous fluid. The details of the cryogenic system are outlined in Appendix A.

The resonant frequencies may be detected by sweeping the antenna with an RF sweep generator; where the generator frequency ranges between f_A and f_B and the resonant frequency (or frequencies) of interest lies between f_A and f_B. When the generator frequency coincides with the resonant frequency there is a decrease in the signal reflected from the antenna which shows up as a spike in the detector output; this output may be displayed on an oscilloscope (see figure 1).

If the sweep generator frequency output is linear (or at least repeatable) in time then the resonant frequencies may be measured by measuring the time interval between the output of a reference cavity (tuned to a frequency f_0) and the output of the experimental vessel (see figure 1). For example, if the sweep rate r is linear, the resonant frequency of the fundamental mode, f_1, is given by

$$f_1 = f_0 + r (t_1 - t_0) \ . \tag{2}$$

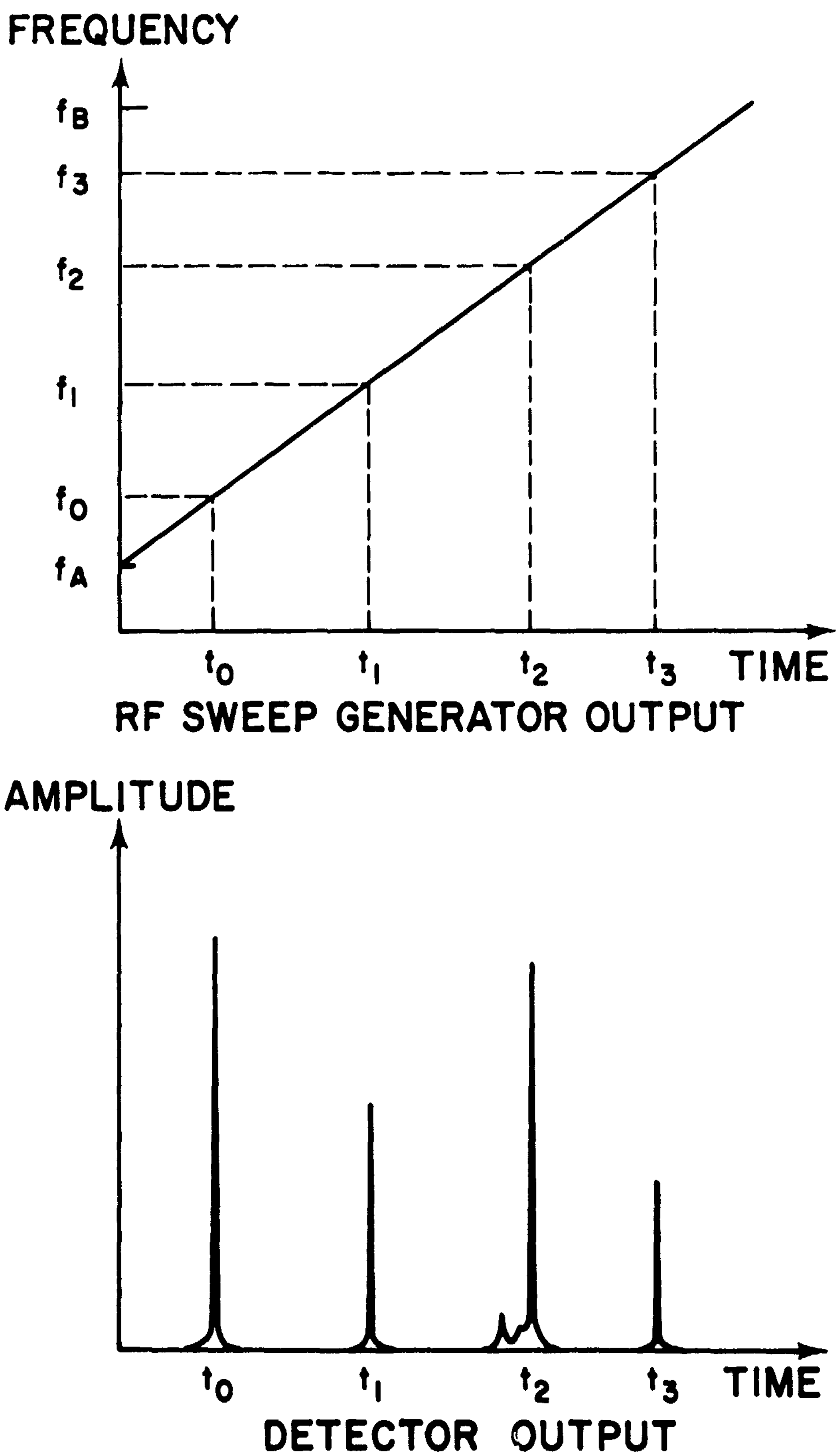

Figure 1. Input and output of RF cavity.

Since f_0 and r are fixed, f_1 is determined by the time interval $(t_1 - t_0)$; this then is a measurement of the resonant frequency in the "time domain".

The time intervals can be measured using a digital clock and a counter. The clock may be triggered in a start and stop process by signals coming from the reference cavity and experimental vessel, respectively. This is shown schematically in Figure 2. The details of the signal conditioner and data acquisition system are contained in Appendix B.

If the detectors are to start and stop the clock in a precise manner then the pulse must be very sharp and narrow so that the signal in real time comes precisely at the time the RF generator is at the resonant frequency. The narrowness of the pulse is related to the Q of the cavity which is defined by

$$Q_n = \frac{f_n}{\delta f_n} \quad . \qquad (3)$$

where δf_n is the width of the spike at the half power points. For example, if Q_n is 10,000 then there will be about a 0.01 percent uncertainty in the measurement of f_n.

The Q_n for several of the resonant modes have been measured in detail for a 19 inch diameter copper sphere, an 18 inch diameter stainless steel sphere and a 5 foot diameter stainless steel sphere. The measured Q values range between 6,200 and 91,000. The detailed results are contained in Appendix C.

The conclusion of Appendix C is that the Q's are high enough to accurately measure the resonant frequencies by the time domain technique even for the large vessel; and it is reasonable to use small vessels for scaling experiments on ultimate large tank configurations.

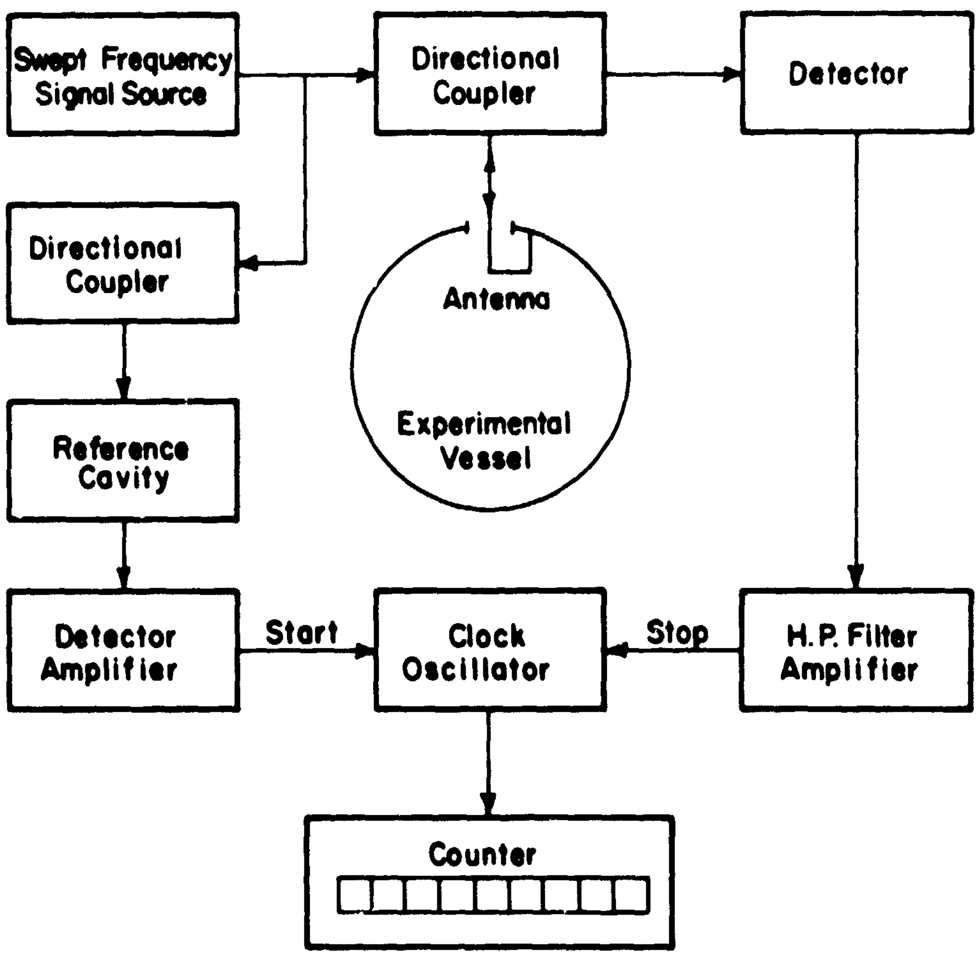

Figure 2. Conversion of resonant frequencies to the "time domain."

THE RF ANTENNA

One of the attractive features of the RF technique is the simplicity of the internal tank hardware, which is simply a small loop of wire. Figure 3 shows two of the antenna configurations which have been used in the experimental vessel; these are connected to high pressure coaxial feedthroughs.

The straight wire antenna is the "TM probe". It generates only the TM modes. The straight wire is simply an extension of the center conductor of the coaxial feedthrough.

In the loop antenna, the center conductor is bent into a U-shape about 3/4 inch by 3/4 inch and the end is grounded to the outer conductor. This antenna will generate both TE and TM modes.

The coupling of the antenna to the cavity (and hence the amplitude of the response) is changed only slightly by changes in the size and shape of the antenna. There appears to be a wide variety of antenna size and shapes which are acceptable for this gauging technique.

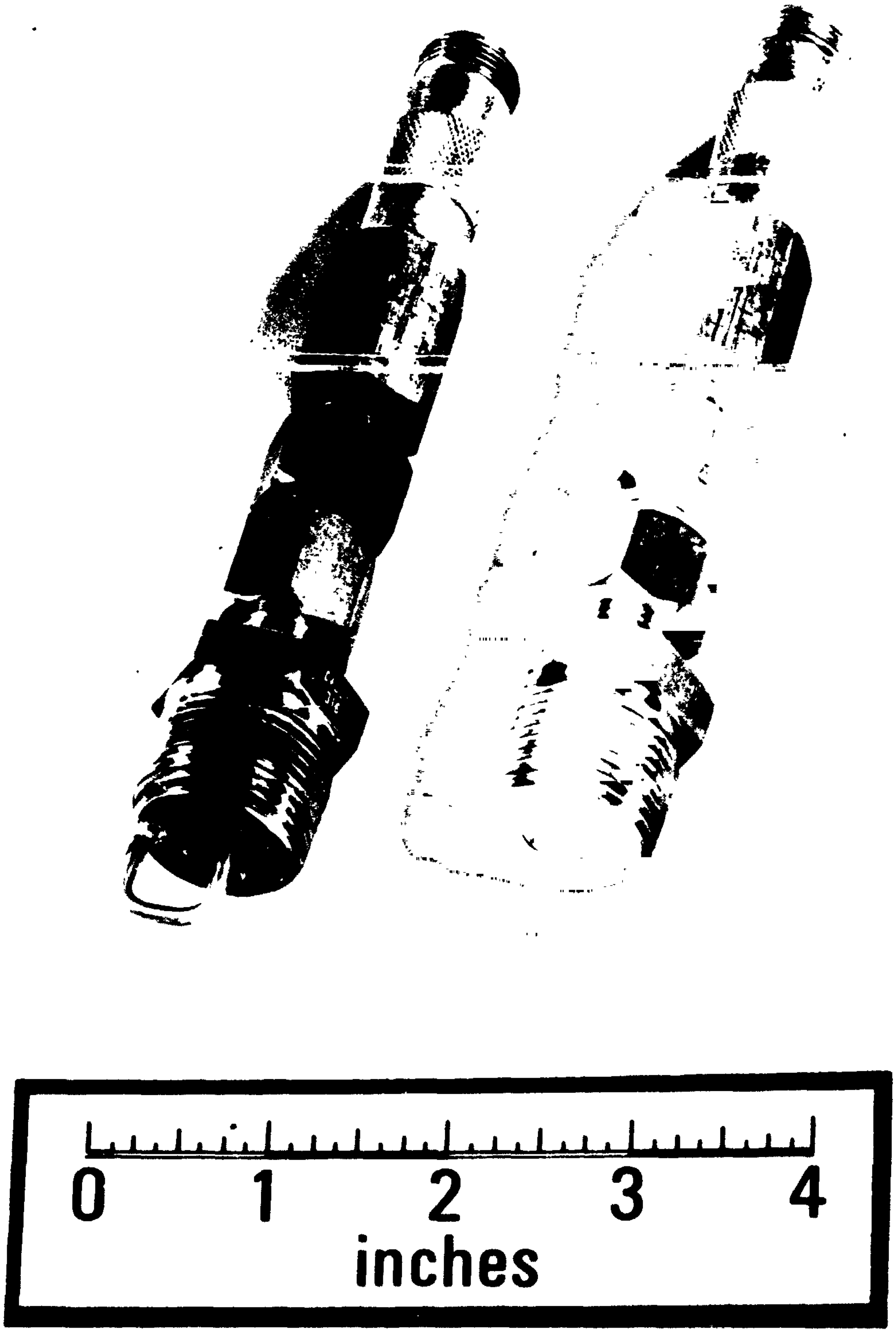

Figure 3. RF Antennas.

UNIFORM DENSITY FLUID

For a non-polar dielectric fluid of density, ρ, (a constant throughout the cavity), the resonant frequency of the nth mode f_n is given by[1]

$$f_n = \frac{f_{on}}{\sqrt{\epsilon(\rho)}} \tag{4}$$

where f_{on} is the empty cavity frequency. Semi-emperically $\epsilon(\rho)$ can be given implicity by[2, 3, 4]

$$\frac{\epsilon(\rho) - 1}{\epsilon(\rho) + 2} = A\rho + B\rho^2 + C\rho^3 \tag{5}$$

where A, B, and C are constants determined experimentally for each fluid. The f_{on} are determined experimentally and serve to calibrate the system. f_{on} depends on the size and shape of the cavity; if the cavity changes size because of thermal contractions or pressure expansions f_{on} must be adjusted accordingly; f_{on} may also change if objects are placed in the cavity. To a good approximation, for most situations of interest B and C may be neglected in equation (5); if V is the total volume of the cavity, the mass M in this case may be given by

$$M = \frac{V}{A}\left(\frac{\epsilon(\rho)-1}{\epsilon(\rho)+2}\right) = \frac{V}{A}\left(\frac{f_{on}^2 - f_n^2}{f_{on}^2 + 2f_n^2}\right) \tag{6}$$

corrections to this formula for non zero B and C may be applied if necessary. It is seen that possible inaccuracies in the total mass come from four sources:

1. The uncertainties in A, B, and C. This is not a serious problem if the properties data taken by careful capacitance measurements

---
1, 2, 3, 4 See references on page 32.

are complete over the ranges of interest. This must be determined for each application involving a specific fluid.

2. The volume of the container. This is usually inferred by weighing a fluid with a known density.

3. The accuracy of f_{on} which can be measured accurately for an empty cavity; however, if the cavity changes size or shape as a function of fluid density the empty cavity value is no longer valid in equation (6) and corrections must be made to equation 6 to account for this fact.

4. The uncertainties in f_n. For normal RF frequency ranges and high Q cavities this measurement can be made very accurately. The inaccuracies in converting this frequency into a useful digital or analog signal are presently about 0.2 percent full scale; this can be improved if necessary.

It should be noted that the factors 1, 2, and 3 above may be bypassed by direct calibration of f_n vs M using a gravimetric weigh system. However, this is not practical to do for every system. The purpose of this work, then, is to examine the validity of equation (6) (and possibly corrections to equation (6)) for general use in a system where the four accuracy factors may be adequately evaluated. This will be described for the cases of nitrogen and hydrogen. It is anticipated that oxygen will also be evaluated in the near future. The general approach will be to directly calibrate f_n vs M using a gravimetric weigh system for measuring M and a calibrated reference cavity for measuring f_n and comparing these results with equation (6) using the "time domain" method of measuring f_n. The amount of any possible density variations will be inferred from an array of thermocouples attached to the cavity.

Data Reduction and Readout

Although equation (6) is fairly complicated in form it is surprisingly linear over the density range of interest. A least squares linear fit to equation (6) for the density range from zero to the normal boiling point shows a maximum deviation of 2.45 percent of the total range for oxygen, 2.2 percent for nitrogen and 1.3 percent for hydrogen. Thus the frequency vs mass relation can be expressed to a good approximation by

$$f_n = f_{on} (\alpha + \beta\rho) \tag{7}$$

where α and β are constants depending only on the fluid. This simple linear readout may be sufficient for many applications. Quadratic fits of the form

$$f_n = f_{on} (\alpha + \beta\rho + \gamma\rho^2) \tag{8}$$

may be found which give less than 1 percent error for all fluids (see Appendix E).

Experimental Data for Nitrogen and Hydrogen

Preliminary experiments were started with liquid nitrogen to check out the experimental apparatus and the theory of uniform density fluids. The pressure was raised to 500-700 psi and the experimental vessel was agitated to achieve nearly uniform density. The frequencies were measured directly using the reference cavity; the line of the reference cavity was shifted to coincide with the resonant line on the face of the oscilloscope. Figures 4 and 5 show the data taken in this manner for the TM_{011} and TM_{021} modes respectively. It is seen that the data are nearly linear (slightly concave downward) and corresponds very well to the theoretical form given by equation (6). We believe that the occasional point which deviates from the theoretical curve is due to non-homogeneous density "stratification." We will give some preliminary results on stratification for the case of hydrogen.

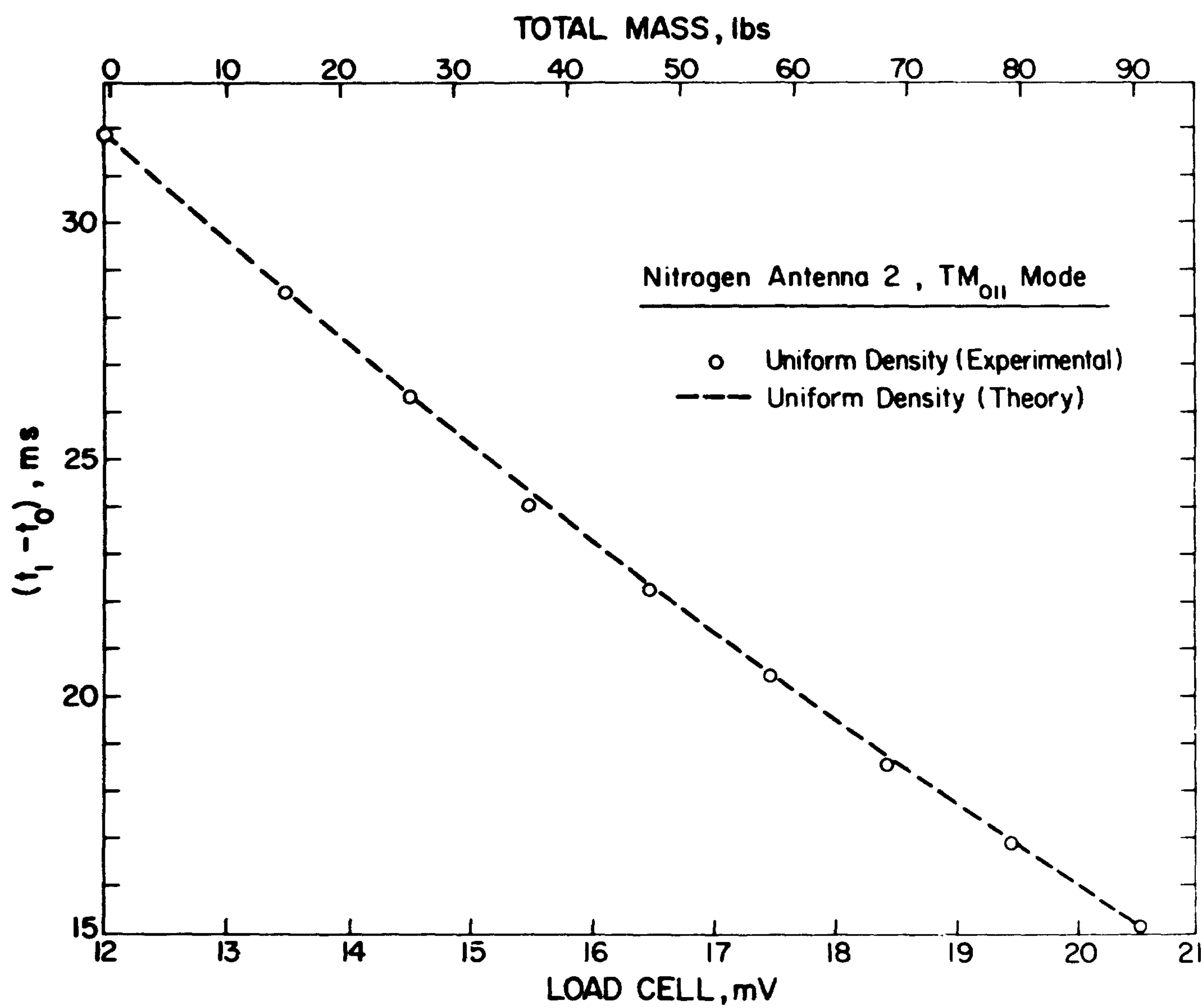

Figure 4. Mass gauging of uniform density LN_2 using the TM_{011} mode.

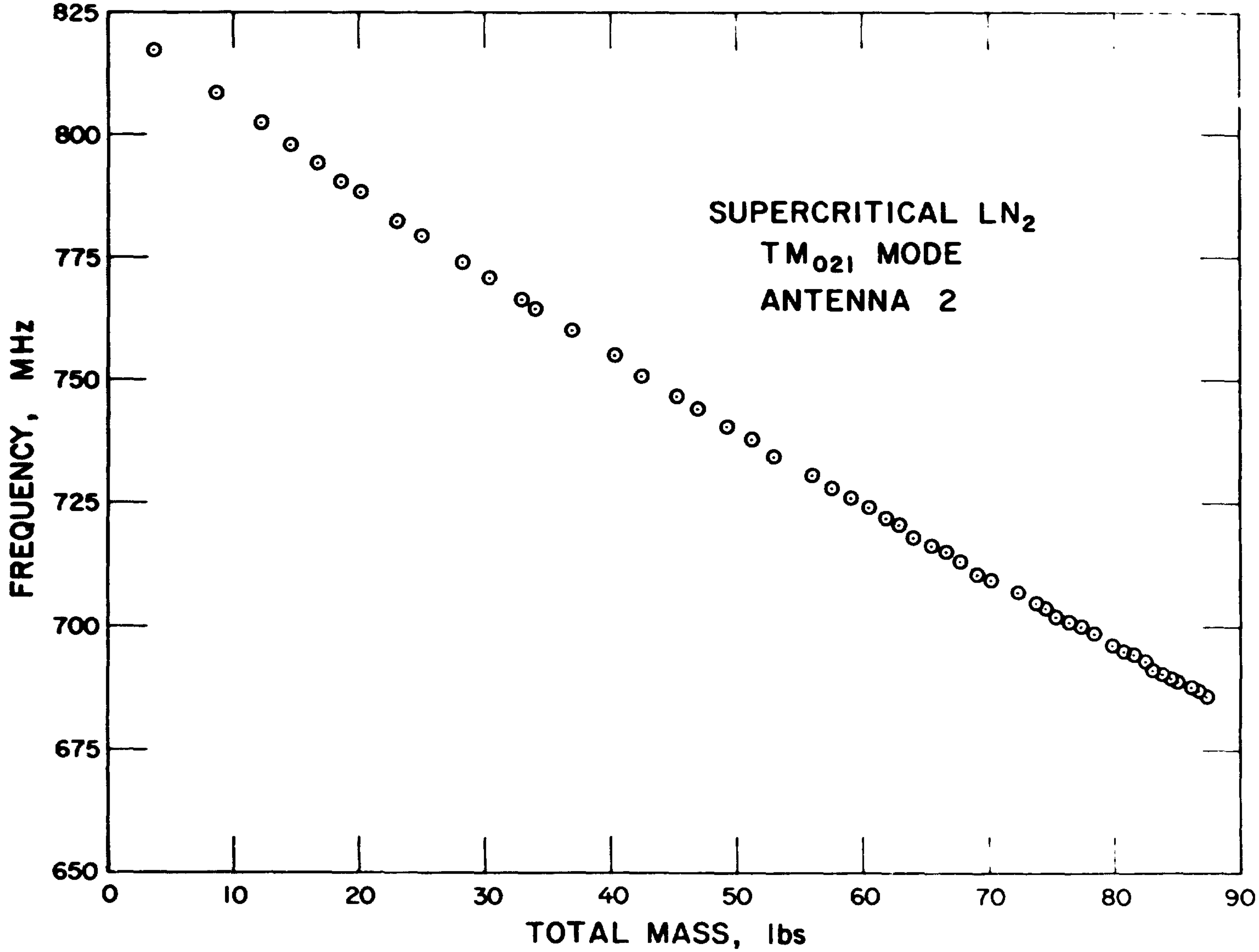

Figure 5. Mass gauging of uniform density LN_2 using the TM_{021} mode.

The hydrogen data were taken with the data acquisition system described in Appendix B. The resonant frequencies for the first five fundamental modes were converted to milliseconds in the time domain (as indicated in equation 2) to the nearest 0.01 msec. These times were digitized by an internal clock and stored on magnetic tape. The tape was used to punch data cards which contain a run code, the time conversion of the resonant frequencies, and the scatter in the time domain data. The scatter in the time domain data (except for an occasional noise spike) was ± 0.01 msec corresponding to the first significant digit. The data cards also contain the pressure, temperature and mass data corresponding to the run identification number. Computer plots of the data for the TM_{011} and TM_{021} modes are shown in figures 6 and 7 respectively. A least squares fit of these data to equation (6) gives a 3σ (99.9% confidence level) for the TM_{011} mode of 1.2 percent, the maximum deviation of the data points taken is 1.10 percent. Further details of the data analysis, and also the accuracy statements are contained in Appendices D and E.

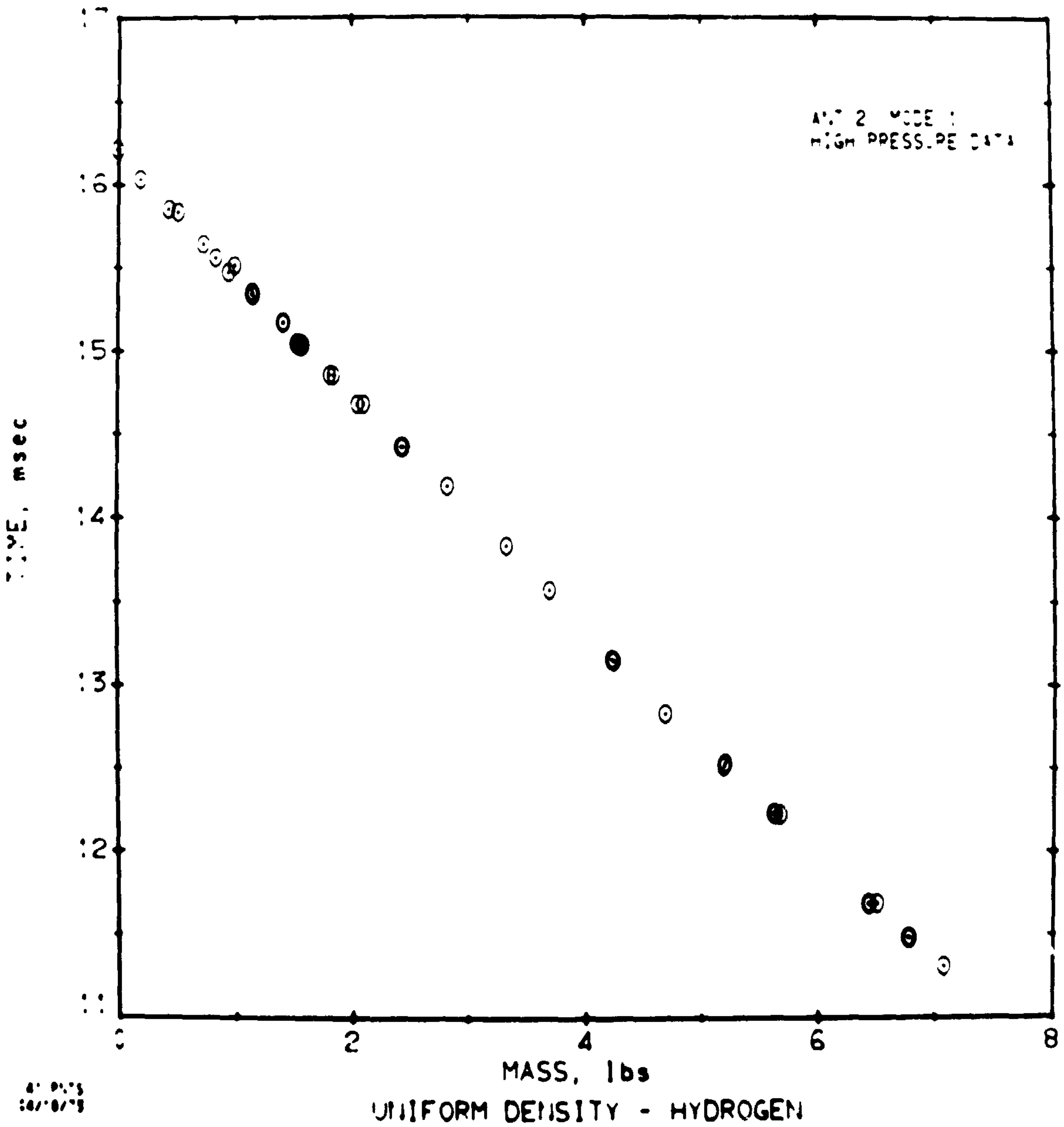

Figure 6. Mass gauging of uniform density LH_2 using the TM_{011} mode.

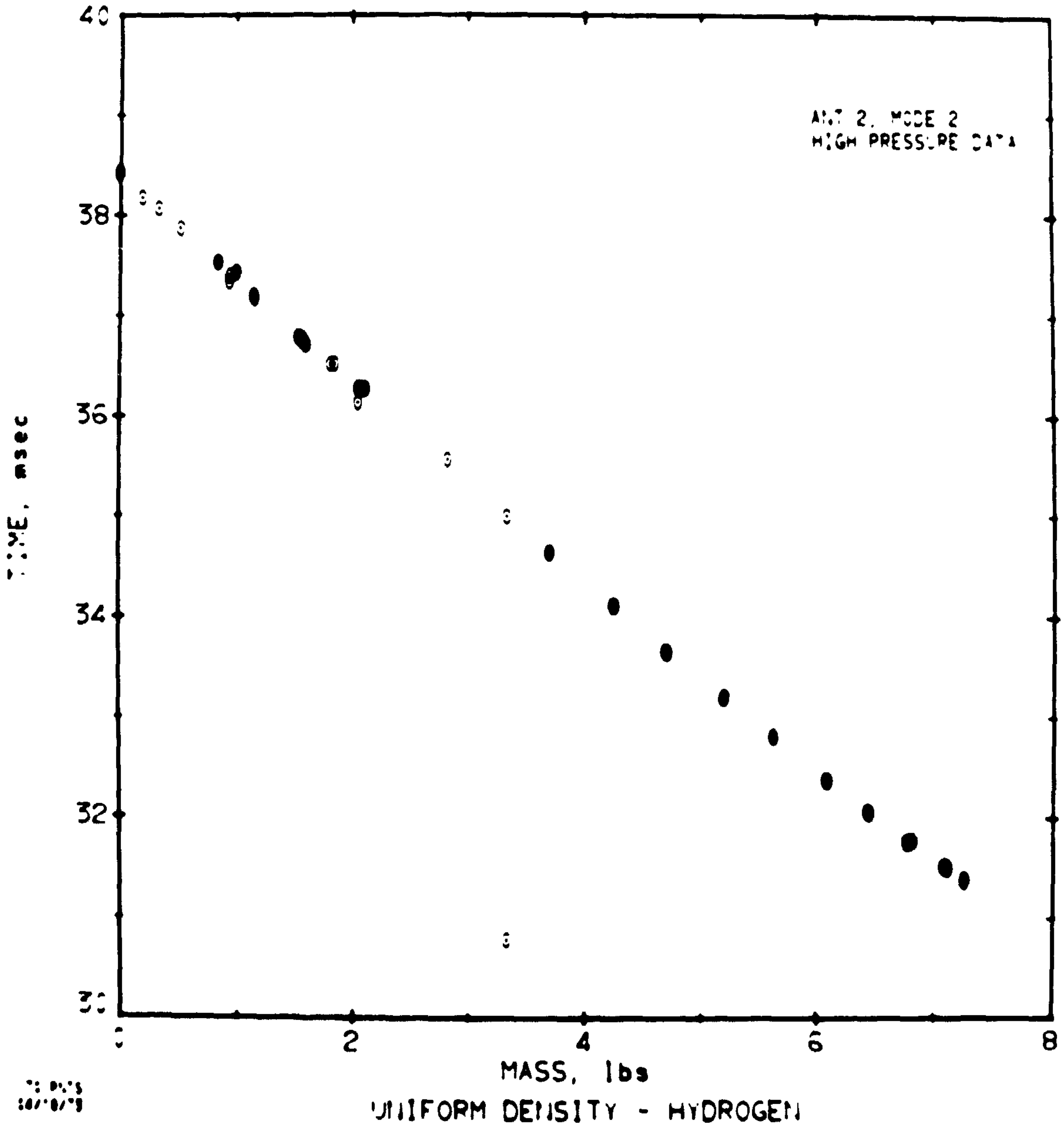

Figure 7. Mass gauging of uniform density LH_2 using the TM_{021} mode.

EFFECTS OF STRATIFICATION

In the data described above, every effort was applied to achieve uniform density; however, a few preliminary data have been obtained concerning the effects of stratification on a single resonant frequency. The following cases (in which the top and bottom temperatures were not equal) gives a rough idea of the effect of stratification on the TM_{011} mode for supercritical hydrogen at 350 psi:

Case I -	Top temperature	=	47.5 K
	Bottom temperature	=	27.5 K
	Top density	~	1 lb/ft^3
	Bottom density	~	4 lb/ft^3
	Average density	~	3.02 lb/ft^3
	Measured weight (load cell)	=	5.35 lbs
	Inferred weight (from fig. 6)	=	5.55 lbs
	% Full scale error	≈	4%
Case II -	Top temperature	=	37.5 K
	Bottom temperature	=	33 K
	Top density	~	2.25 lbs/ft^3
	Bottom density	~	3.45 lbs/ft^3
	Average density	~	2.00 lbs/ft^3
	Measured weight (load cell)	=	3.55 lbs
	Inferred weight (from fig. 6)	=	3.45 lbs
	% Full scale error	≈	1.5%
Case III -	Top temperature	=	31.5 K
	Bottom temperature	=	53 K
	Top density	~	3.8 lbs/ft^3
	Bottom density	~	0.8 lbs/ft^3
	Average density	~	1.07 lbs/ft^3

Measured weight	=	1.9 lbs
Inferred weight (from fig. 6)	=	1.9 lbs
% Full scale error	~	0.0%

In Case I, the stratification is cold fluid on the bottom, warm on top with a good share of the fluid in between at the colder temperature; definitely not a linear thermal gradient.

In Case II, there is a cold fluid on top, a colder fluid on the bottom and warmer fluid in the middle as inferred from the average density.

In Case III, there is a cold fluid on top, a warm fluid on the bottom with most of the fluid in the cavity at the warmer temperature.

From these cases, it is seen that certain small amounts of stratification may be tolerable; this is because the antenna senses the entire cavity and tends to have an integrative effect over all the mass within the cavity. For larger amounts of stratification, one antenna and one mode may not be sufficient to achieve the desired accuracy, and more information from other antennas or modes may be necessary to properly use the RF technique as a gauge. This situation is discussed in the next section on non-uniform density fluids.

NON-UNIFORM DENSITY FLUIDS - RF MODE ANALYSIS

Non-uniform (inhomogeneous) density (or dielectric constant) may occur either in a single phase fluid under temperature gradients or in a two phase fluid with a liquid-gas interface. The spacial gradients in the dielectric constant have a diffractive effect on the propagation of the electro-magnetic wave and this changes the shape of the standing wave patterns of each resonant mode. These changes will be different for each mode because of the dissimilar field patterns of the modes. The resonant frequency of the nth mode will be given by

$$f_n = f_{un} + \Delta f_n$$

Where f_{un} is the resonant frequency expected for the uniform density case assuming that the total mass in the cavity is spread uniformly over the cavity; Δf_n is the change in resonant frequency due to the non-uniform geometry of the fluid and will be different for each mode even to the extent of being positive or negative depending on the mode.

It is natural to ask: what are the extreme limits of Δf_n as the fluid ranges over all possible configurations? This is a difficult and possibly impractical question to answer. The reason is that for a given mass of fluid, there are two fluid geometries which will give the maximum and minimum values for Δf_n; but these geometries appear to be very complicated and it is unlikely that they will occur in practice. It is more feasible to talk about the practical limits of Δf_n which are determined by experimentation and calculation of Δf_n for likely fluid geometries.

Theoretical Approach

Theoretical work which was initiated in early stages of Phase I was directed along two lines. The first was to develop approximation techniques for calculating how fluid geometry affects the resonant frequencies; the second was to investigate the mode geometries to get a qualitative picture of how fluid location may affect the resonant frequencies.

Earlier work had calculated in closed form the resonant frequencies expected for a two phase fluid with a concentric spherical phase boundary ("zero-g" geometry). This work is contained in Appendix F for reference purposes. Further work on two phase geometry effects must be handled by approximation or numerical techniques. Appendix G is a survey of relevant approximation techniques and how they may be applied to the cavity problem. Several of the examples are worked out for the case of the normal two phase fill geometry. One of the conclusions of this work is that the resonant frequencies are most affected when the dense portion of the fluid moves in and out of the high field region. These high field regions are different for different modes. The field profiles for a few of the lowest order modes are plotted in figures 8 through 13. It is seen that the modes partition the cavity into several distinct high field regions; from this, it is expected qualitatively that an average of the resonant frequencies of the lowest order modes may give a mass value that is relatively independent of the location of the dense fluid. The numerical derivation of these graphs as well as numerical solutions of some of the approximation techniques are contained in Appendix H.

Experimental Approach

The experimental system described earlier is designed to record on magnetic tape the resonant frequencies of the first five modes for three different antenna locations; the data for each antenna is collected every 0.1 sec. thus making it possible to study dynamic effects where the fluid is in motion. It is anticipated that this system will give useful information in "zero-g" simulation experiments. Some preliminary data

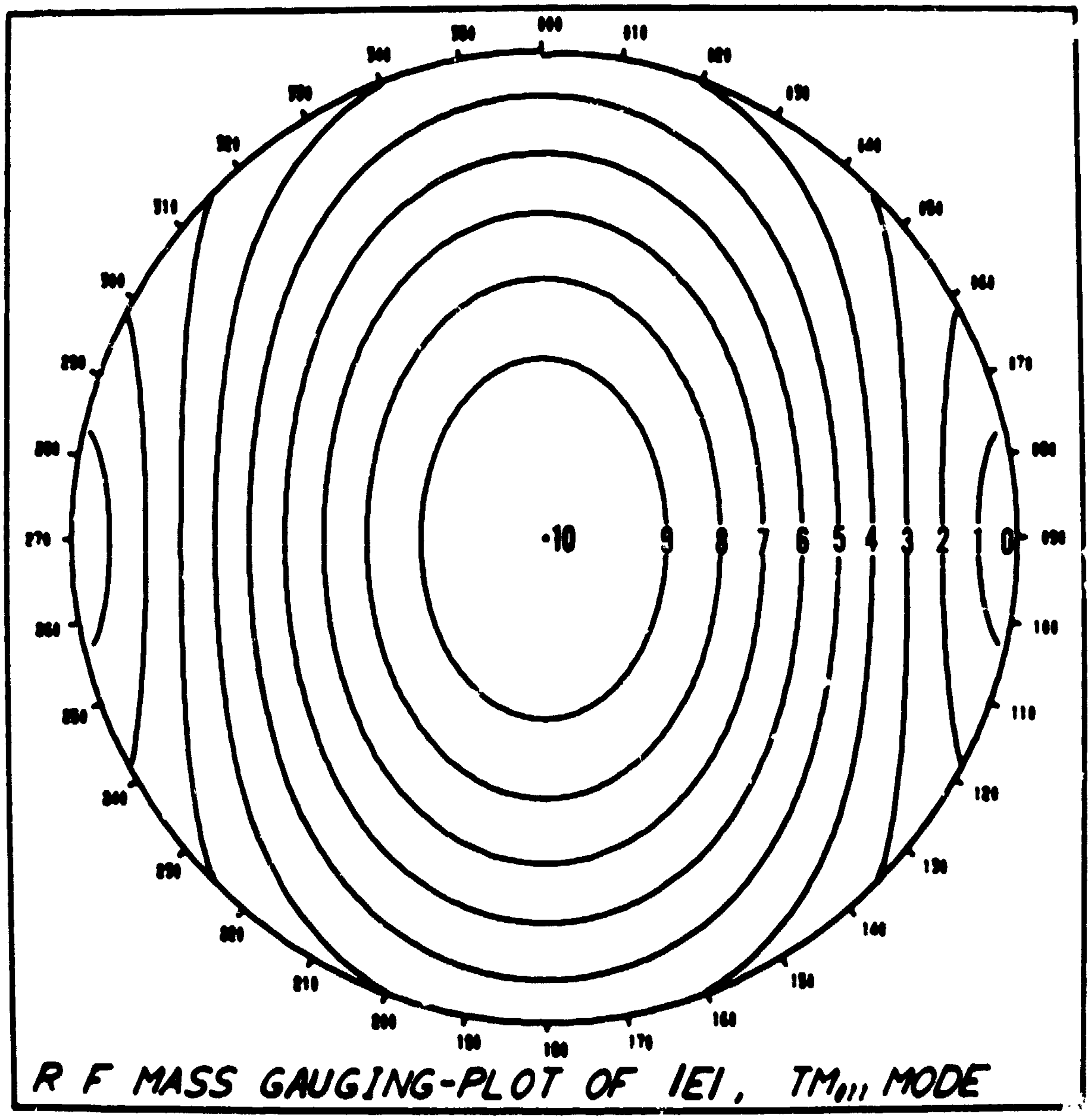

Figure 8. Field magnitude contours for the TM_{011} mode.

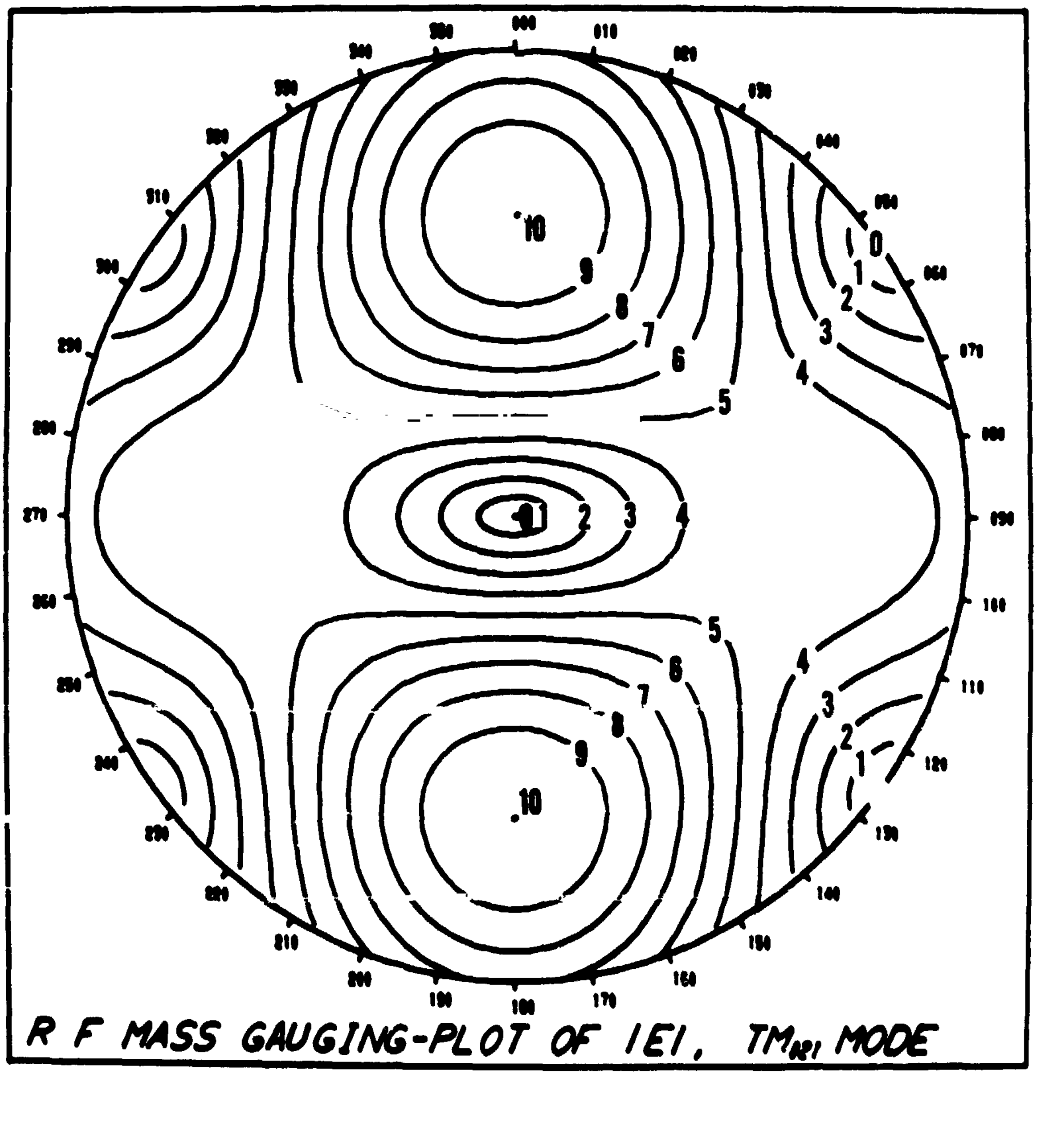

Figure 9. Field magnitude contours for the TM_{021} mode.

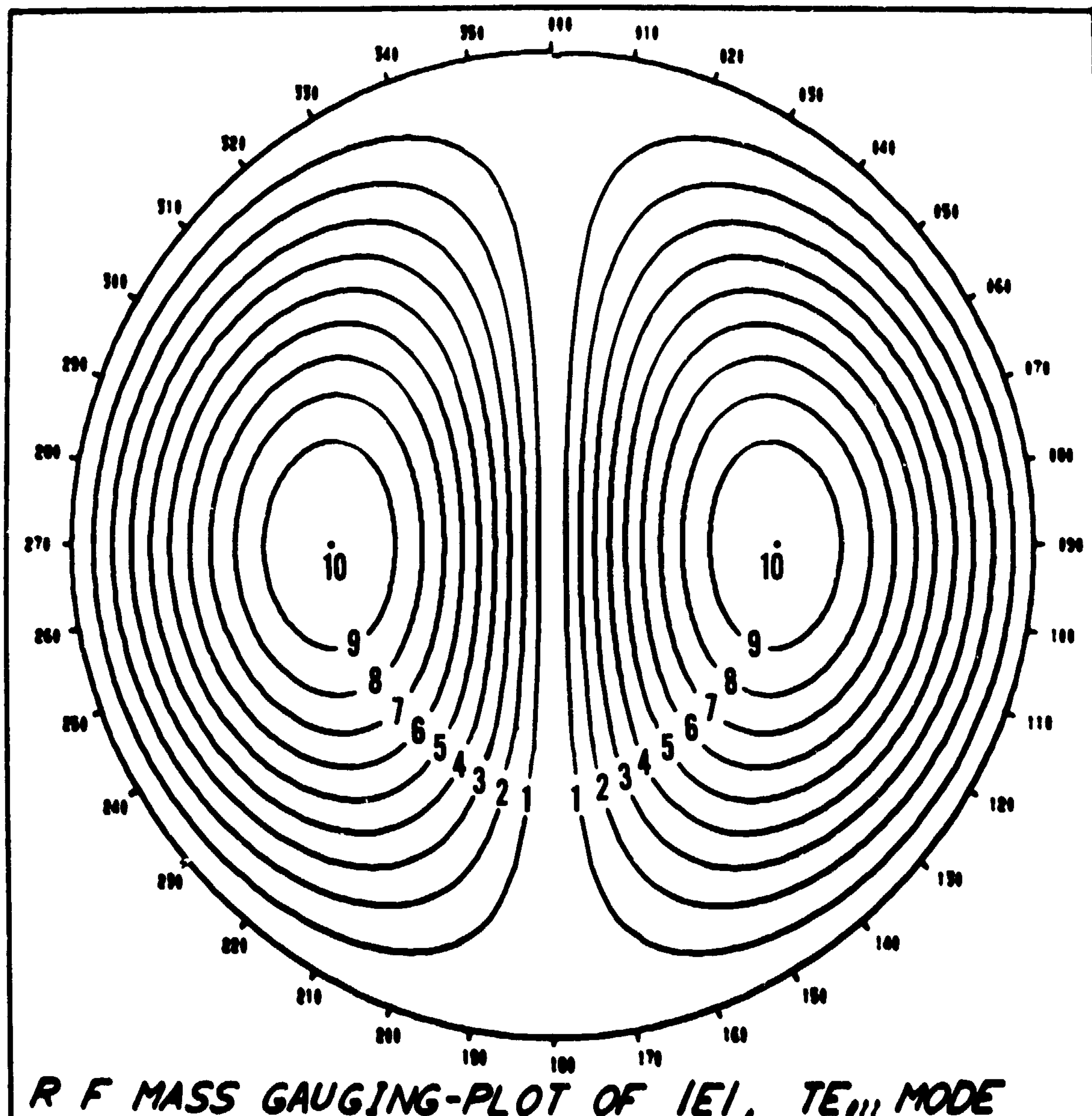

Figure 10. Field magnitude contours for the TE$_{011}$ mode.

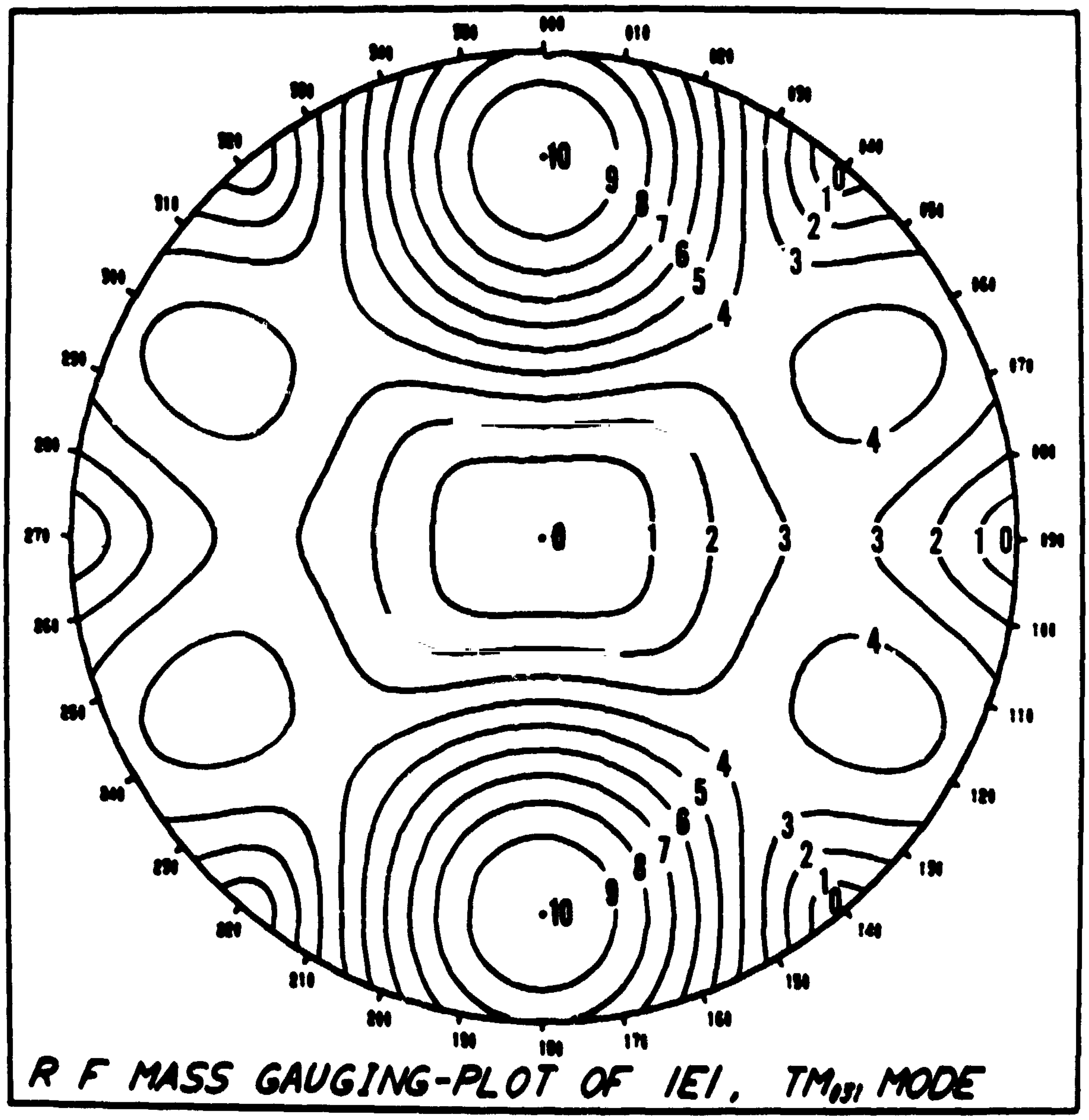

Figure 11. Field magnitude contours for the TM$_{031}$ mode.

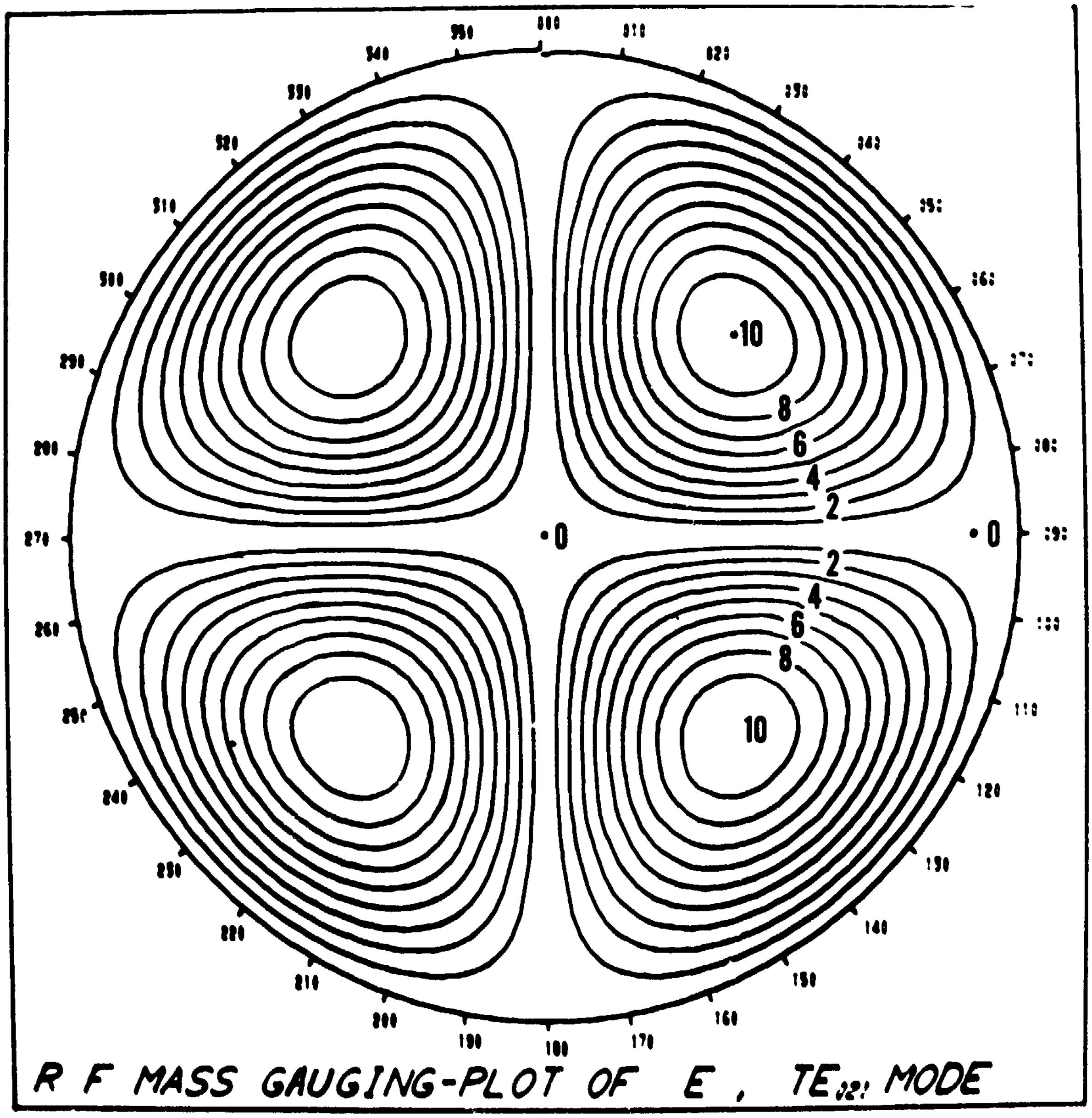

Figure 12. Field magnitude contours for the TE_{021} mode.

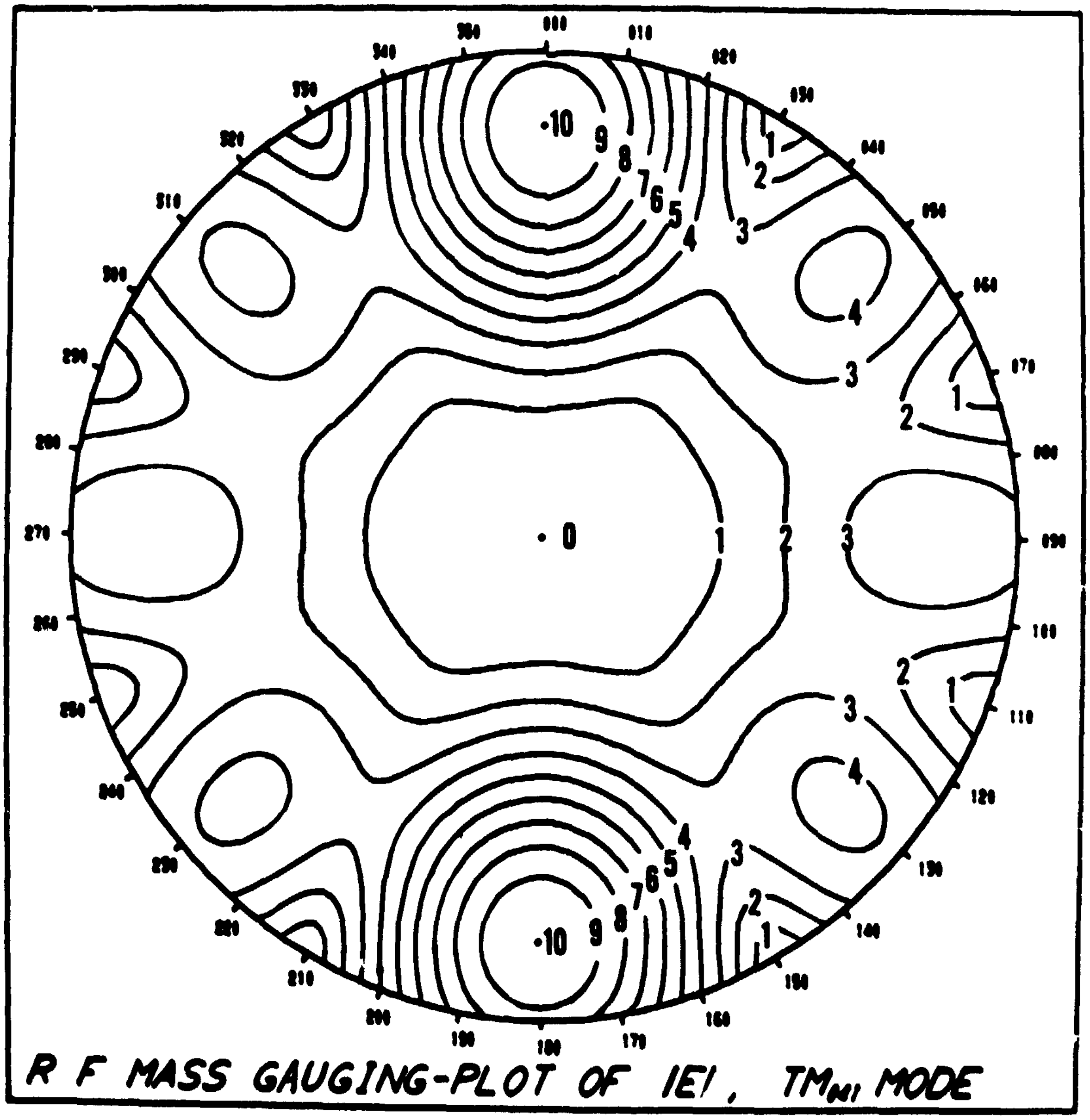

Figure 13. Field magnitude contours for the TM_{041} mode.

has been taken for normal gravity LN_2 two phase fill. Since the liquid surface breaks the spherical symmetry, it is found that some of the resonant lines split into two or more closely spaced lines; some of the modes do not split. For example, the TM_{011} mode stays as a single line and the frequency shifts as a function of total mass (see figure 14) giving some idea of the magnitude of Δf_1. Figure 15 shows the response of the TM_{021} mode which splits into three lines during normal fill. In this case, a straight forward average of the three modes is very close to uniform density curve for this mode as shown in figure 16.

These two cases indicate two alternate methods of gauging the situation of normal fill together with uniform density:

(1) In the case of TM_{011} mode, the readout can be designed for uniform density and then a correction factor can be applied for the normal fill condition.

(2) In the case of the TM_{021} mode, the readout can be designed for uniform density, with electronic averaging of the three split resonant lines in the TM_{021} time frame.

It is reasonable to expect that both of these techniques could be developed to give readout accuracies on the order of 1 percent; however, the averaging technique may be more useful if it can be generalized to tilt geometries and "low gravity" geometries.

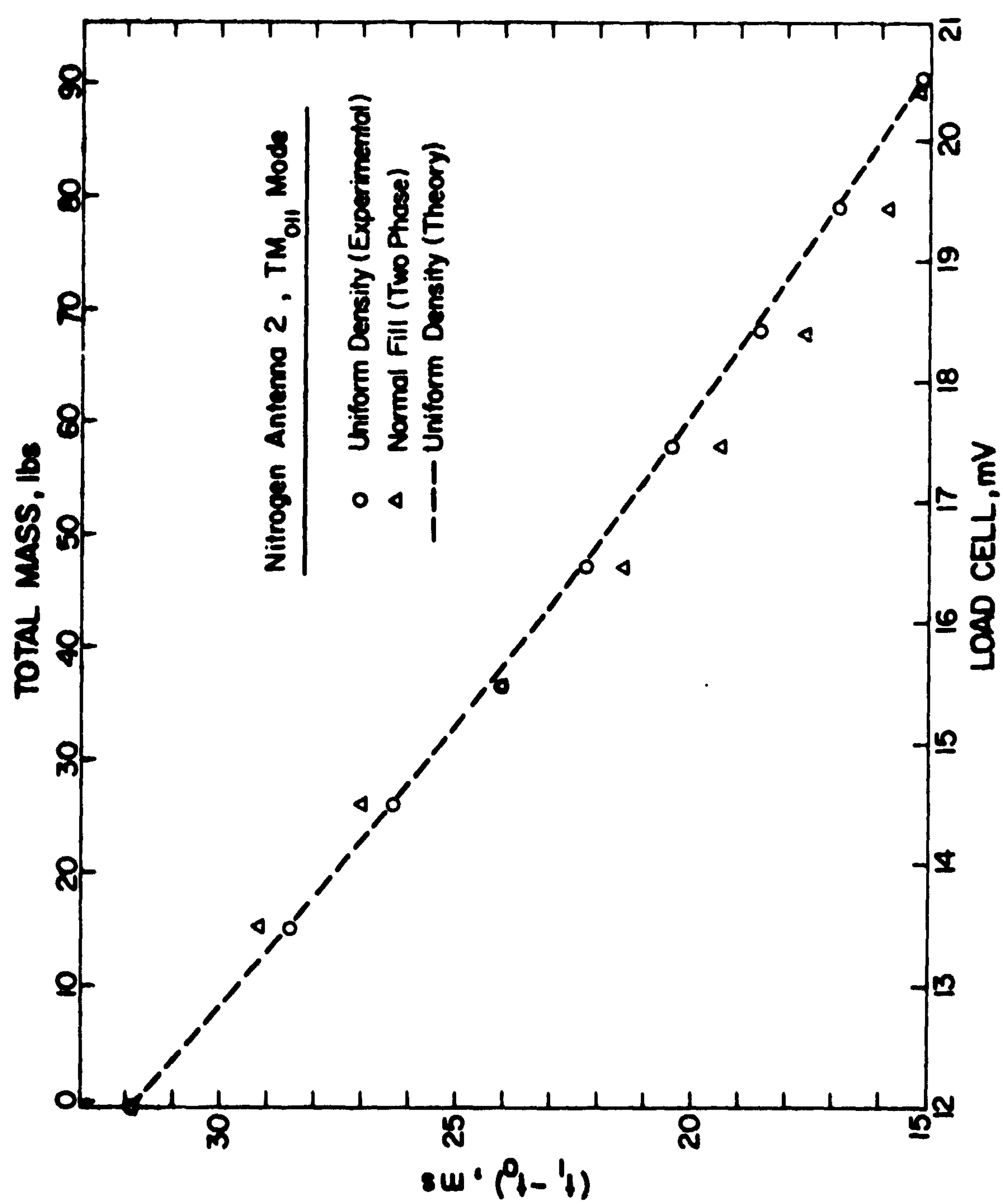

Figure 14. Comparison between supercritical and normal fill for nitrogen, TM_{011} mode.

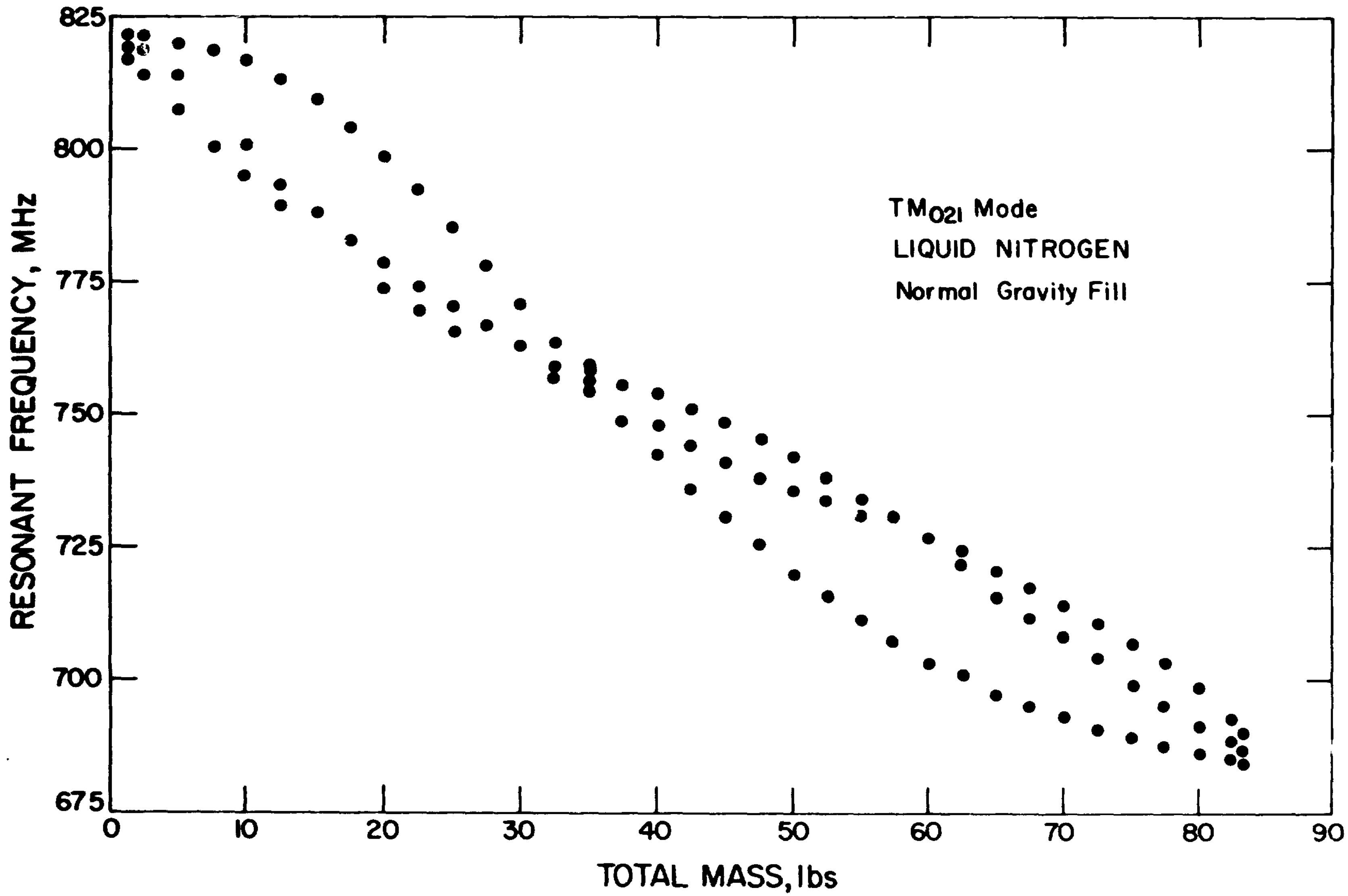

Figure 15. Normal fill data for liquid nitrogen TM_{021} mode.

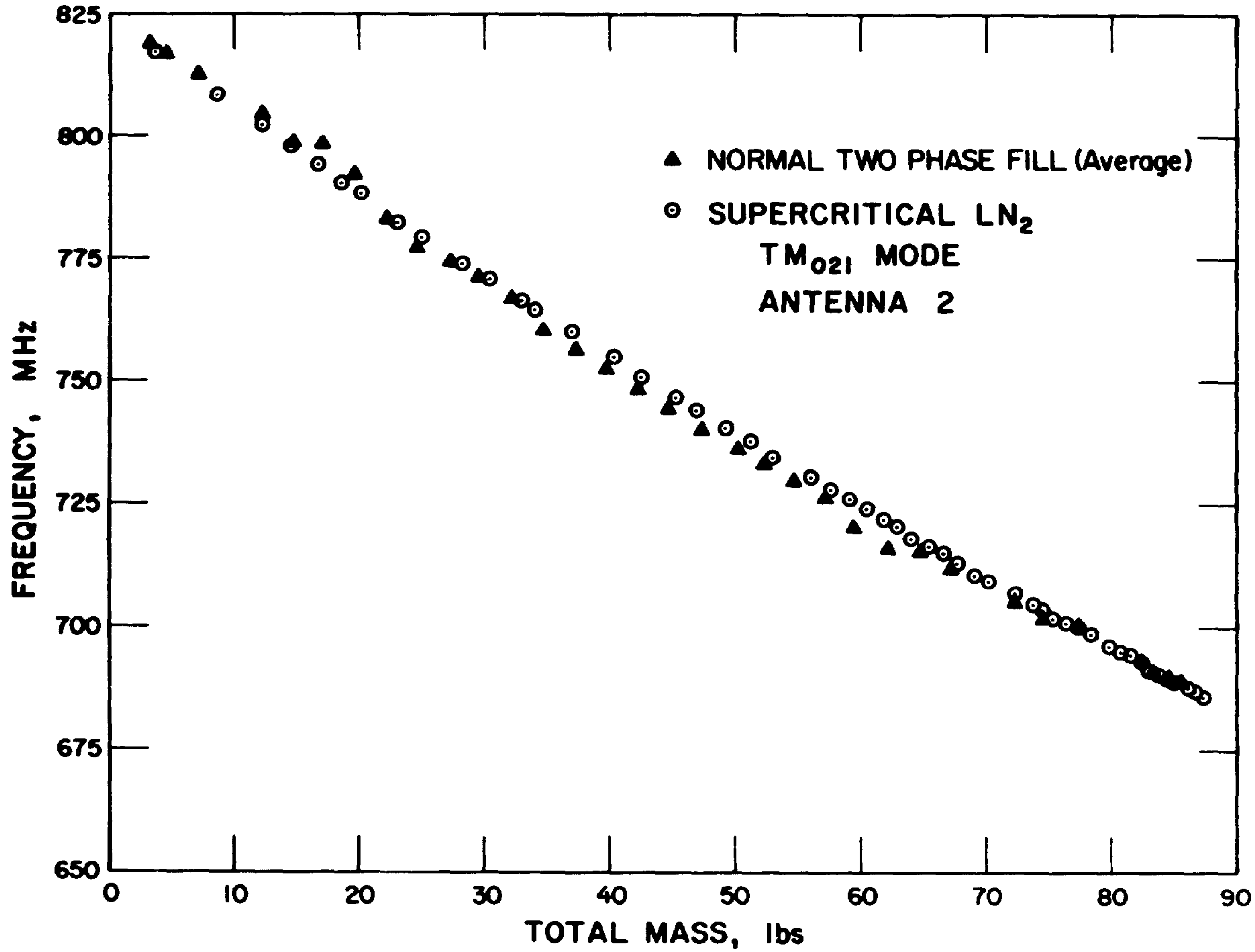

Figure 16. Comparison between supercritical and normal fill (average) for nitrogen, TM_{021} mode.

CONCLUSIONS

We have demonstrated using hydrogen and nitrogen that the RF Mode Analysis Technique is conceptually sound for uniform density fluids and that there are encouraging results for non-uniform density fluids. The results for uniform density fluids should apply to any size or shape of tank as long as the factors listed on pages 8 and 9 can be adequately evaluated. Further work should be done on non-uniform density fluids for the spherical tank and also on tank shapes which are not spherical.

REFERENCES

1. See Appendix F.

2. Johnston, Andrews and Cole, J. Chem. Phys. 33, 1310 (1960). Orantt and Cole, J. Chem. Phys. 46, 697 (1967) (Nitrogen).

3. Younglove, B. A., Journal of Research (NBS), Vol. 76A No. 1 Jan-Feb 1972. (Oxygen).

4. Stewart, John W., J. Chem. Phys. 40, 3297 (1964) (Hydrogen).

APPENDIX A

CRYOGENIC SYSTEMS

The basic system includes a pressure vessel, a heater, a piping system and an insulation system. These components were common to all the test configurations. The normal gravity calibrations utilized a load cell to measure the mass accurately. The design of the flight pallet for the zero gravity tests included an additional storage dewar. The major components of these systems are described.

The Pressure Vessel

The vessel is a sphere constructed of 304 stainless steel. It was formed by welding together two spun hemispherical heads. The inside diameter is 17 - 13/16 inches. It was designed and constructed per the A.S.M.E. Code for Unfired Pressure Vessels. The minimum wall thickness is 0.21 inches and the maximum allowable working pressure is 750 psig as defined in this code. The pressure vessel has been hydrostatically tested to 1-1/2 times its working pressure at room temperature. Access ports for instrumentation and piping are provided. All ports, except the port on the bottom, are 3/4" female pipe threads. The bottom port is 1-1/2" female pipe thread to accommodate the heater. All ports are reinforced with welding spuds.

The Heaters

Two heater configurations have been used. The first was designed for use with liquid nitrogen and the second for liquid hydrogen. Both were designed to pressurize the fluids to their critical pressures in forty minutes. Both were constructed with temperature independent resistance wire. Pressurization lines as a function of heater power and current are presented in figure A1.

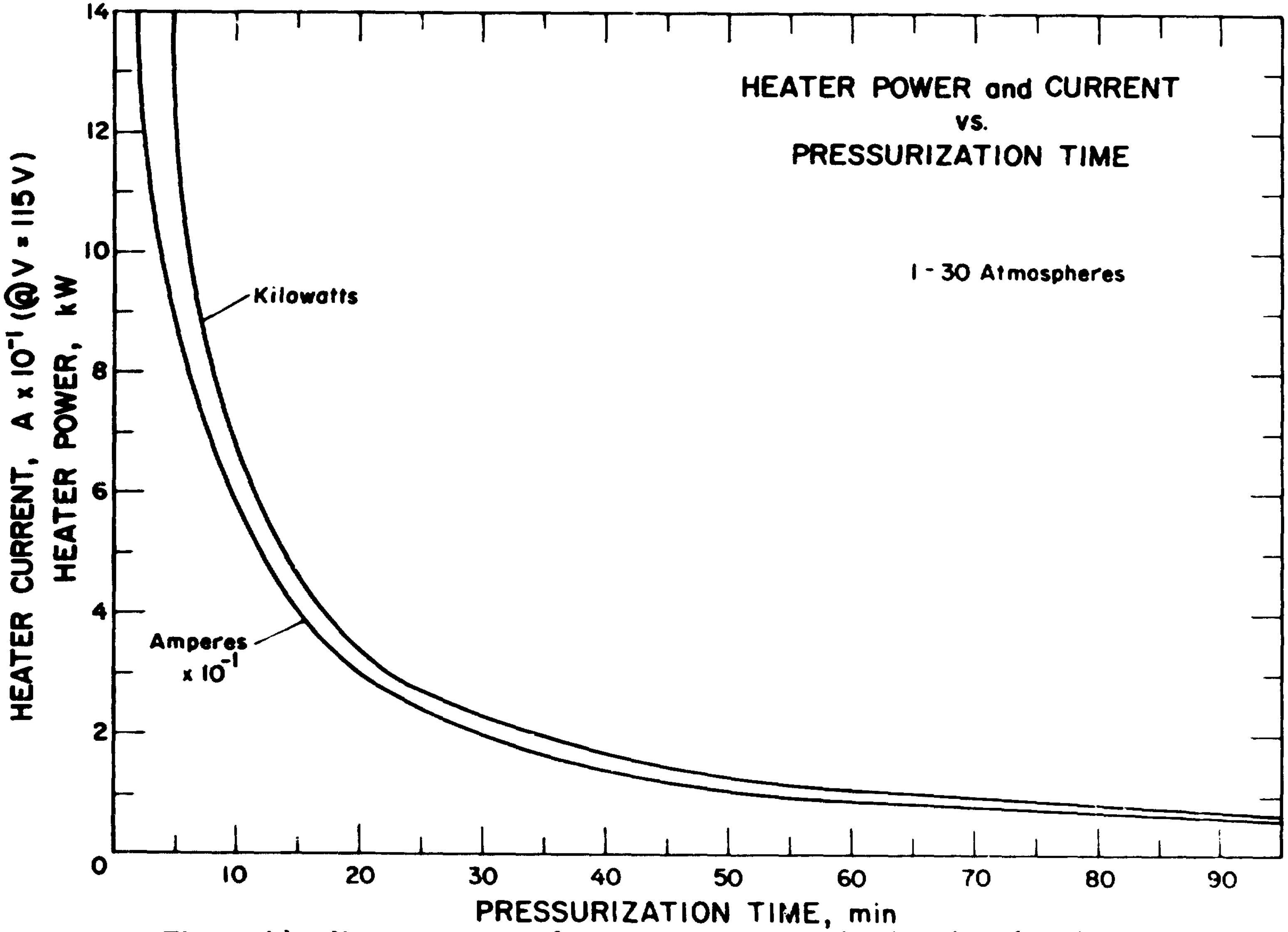

Figure A1. Heater power and current vs. pressurization time for nitrogen.

The nitrogen heater system consisted of two separate one kilowatt heaters that could be separately controlled. Each heater was wound with ten feet of 22 gage wire. Each had a room temperature resistance of 12 ohms. The wire was wound on two separate coils. The coils were then inserted in the bottom access port with the wire in direct contact with the nitrogen.

The hydrogen heater was constructed differently because of safety considerations with the flammable fluid. This heater consisted of one 300 watt coil of wire. It was wound with four feet of 28 gage wire with a room temperature resistance of 20 ohms. The wire was covered with ceramic beads and inserted into a coil of 1/4" O.D. copper tubing. The tubing was then soldered on the outside of a brass spindle which was screwed into the bottom port. The heater element does not contact the hydrogen but heats the pressure vessel from the outside. The copper tubing is purged with helium gas and is electrically grounded.

The Normal Gravity Calibration Tests

For these tests, the pressure vessel was hung in a cubical frame constructed of aluminum angle. The piping system and the insulation system was also supported from the frame. The frame, and the systems it supported, was suspended from the load cell. All interface piping and instrument lines were flexible to minimize their effect on the load cell. Figure A-2 is a photograph of this system without the insulation.

The piping was designed for use with liquid hydrogen and was used with liquid nitrogen as well. The system is equipped with a 750 psig

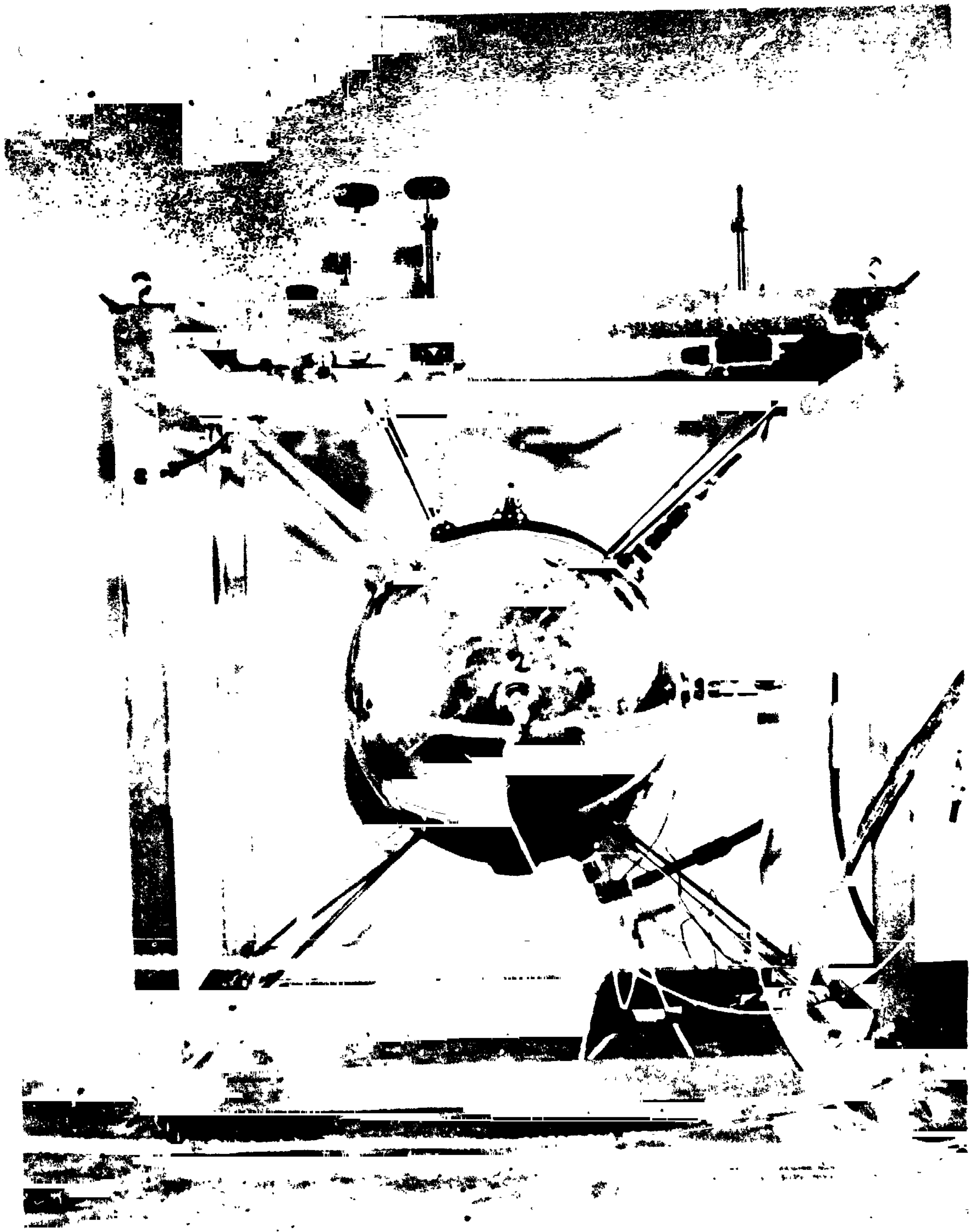

Figure A2. Experimental vessel.

relief valve. The system has been pressure tested to 700 psig with liquid nitrogen as the test fluid and it has been tested to 300 psig with liquid hydrogen.

The insulation system was made up of six inches of fiberglass batting. To prevent cryopumping the fiberglass was covered and sealed with aluminized mylar. The insulation was then purged with helium gas and a slight overpressure was maintained during the tests.

The load cell used was a strain gage type rated at 300 pounds maximum load; it has a load sensitivity of 0.1 mv/lb with a 10 volt excitation voltage. Using a high precision digital voltmeter on the output, the resolution is approximately 0.01 lbs.

The pressure vessel was instrumented with several temperature measuring transducers to determine the temperature and density gradients during the supercritical tests. Nine copper-constantan thermocouples were attached to the outside wall of the pressure vessel at six inch vertical increments. Platinum resistance thermometers were inserted into the fluid at the top and bottom to determine actual fluid temperature.

The Zero Gravity Tests

The design of this system utilizes the same pressure vessel, heater and support frame as the normal gravity system. The piping and insulation systems have been changed.

The piping system flow diagram is shown in figure A3. All the valves are manually operated. The design utilizes a common overboard vent and liquid dump, which will be compatible with the aircraft. The system can be refilled and pressurized in flight if necessary.

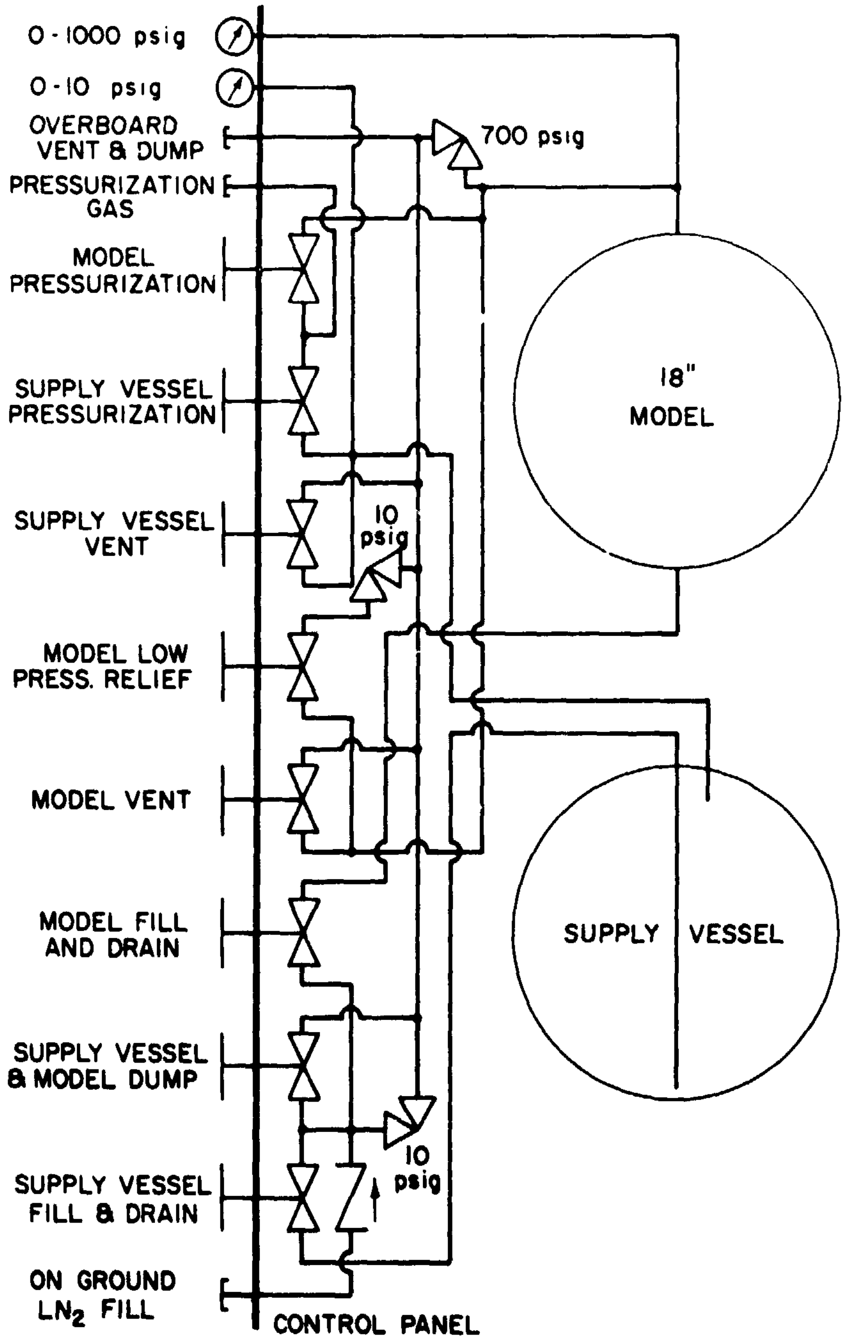

Figure A3. Cryogenic flow system for zero-g simulation tests.

The complete system will be packaged in an aluminum paneled container six feet long by three feet high and three feet wide. The total weight will be approximately 700 pounds.

The system is designed to withstand an acceleration load of 16 g's in any direction. This will be accomplished by using a polyurethane foam insulation system. After the entire system has been assembled in the paneled container, the foam will be poured, filling all remaining space. The foam, then, will not only insulate but will support the system. The outside paneling shall be 3/8 inch aluminum plate.

With this insulation system, the total heat leak will be approximately 15 BTU per hour. The rate of pressure rise, as a result of this heat leak, will be 1.5 psi per hour.

APPENDIX B

MASS TANK GAGING SIGNAL CONDITIONER AND DATA ACQUISITION SYSTEM

Purpose

To condition the resonant frequencies of the mass tank, to measure these frequencies as a function of time and store the data in a magnetic tape unit.

Operation

A radio frequency generator is swept through a designated frequency spectrum of a starting frequency f_A, to an ending frequency f_B.

This generator is connected to a cryogenic mass tank. The mass tank has resonant frequencies (modes) which are enhanced each time the tank is energized with the generator sweep of selected frequencies.

The design objective of the data acquisition system and signal conditioner is to measure these enhanced resonant modes with respect to a known frequency and record them.

In the system this measurement is accomplished by using a time measurement technique. The generator sweep is used as a time base for all of these measurements.

A reference cavity tuned to a frequency, f_o, which is lower than the lowest cryogenic cavity mode, is the reference starting time for the time measurement of the mass tank system.

When the generator energizes the reference cavity tuned to f_o, a pulse is generated by the cavity. This pulse is used to start a counting sequence using a 100 kHz clock as the basic counting device.

The first resonant mode, f_1, from the mass tank strobes the counter into a buffer register which loads the data to a shift register.

The shift register then sends the data to a magnetic tape unit. All these data transfers occur before the next resonant mode of the mass tank is generated.

The counter continues counting with its data being strobed into the shift register every time a resonant mode is generated.

Upon completion of the generator sweep, the counter is reset, another antenna in a different location on the mass tank is multiplexed, and the generator initiates a new sweep. Beginning of the sweep initiates a new set of data.

Using this technique, a measurement of mass in the cryogenic tank is obtained as a function of time with respect to the reference cavity tuned to f_o.

Data Acquisition Schematic I

Functional Description

This schematic shows the timing sequences necessary to start the counting sequence and data transfer functions. All timing events are referred to the initiating pulse, t_o, generated by the reference cavity.

The pulse t_o, opens the gate to the counter and enables the real time clock to send 100 KHz pulses to the six stage counter.

The next timing event occurs when the cryogenic mode pulse t_n is generated. This pulse generates a strobe command to the storage buffer, a parallel load command to the shift register, a serial-parallel mode control pulse to the shift register, and a shift command gate enable pulse to the serial shift clock.

The mode counter generates a clock disable signal at the end of the last mode to be measured and resets itself.

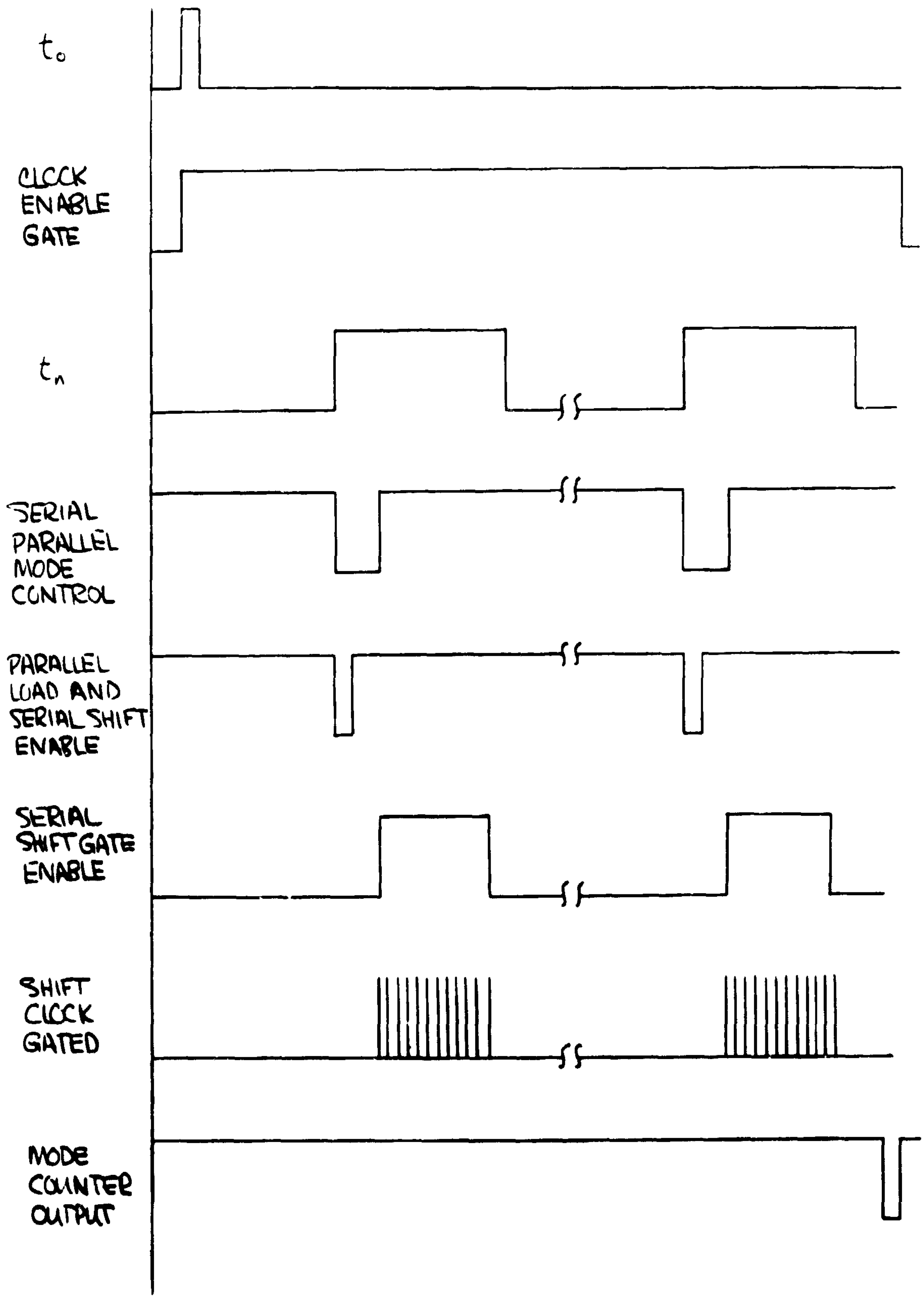

t_o
CLOCK ENABLE GATE
t_n
SERIAL PARALLEL MODE CONTROL
PARALLEL LOAD AND SERIAL SHIFT ENABLE
SERIAL SHIFT GATE ENABLE
SHIFT CLOCK GATED
MODE COUNTER OUTPUT

DATA ACQUISITION SCHEMATIC I

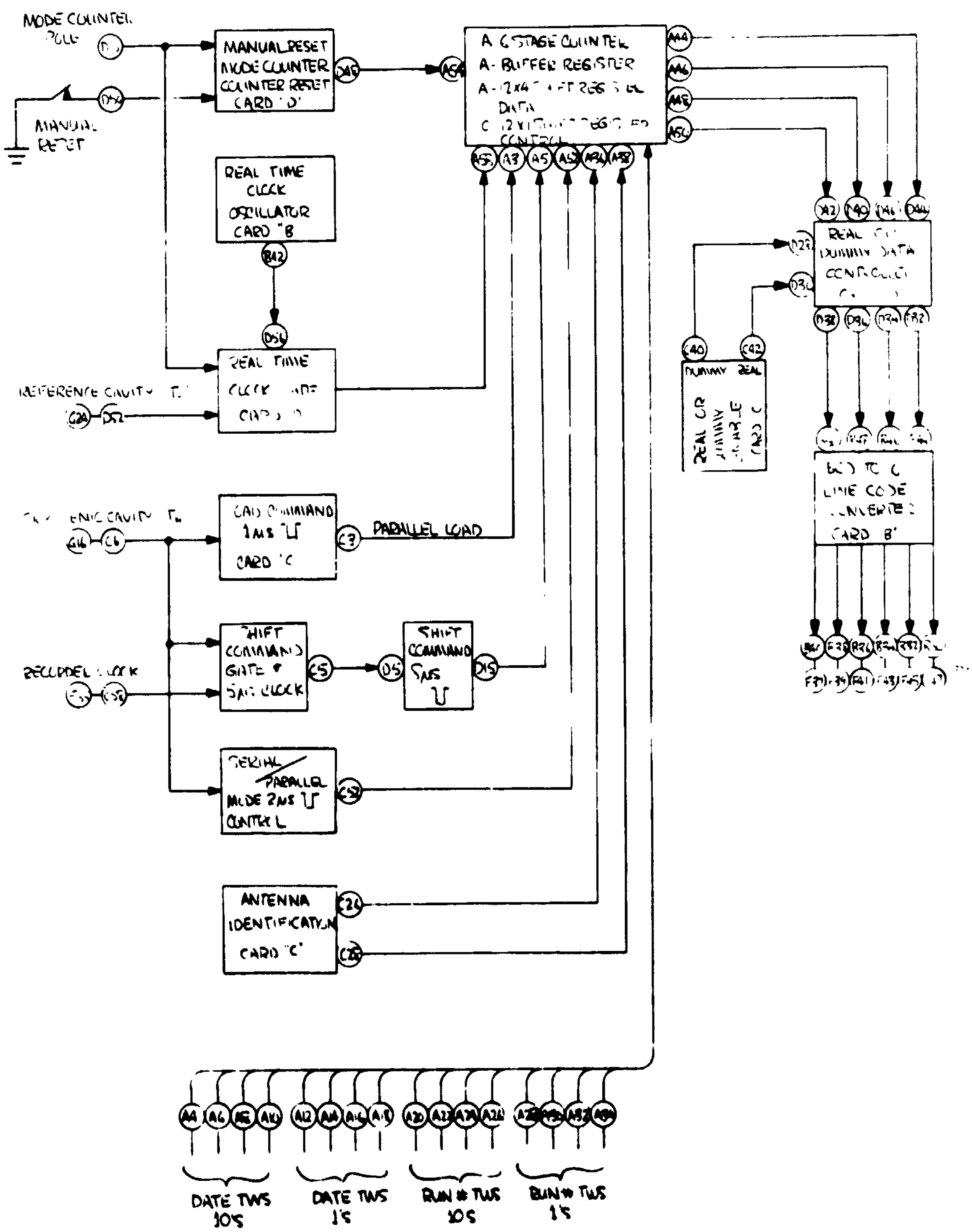

Data Acquisition Schematic II

Functional Description

This schematic shows the timing sequence necessary for control of the mode counter, antenna multiplexer, sequence counter and magnetic tape recording unit. All timing events are referred to the mass tank pulse t_n generated by the modes f_n.

A recording sequence is initiated by depressing the manual reset and manual start push buttons. The manual reset button resets all counters and controls flip flops to initial status for recording and controlling. The start push button starts the magnetic tape unit.

The t_n pulses are counted by the mode counter until a preselected output is generated in the counter. This output multiplexes the antenna or sends a counting pulse to the sequence counter if the antenna multiplexer is disabled.

The antenna multiplexer generates an output for every complete cycle of antenna multiplexing. This output sends a counting pulse to the sequence counter when multiplexing is enabled.

The sequence counter has a preselected number of counts it can accept before it overflows and stops the magnetic tape recorder.

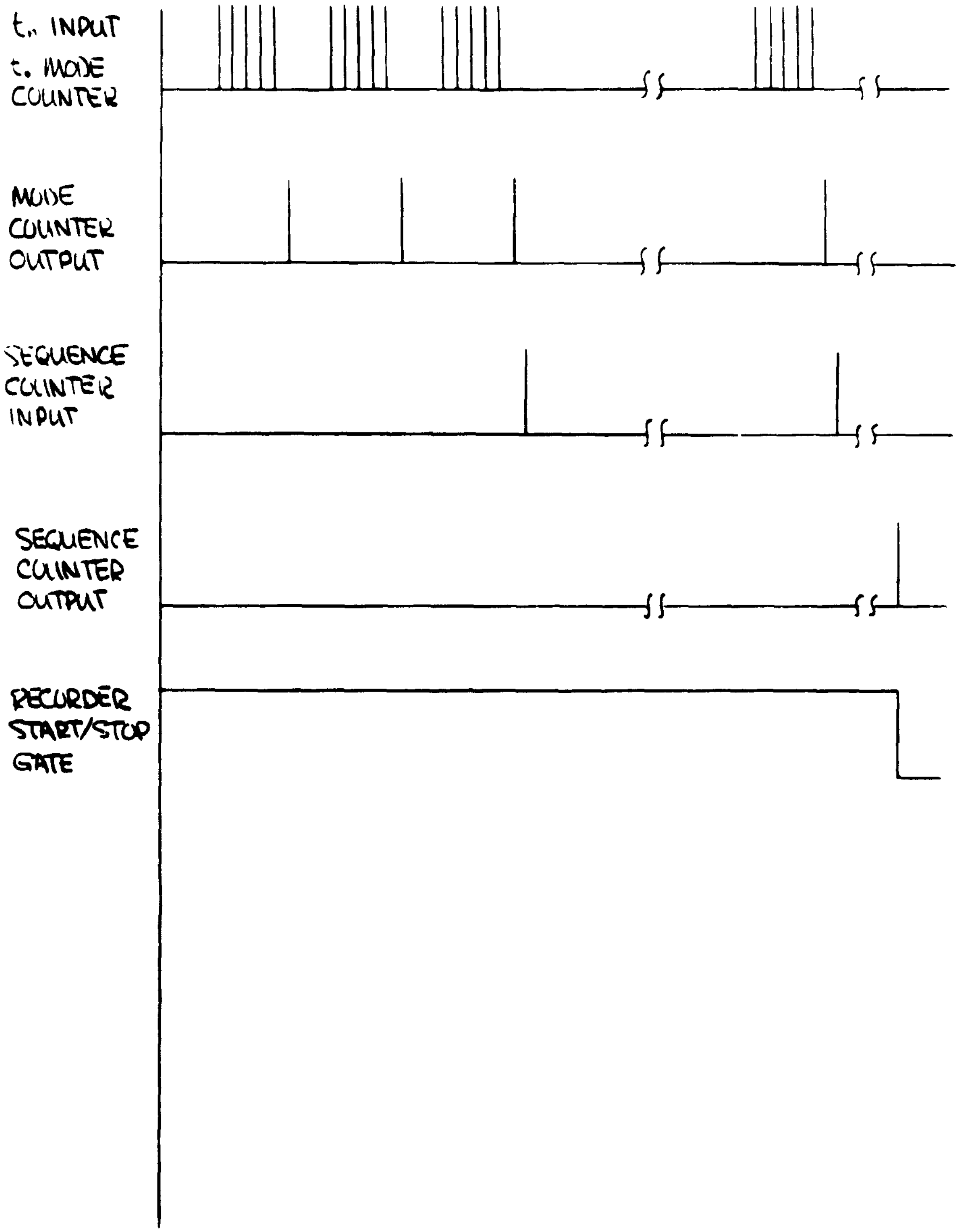
t. INPUT
t. MODE COUNTER
MODE COUNTER OUTPUT
SEQUENCE COUNTER INPUT
SEQUENCE COUNTER OUTPUT
RECORDER START/STOP GATE

DATA ACQUISITION SCHEMATIC II

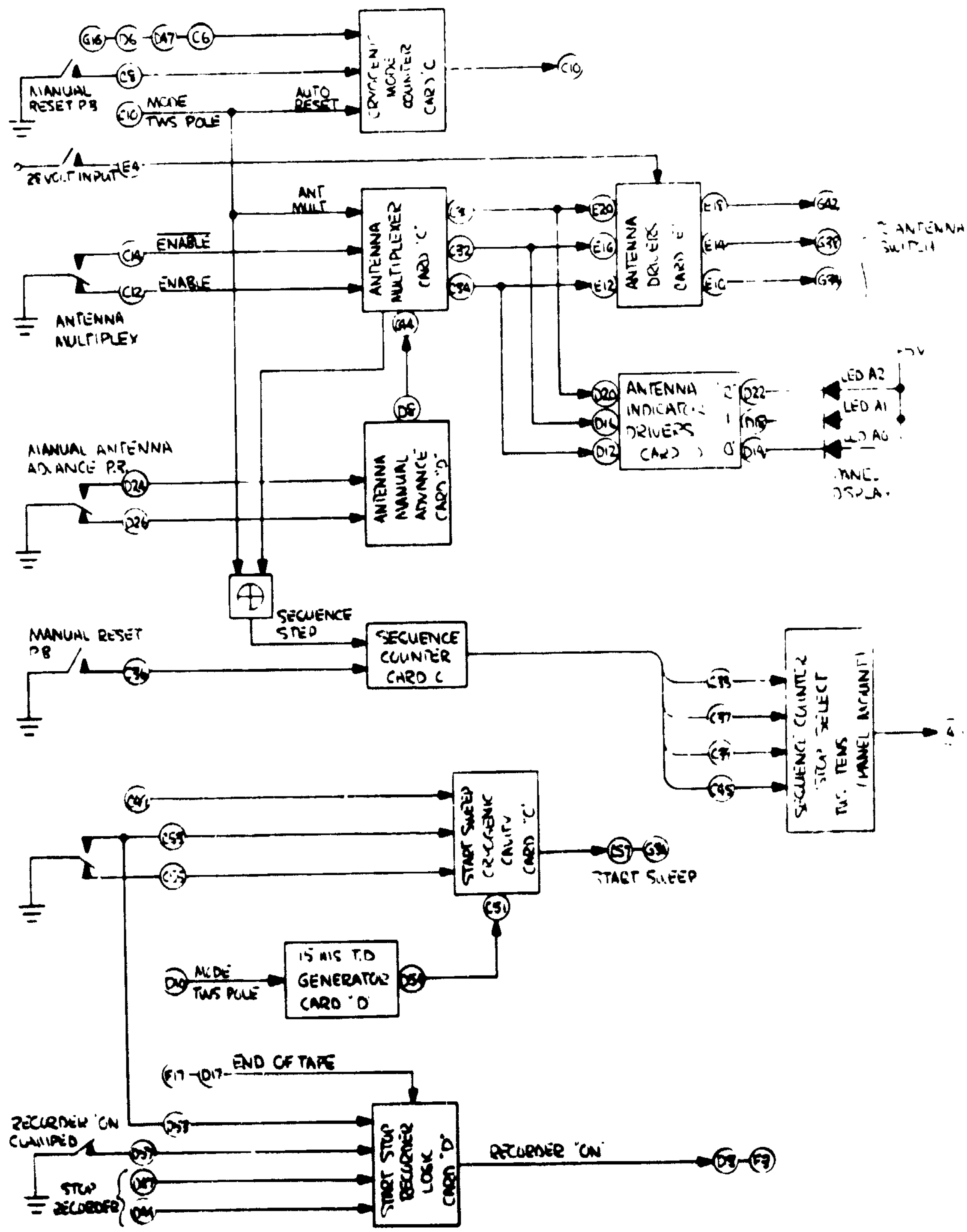

COUNTER-SHIFT REGISTER CARD

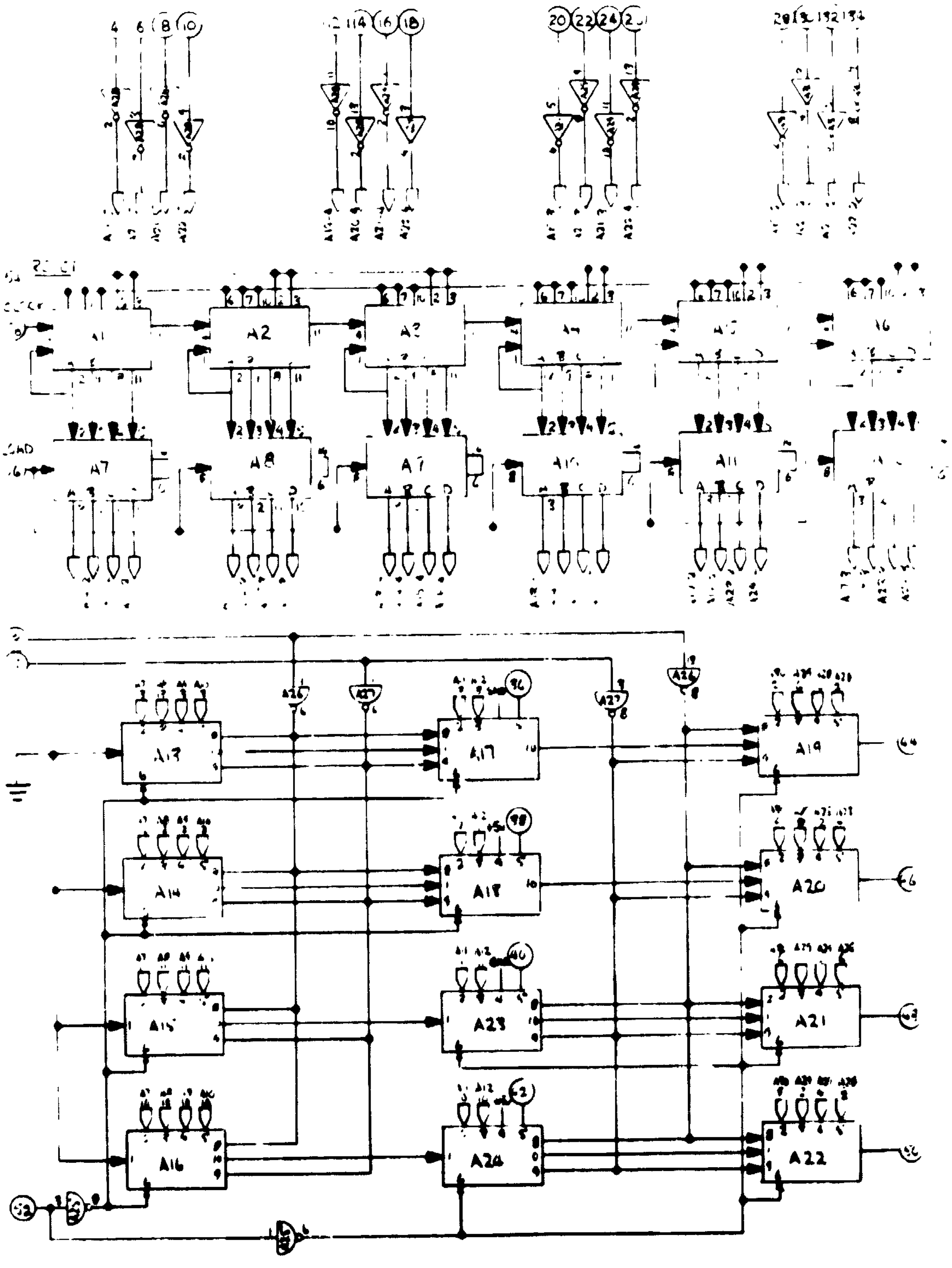

COUNTER-SHIFT REGISTER CARD A

From	To	Function	Condition
A3	A56-C3	load shift register	input
A5	D15-C4	8μs serial shift register	input
A2	B2	+ 5 volt distribution	
A4	Tens thumbwheel switch	date-1	input
A6	Tens thumbwheel switch	date-2	input
A8	Tens thumbwheel switch	date-4	input
A10	Tens thumbwheel switch	date-8	input
A12	Ones thumbwheel switch	date-1	input
A14	Ones thumbwheel switch	date-2	input
A16	Ones thumbwheel switch	date-4	input
A18	Ones thumbwheel switch	date-8	input
A20	Tens thumbwheel switch	run no. 1	input
A22	Tens thumbwheel switch	run no. 2	input
A24	Tens thumbwheel switch	run no. 4	input
A26	Tens thumbwheel switch	run no. 8	input
A28	Ones thumbwheel switch	run no. 1	input
A30	Ones thumbwheel switch	run no. 2	input
A32	Ones thumbwheel switch	run no. 4	input
A34	Ones thumbwheel switch	run no. 8	input
A36	C26	antenna identification 1	input
A38	C28	antenna identification 2	input
A40	A42-A60	antenna identification 4	ground input
A42	A40-A60	antenna identification 8	ground input
A44	D44	shift register output 1	
A46	D46	shift register output 2	
A48	D40	shift register output 4	
A50	D42	shift register output 8	
A52	C52	2μs shift register mode control	input
A54	D48	real time counter reset	input
A56	A3-C3-G44	load buffer register	input
A58	D58-G56	gated oscillator 100 K Hz clock	input
A60	A40-A42-B60	common distribution	

A1	7490	decade counter
A2	7490	decade counter
A3	7490	decade counter
A4	7490	decade counter
A5	7490	decade counter
A6	7490	decade counter
A7	7495	4-bit right/left shift register
A8	7495	4-bit right/left shift register
A9	7495	4-bit right/left shift register
A10	7495	4-bit right/left shift register
A11	7495	4-bit right/left shift register
A12	7495	4-bit right/left shift register
A13	7495	4-bit right/left shift register
A14	7495	4-bit right/left shift register
A15	7495	4-bit right/left shift register
A16	7495	4-bit right/left shift register
A17	7495	4-bit right/left shift register
A18	7495	4-bit right/left shift register
A19	7495	4-bit right/left shift register
A20	7495	4-bit right/left shift register
A21	7495	4-bit right/left shift register
A22	7495	4-bit right/left shift register
A23	7495	4-bit right/left shift register
A24	7495	4-bit right/left shift register
A25	832	dual 4 input NAND gate
A26	832	dual 4 input NAND gate
A27	832	dual 4 input NAND gate
A28	7404	HEX inverter
A29	7404	HEX inverter
A30	7404	HEX inverter

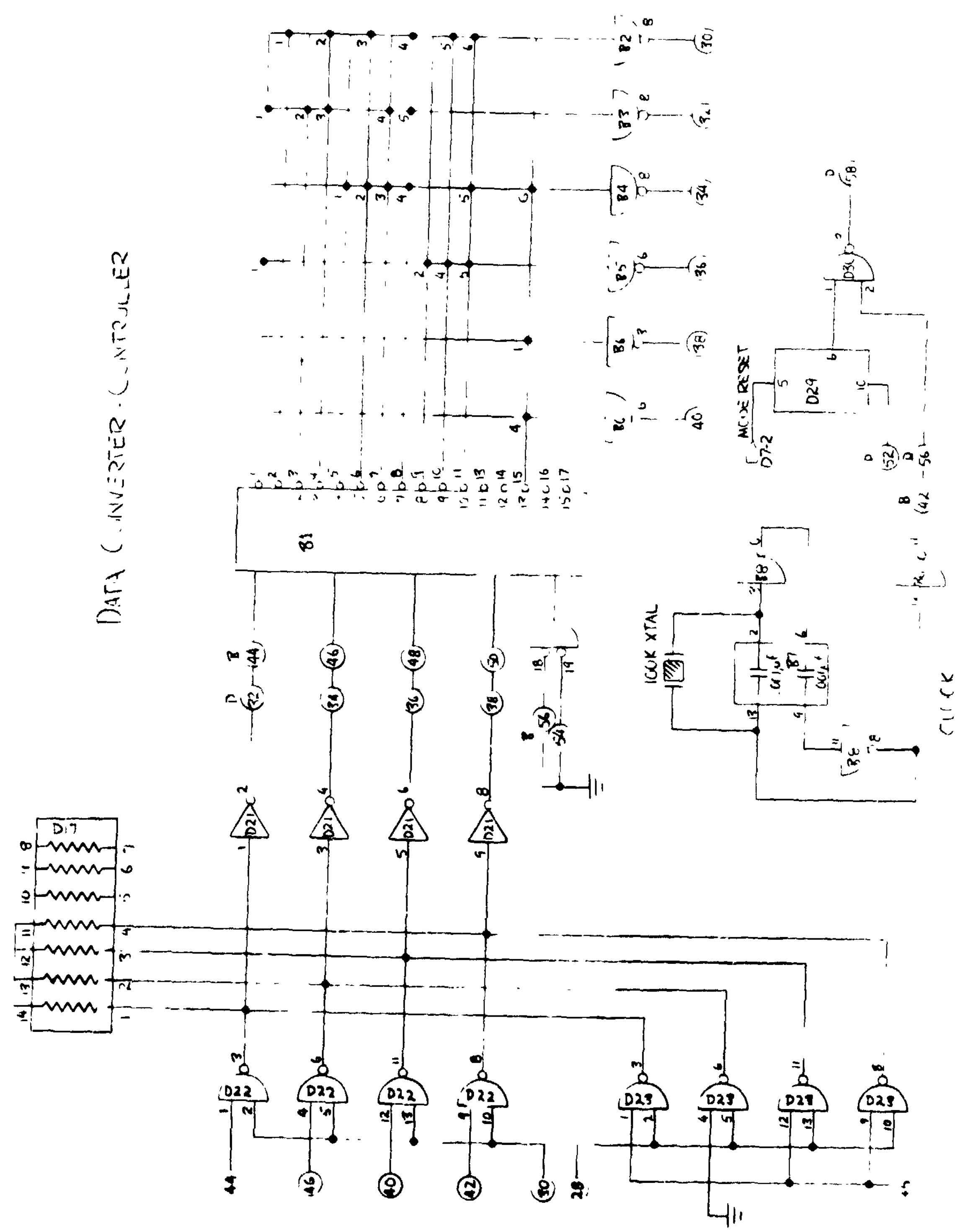
DATA CONVERTER CONTROLLER
100K XTAL
MODE RESET
CLOCK

DATA CONVERTER-CONTROLLER CARD "B" AND CARD "D"

From	To	Function	Condition
B2	A2-C2	+ 5 volt distribution	
B30	F47	magnetic tape 1	output
B32	F45	magnetic tape 2	output
B34	F43	magnetic tape 4	output
B36	F41	magnetic tape 8	output
B38	F39	magnetic tape A	output
B40	F37	magnetic tape B	output
B42	D56	100 K Hz clock free running	output
B44	D32	shift register data 1	input
B46	D34	shift register data 2	input
B48	D36	shift register data 4	input
B50	D38	shift register data 8	input
B54	B56-B60	code conversion enable	input
B60	A60-C60	common distribution	
D28	C40	dummy data enable	input
D30	C42	real data enable	input
D32	B44	shift register data 1	output
D34	B46	shift register data 2	output
D36	B48	shift register data 4	output
D38	B50	shift register data 8	output
D40	A48	shift register data 1	input
D42	A50	shift register data 2	input
D44	A44	shift register data 4	input
D46	A46	shift register data 8	input
D52	G24	reference cavity	input
D56	B42	100 K Hz clock free running	input
D58	A58-G56	100 K Hz clock gated	output

B1	9311	one of sixteen decoder
B2	7430	8-input positive NAND gate
B3	7430	8-input positive NAND gate
B4	7430	8-input positive NAND gate
B5	7420	dual 4-input positive NAND gate
B6	7400	quad 2-input positive NAND gate
B7	2 capacitor cambion	
B8	832	dual buffer

D17	2 K resistors	
D21	7404	HEX inverter
D22	7403	quad 2-input positive NAND gate
D23	7403	quad 2-input positive NAND gate
D29	848	clocked flip-flop
D30	7400	quad 2-input positive NAND gate

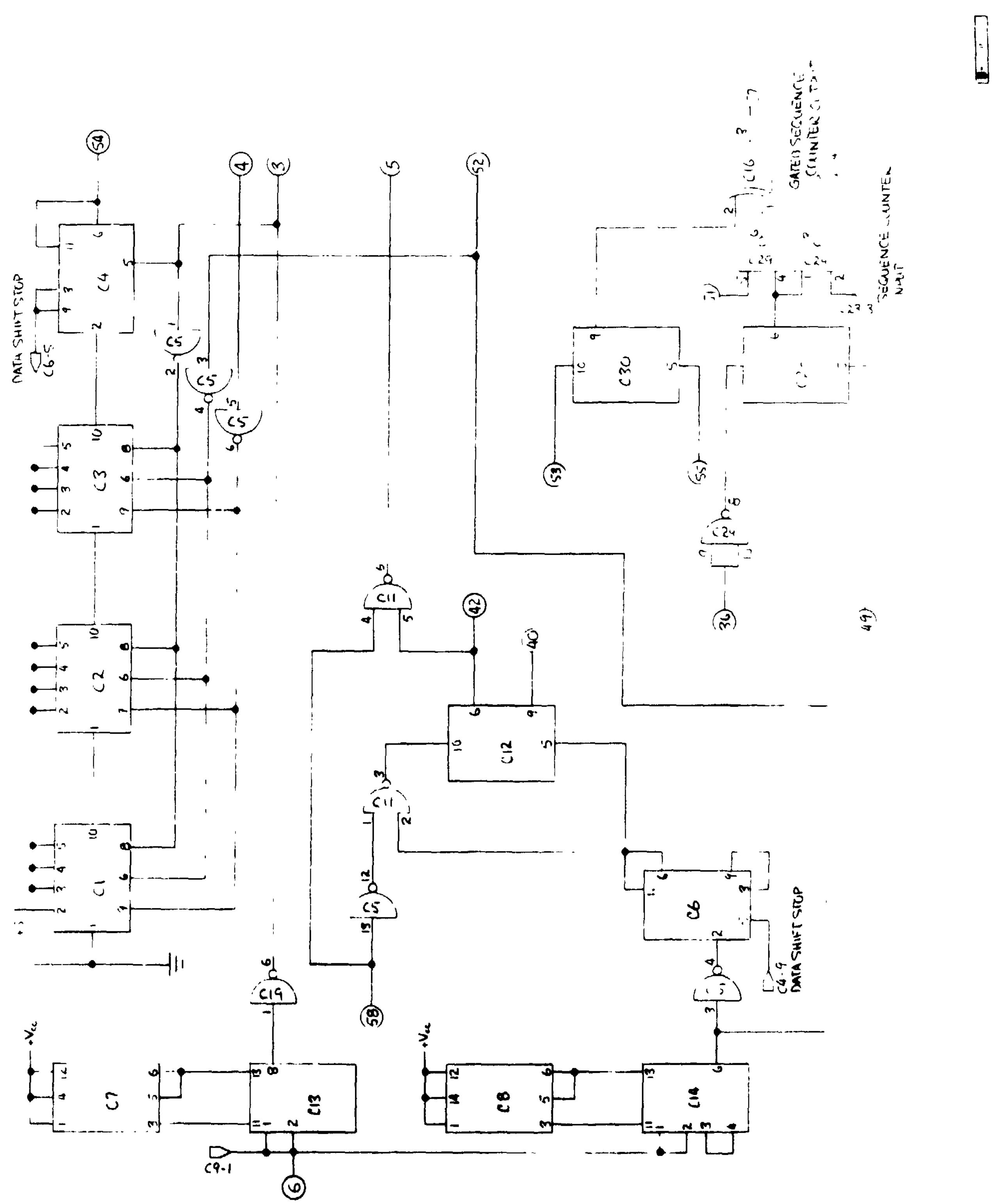
DATA SHIFT STOP
C1
C2
C3
C4
C6
C7
C8
C12
C13
C14
C30
C9-1

CONTROL REGISTER-TIMING GENERATORS CARD "C"

From	To	Function	Condition
C3	A3-G44	1 μs parallel load	output
C5	D5	serial shift gated clock	output
C49	D49-10's tws pole	sequence counter stop sweep	input
C51	D54	15 ms T.D. start sweep	input
C53	D53-N.O. SW	manual start pushbutton	input
C55	N.C. SW	manual start pushbutton	input
C57	G30	start sweep	output
C4	D15-A5	8μs shift clock	output
C6	G16	cryogenic cavity	input
C36	D50 N.C. SW	manual reset pushbutton	input
C40	D28	dummy data enable	output
C42	D30	real data enable	output
C52	A52	2μs shift register mode control	output
C58	F55	recorder clock	input

C1	7495	4-bit right/left shift register
C2	7495	4-bit right/left shift register
C3	7495	4-bit right/left shift register
C4	848	clocked flip-flop
C5	7404	HEX inverter
C6	848	clocked flip-flop
C7	RC network for one shot (C13)	
C8	RC network for one shot (C14)	
C11	7400	quad 2-input positive NAND gate
C12	848	clocked flip-flop
C13	9601	one shot multivibrator
C14	9601	one shot multivibrator
C16	7486	quad exclusive OR gate
C19	832	dual buffer
C26	848	clocked flip-flop
C29	7400	quad 2-input positive NAND gate
C30	848	clocked flip-flop

MODE & SEQUENCE COUNTER & ANTENNA MULTIPLEXER

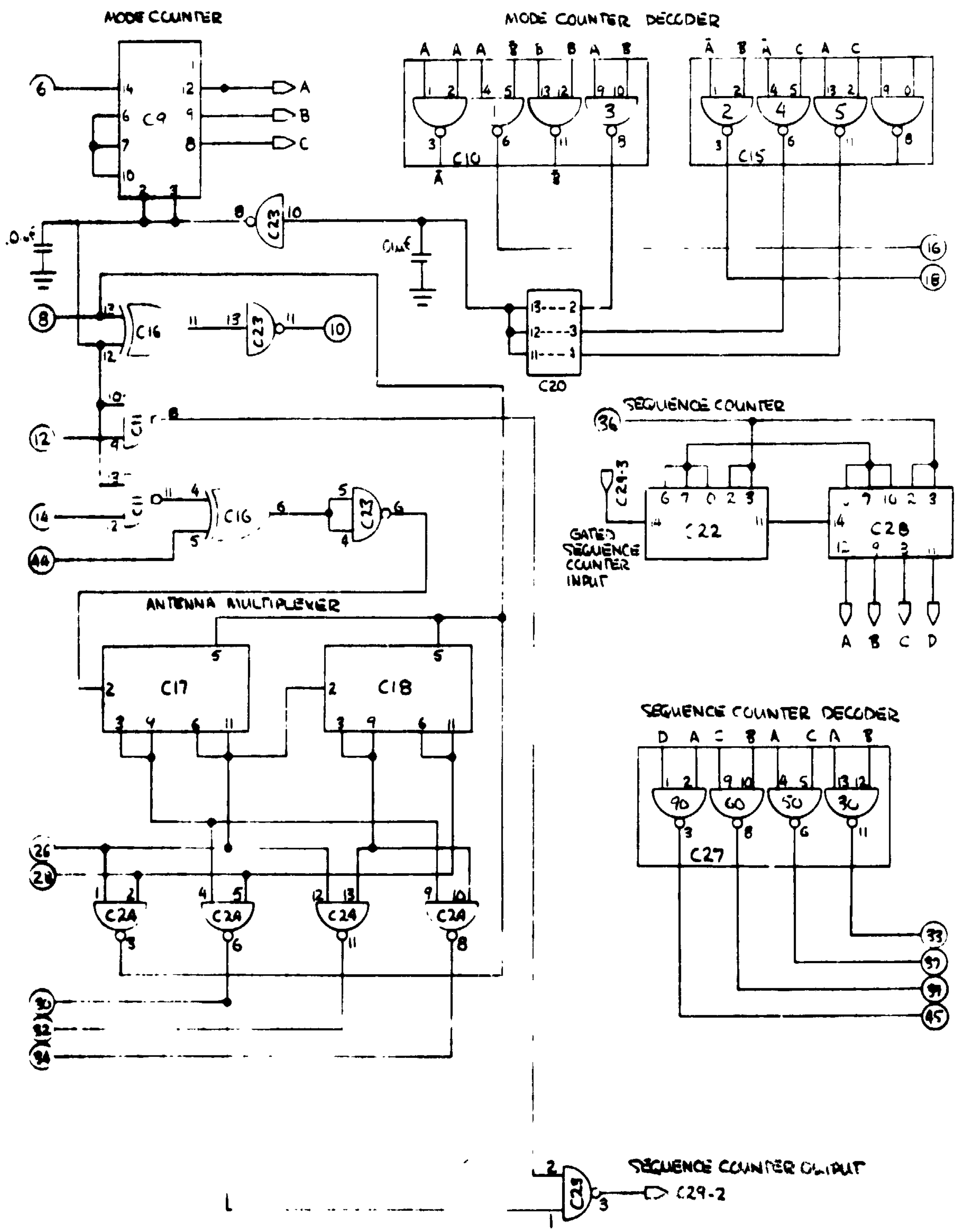

MODE COUNTER-SEQUENCE COUNTER-ANTENNA MULTIPLEXER
CARD "C"

From	To	Function	Condition
C33	10's tws pos 3	sequence counter 30 counts	output
C37	10's tws pos 5	sequence counter 50 counts	output
C39	10's tws pos 6	sequence counter 60 counts	output
C45	10's tws pos 9	sequence counter 90 counts	output
C6	D47	cryogenic cavity gated	input
C8	N.O. sw	manual reset pushbutton	input
C10	D10-G44	reset and antenna multiplex	input
C12	N.C. sw	antenna multiplex enable	input
C14	N.O. sw	antenna multiplex enable	input
C16	G46	mode 1 reset	output
C18	G48	mode 2 reset	output
C20	G50	mode 3 reset	output
C22	G52	mode 4 reset	output
C24		mode 5 reset	output
C26	A36	antenna identification 1	output
C28	A38	antenna identification 2	output
C30	D20-E20-G40	antenna driver 1	output
C32	D16-E16-G36	antenna driver 2	output
C34	D12-E12-G32	antenna driver 4	output
C36	D50-N.C. sw	manual reset pushbutton	input
C44	D48	manual antenna advance	input

C9	7490	decade counter
C10	7400	quad 2-input NAND gate
C11	7400	quad 2-input NAND gate
C15	7400	quad 2-input NAND gate
C16	7486	quad exclusive OR gate
C17	848	clocked flip flop
C18	848	clocked flip flop
C20	cambion for wire connections	
C22	7490	decade counter
C23	7400	quad 2-input positive NAND gate
C24	7400	quad 2-input positive NAND gate
C27	846	quad 2-input NAND gate
C28	7490	decade counter

GENERAL PURPOSE TIMING EVENTS

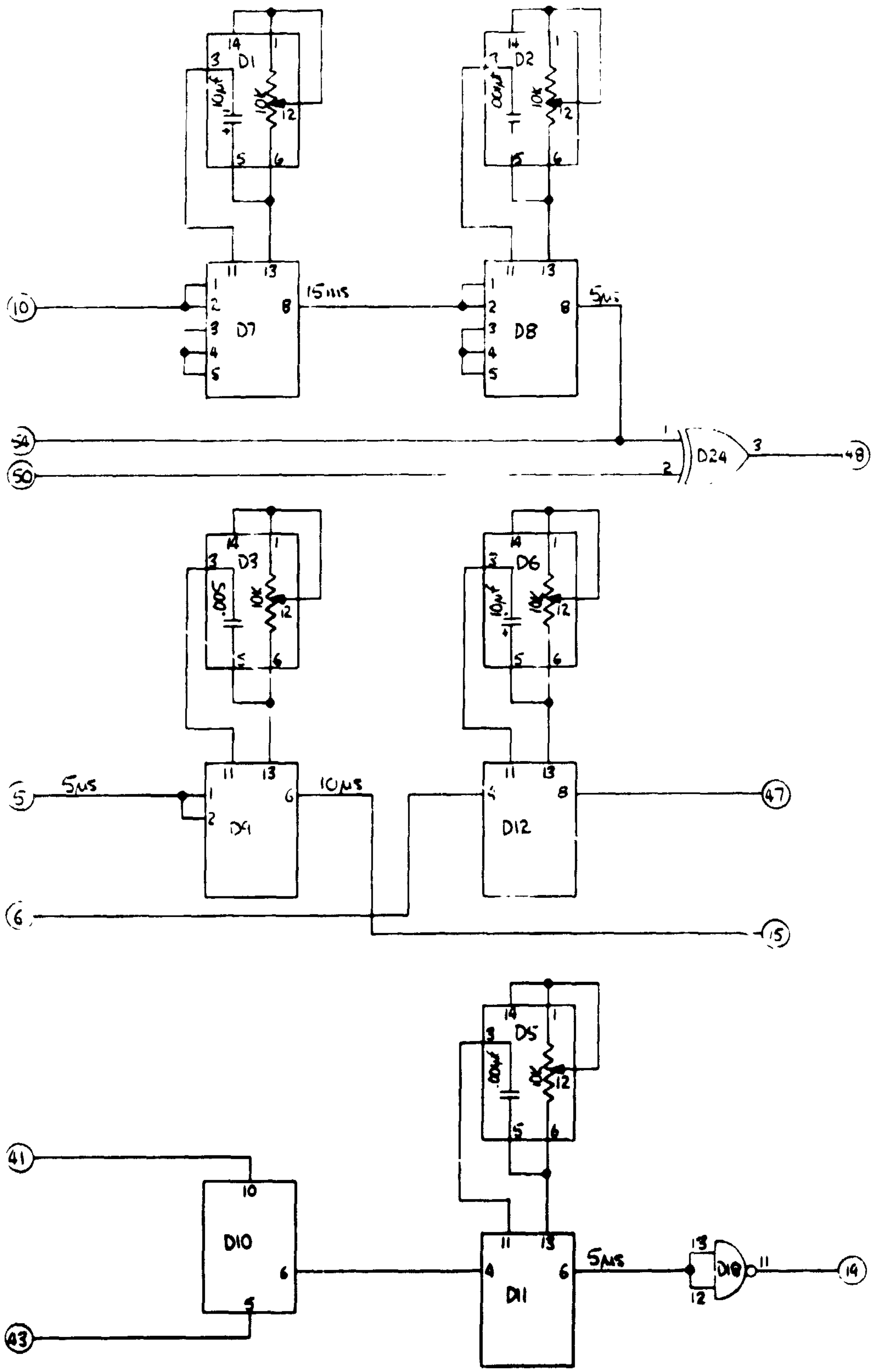

GENERAL PURPOSE TIMING EVENTS CARD "D"

From	To	Function	Condition
D3			
D5	C5	5μs serial shift gated clock	input
D15	A5-C4	8μs serial shift gated clock	output
D19	F16	end of file 5μs	output
D41	N.O. sw	end of file pushbutton	input
D43	N.C. sw	end of file pushbutton	output
D47	C6	cryogenic cavity gated 5ms	output
D6	G16	cryogenic cavity gated	input
D10	C10	reset, antenna multiplex and 15ms TD	input
D48	A54-G54	real time counter reset	output
D50	C36-N.C. sw	manual reset pushbutton	input
D54	C51	15ms time delay	output

D1	RC network for one shot (10μf, 10 K)	
D2	RC network for one shot (.001μf, 10 K)	
D3	RC network for one shot (.005μf, 10 K)	
D5	RC network for one shot (.001μf, 10 K)	
D6	RC network for one shot (10μf, 10 K)	
D7	9601	one shot multivibrator
D8	9601	one shot multivibrator
D9	9601	one shot multivibrator
D10	848	clocked flip-flop
D11	9601	one shot multivibrator
D12	9601	one shot multivibrato
D18	7400	quad 2-input positive AND gate
D24	7486	quad 2-input exclusive OR gate

GENERAL PURPOSE FUNCTIONS

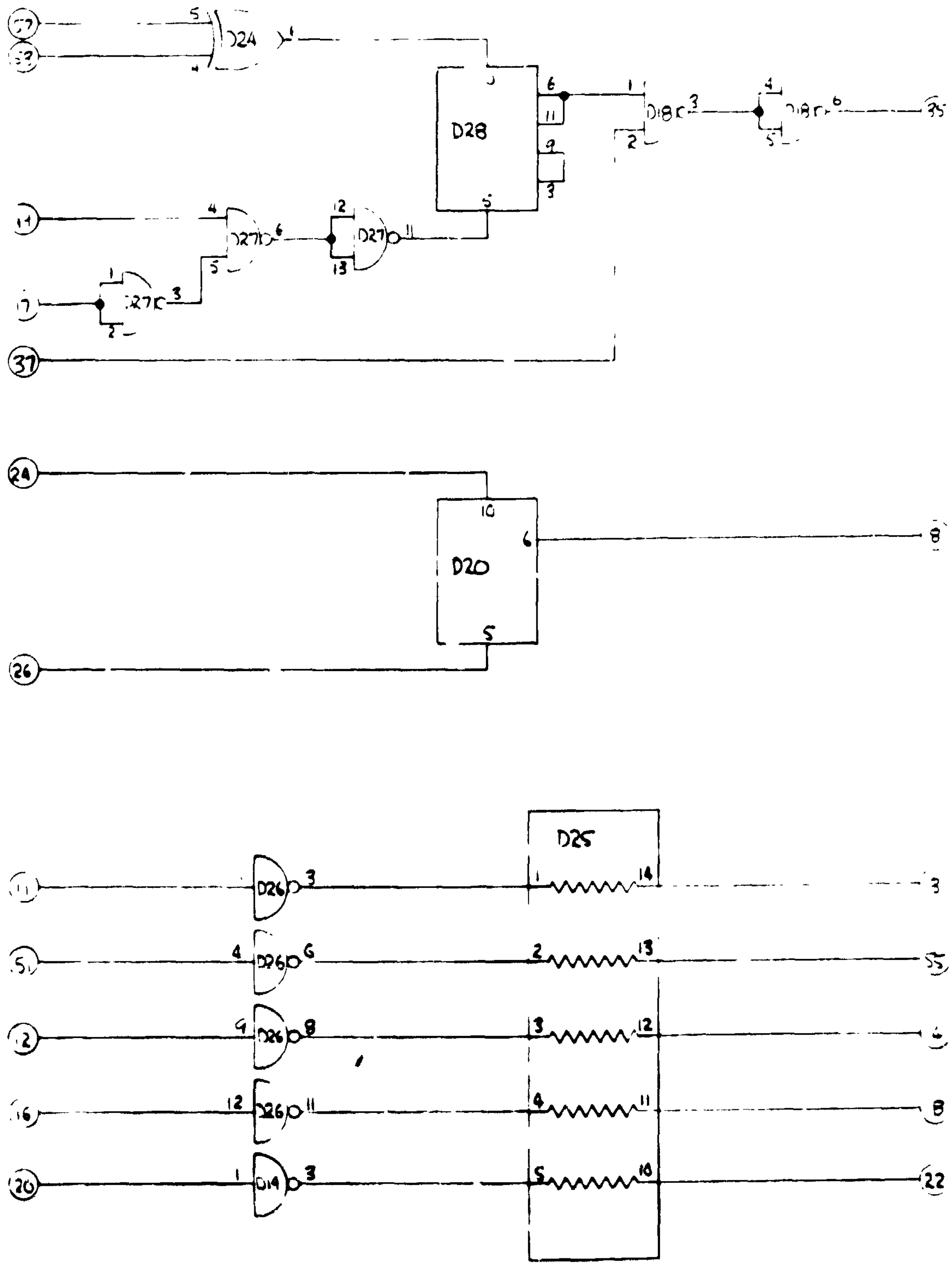

GENERAL PURPOSE FUNCTIONS CARD "D"

From	To	Function	Condition
D11	F11	tape running	input
D13	led 1 panel	tape running indicator	output
D17	F15	end of tape	input
D35	F35	write command	output
D37	F55-C58	write shift clock	input
D49	C49 10's tws	sequence counter switch pole	input
D51	F53	file protect missing	input
D53	C53-N.O. sw	manual start pushbutton	input
D55	led 2 panel	file protect missing indicator	output
D57	N.O. sw	recorder on clamp	input
D8	C44	manual advance antenna	output
D12	E12-G32-C34	antenna "0"	input
D14	led ant "0"	antenna "0" indicator	output
D16	E16-G36-C32	antenna "1"	input
D18	led ant "1"	antenna "1" indicator	output
D20	E20-G40-C30	antenna "2"	input
D22	led ant "2"	antenna "2" indicator	output
D24	N.O. sw	manual antenna advance	input
D26	N.C. sw	manual antenna advance	input

D18	7400	quad 2-input positive NAND gate
D19	7403	quad 2-input positive NAND gate
D20	848	clocked flip-flop
D24	7486	quad 2-input exclusive OR gate
D25	510Ω resistors	
D26	7403	quad 2-input positive NAND gate
D27	7400	quad 2-input positive NAND gate
D28	848	clocked flip-flop

ANTENNA SWITCH DRIVERS

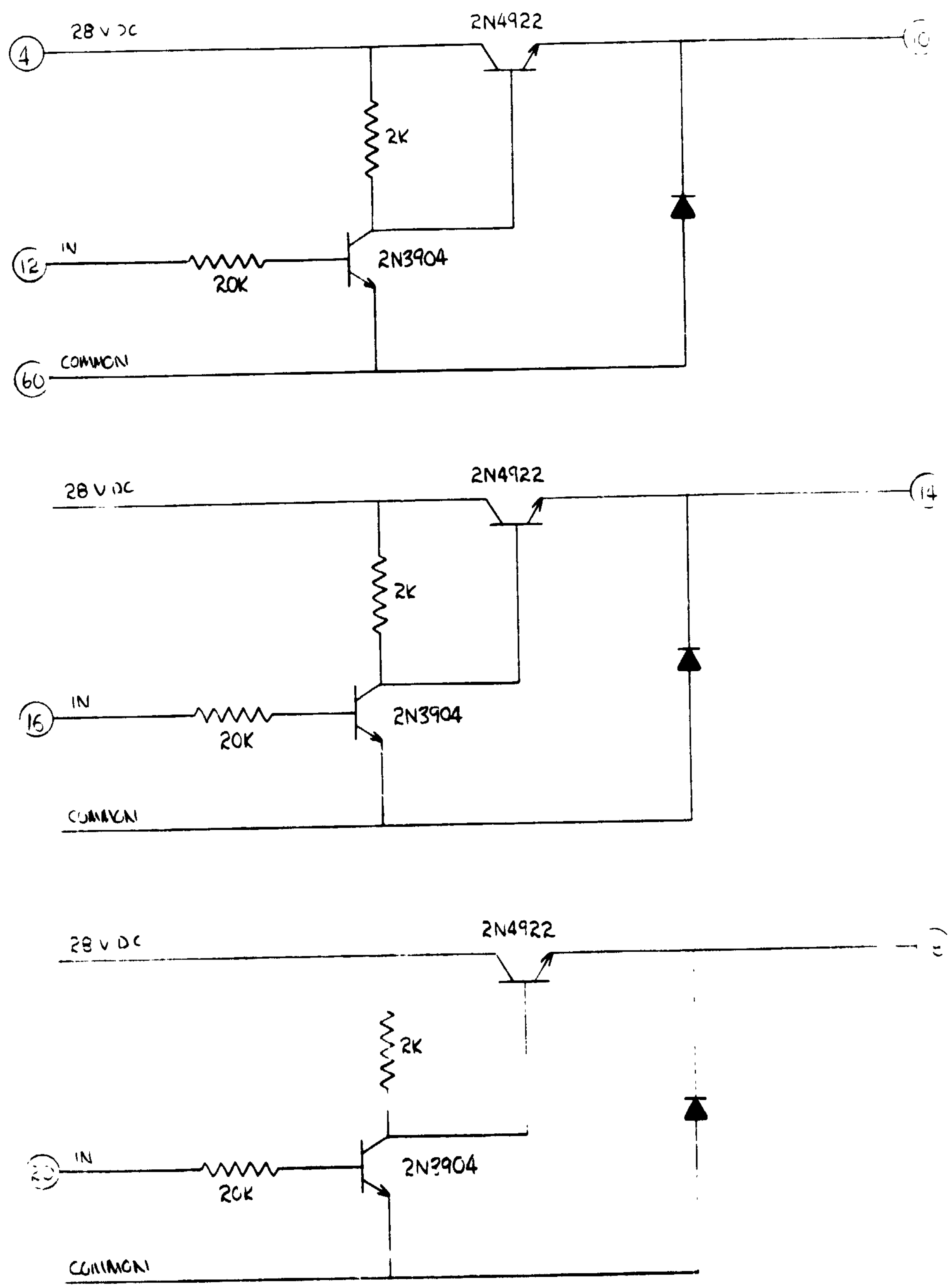

ANTENNA SWITCH DRIVERS CARD "E"

From	To	Function	Condition
E4	G28	+ 28 volts	input
E10	G34	antenna "0"	output
E12	C34-D12-G32	antenna "0"	input
E14	G38	antenna "1"	output
E16	C32-D16-G36	antenna "1"	input
E18	G42	antenna "2"	output
E20	C30-D20-G40	antenna "2"	input

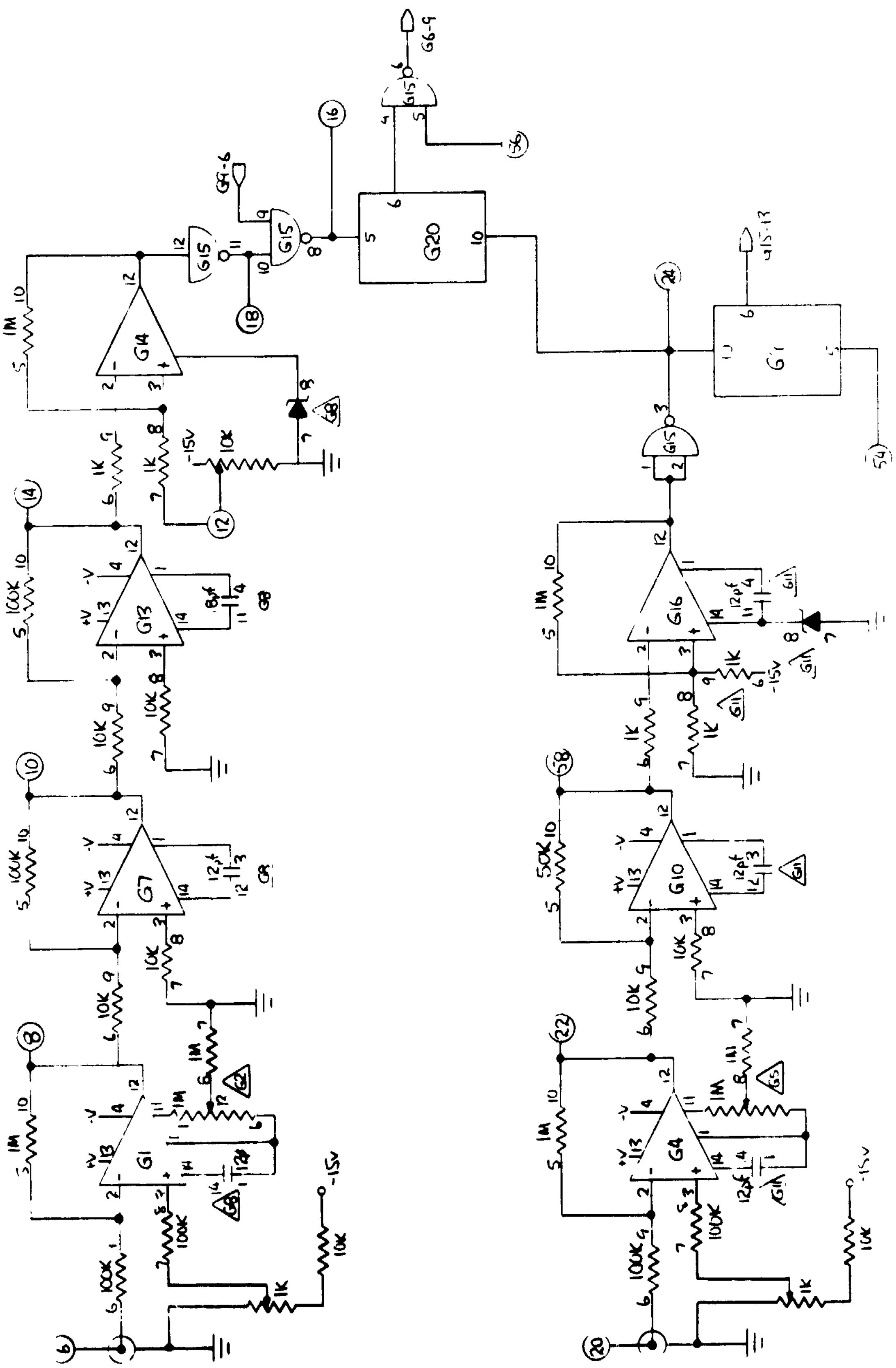
G1
G4
G7
G10
G13
G14
G15
G16
G20
-15V
G6-9

CARD "G"

From	To	Function	Condition
G6	connector 1	cryogenic cavity signal	input
G8		amplifier "1"	test point
G10		amplifier "2"	test point
G14		amplifier "3"	test point
G16	D6	cryogenic signal gated	output
G18		cryogenic comparator signal	test point
G20	connector 2	reference cavity signal	input
G22		reference cavity amplifier "1"	test point
G24	D52	reference cavity comparator	output
G54	D10-C10	mode counter reset signal	input
G56	D58-A58	100 K Hz clock	input
G58		reference cavity amplifier "2"	test point

G1	LM301 operational amplifier	
G2	1MΩ pot and 1MΩ resistor	
G4	LM301 operational amplifier	
G5	1MΩ pot and 1MΩ resistor	
G7	LM301 operational amplifier	
G8	capacitor cambion	
G9	848	clocked flip-flop
G10	LM301 operational amplifier	
G11	capacitor cambion	
G13	LM301 operational amplifier	
G14	LM301 operational amplifier	
G15	7400	quad 2-input NAND gate
G20	848	clocked flip-flop

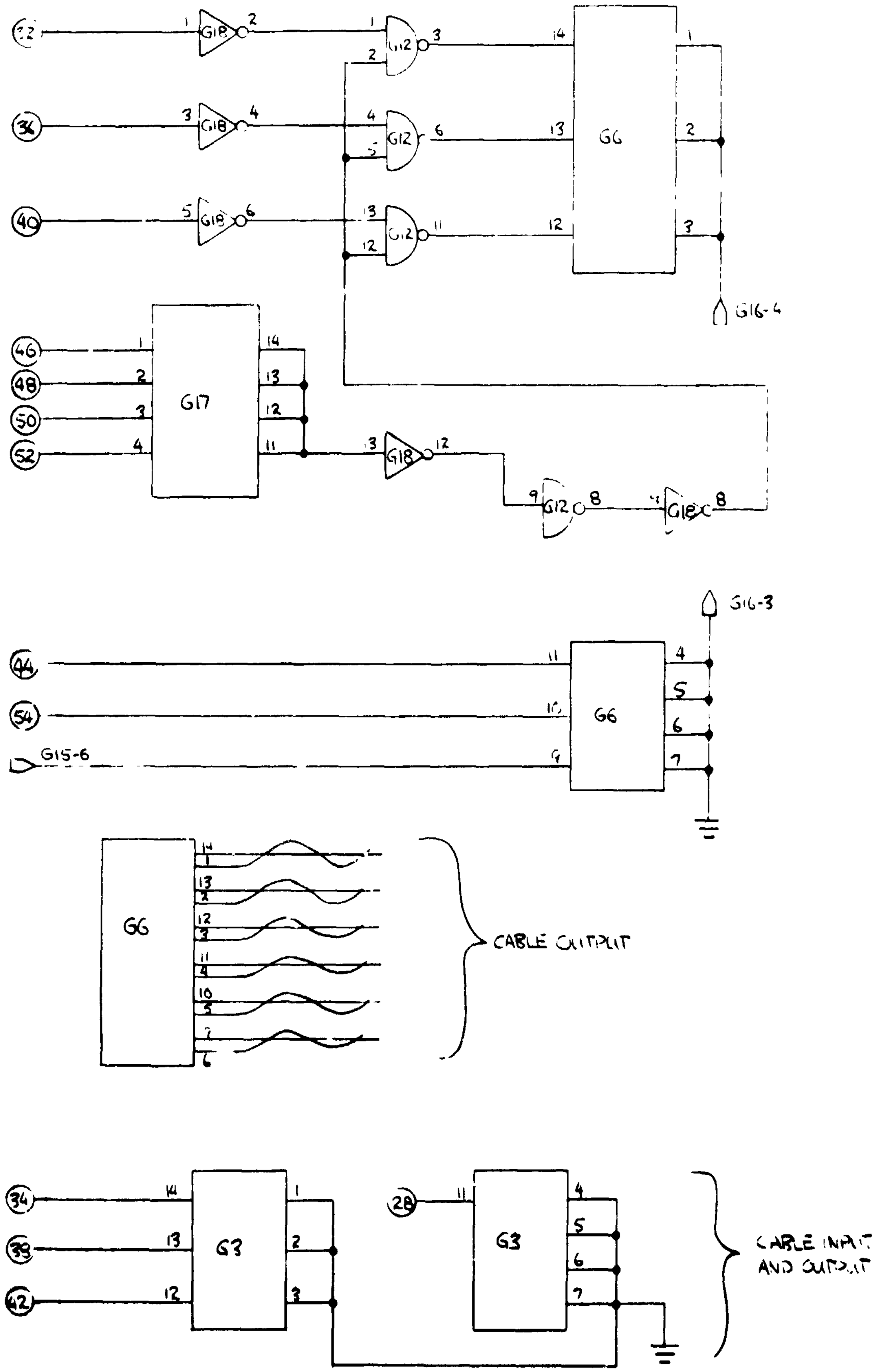
G18
G12
G6
G17
G16-4
G16-3
G15-6
G3
CABLE OUTPUT
CABLE INPUT AND OUTPUT

From	To	Function	Condition
G28	E4	+ 28 volt	output
G32	D12-E12-C34	antenna "0"	input
G34	E10	antenna "0" drive	input
G36	D16-E16-C32	antenna "1"	input
G38	E14	antenna "1" drive	input
G40	D20-E20-C30	antenna "2"	input
G42	E18	antenna "2" drive	input
G44	C3-A3	parallel load	input
G46	C16	mode 1 counter	input
G48	C18	mode 2 counter	input
G50	C20	mode 3 counter	input
G52	C22	mode 4 counter	input
G54	D48-A54	15 ms time delay reset	input

G3	cambion for wire connections	
G6	cable cambion	
G12	7400	quad 2-input positive NAND gate
G17	cambion for wire connections	
G18	7404	HEX inverter

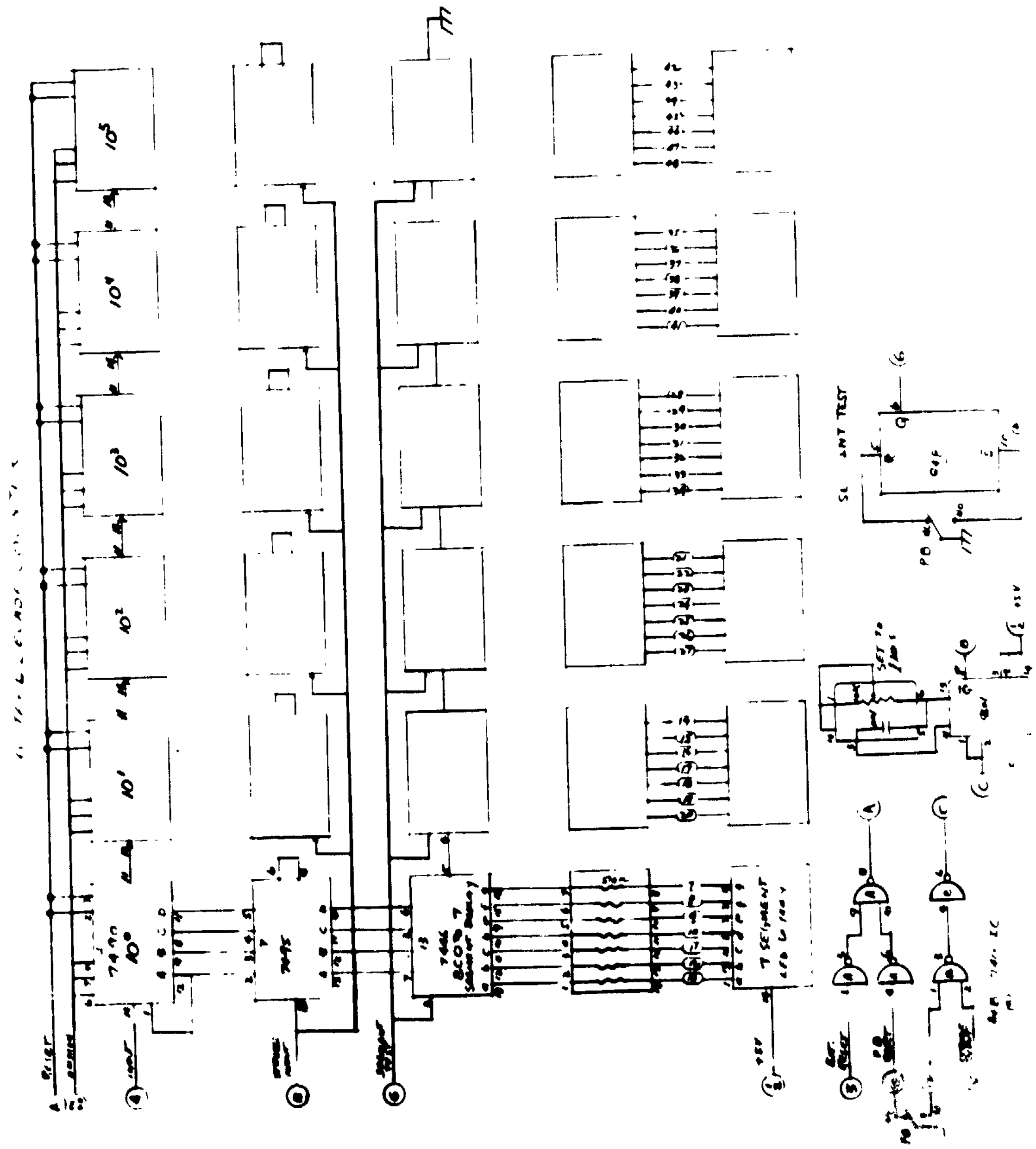

6 STAGE DECADE COUNTER CARD

2/28/73

Connector Pins	Function
1	+ 5V
2	+ 5V
3	external reset
4	signal input
5	strobe input
6	segment test
56	push button reset (N. O.)
57	
58	push button reset (N. C.)
59	common
60	common

INTERFACE CARD

2/28/73	Connector Pins	Function
	1	+ 5V
	2	+ 5V
	3	100 KHz clock
	4	common
	5	
	6	
	7	
	8	
	9	strobe #1 ANT "0"
	10	common
	11	strobe #2 ANT "1"
	12	common
	13	strobe #3 ANT "2"
	14	common
	15	external reset (all resets)
	16	common
	17	
	18	
	19	parallel load
	20	common
	59	common
	60	common

Table B-I. Interface Connector Pin List

ACT. PIN	SIG. GRD.	SIGNAL (see notes 1 through 3)		ACTIVE WIRE COLOR	7-TRACK	9-TRACK	BASIC	WRITE ONLY	READ ONLY	READ WRITE	RAW	SPECIAL
TRANSPORT CONTROL SIGNALS												
3		Run Normal Speed	input level	80	X	X	X	X	X	X	X	
5		Run High Speed	input level	30	X	X	X	X	X	X	X	
7		Forward Select	input level	70	X	X	X	X	X	X	X	
9		Reverse Select	input level	60	X	X	X	X	X	X	X	
11		Tape Running	output level	50	X	X	X	X	X	X	X	
13		Load Point	output level	8	X	X	X	X	X	X	X	
15		End of Tape	output level	6	X	X	X	X	X	X	X	
17		Broken Tape	output level	5	X	X	X	X	X	X	X	
19		Unload Command	input pulse	10	X	X	X	X	X	X	X	
21		Rewind to Load Point	input pulse	90	X	X	X	X	X	X	X	
23		Off Line	input pulse	9	X	X	X	X	X	X	X	
25		Rewind in Process	output level	20	X	X	X	X	X	X	X	
27		On Line	output level	40	X	X	X	X	X	X	[illegible]	
		Reserved - Do Not Use		-								X
		Reserved - Do Not Use		0								X
29		Chassis Ground (see note 4)		1	X	X	X	X	X	X	X	
WRITE SIGNALS												
31		Write Select	input level	7	X	X	X			X	X	
33		Write Parity Select (odd)	input level	92	X			X		X	X	
		Reserved		0	X	X						X
35		Write Command	input pulse	50	X	X		X		X	X	
18		Data Channel 0 (Write)	input level	97		X		X		X	X	
20		Data Channel 1 (Write)	input level	90		X		X		X	X	
37		Data Channel 2-B (Write)	input level	93	X	X		X		X	X	
39		Data Channel 3-A (Write)	input level	96	X	X		X		X	X	
41		Data Channel 4-8 (Write)	input level	95	X	X		X		X	X	
43		Data Channel 5-4 (Write)	input level	94	X	X		X		X	X	
45		Data Channel 6-2 (Write)	input level	9	X	X		X		X	X	
47		Data Channel 7-1 (Write)	input level	98	X	X		X		X	X	
49		Data Channel P-C (Write)	input level	30	X	X		X				X
51		Write Status	output level	90	X	X		X		X	X	
53		File Protect Ring Missing	output level	98	X	X		X		X	X	
55		Write Clock	output pulse	70	X	X		X		X	X	
57		Write Clock Gate	output level	60	X	X		X		X	X	
22		Write Echo Error	output pulse	10	X	X		X		X		
12		2X Write Clock	input pulse	[illegible]	X	X						X
14		Write $\overline{LRC}$	input pulse	20	X	[illegible]		X		X	X	
16		EOF Command	input pulse	80	X	X		X		X	X	

APPENDIX C

Q MEASUREMENT SUMMARY

The objective of the Q measurement task was to determine the spherical vessel Q as a function of diameter and wall material. The results of this measurement task are summarized in tabular form.

Spherical Vessels

Mode	19" Cu	18" SS	60" SS
TM_{11}	91,000	11,600	6,200
TM_{21}	85,200	10,900	13,600
TE_{11}	81,100	19,700	28,400
TM_{31}	41,200	10,900	17,500

Considering the lowest Q (TM_{11} in the 60" SS), f_1 is 172 MHz when empty and would be 155 MHz when filled with boiling point LH_2. The total frequency shift from empty to full would be 17 MHz. The bandwidth at the 3dB points is 0.028 MHz, or approximately 0.15% of the empty-full bandwidth. For LOX the 3dB bandwidth is approximately 0.10% of the empty-full bandwidth. Thus it appears that the Q will not seriously degrade the RF resonance technique in stainless steel spherical vessels up to 5 feet in diameter.

Let us assume that the change in Q pattern measured with the 18" and 60" stainless steel vessels continues to even larger diameters. Then for a 15 foot diameter stainless steel vessel, the 3dB bandwidth is 0.3% of the empty full LH_2 bandwidth. The LOX 3dB bandwidth is approximately 0.2% of the empty-full bandwidth.

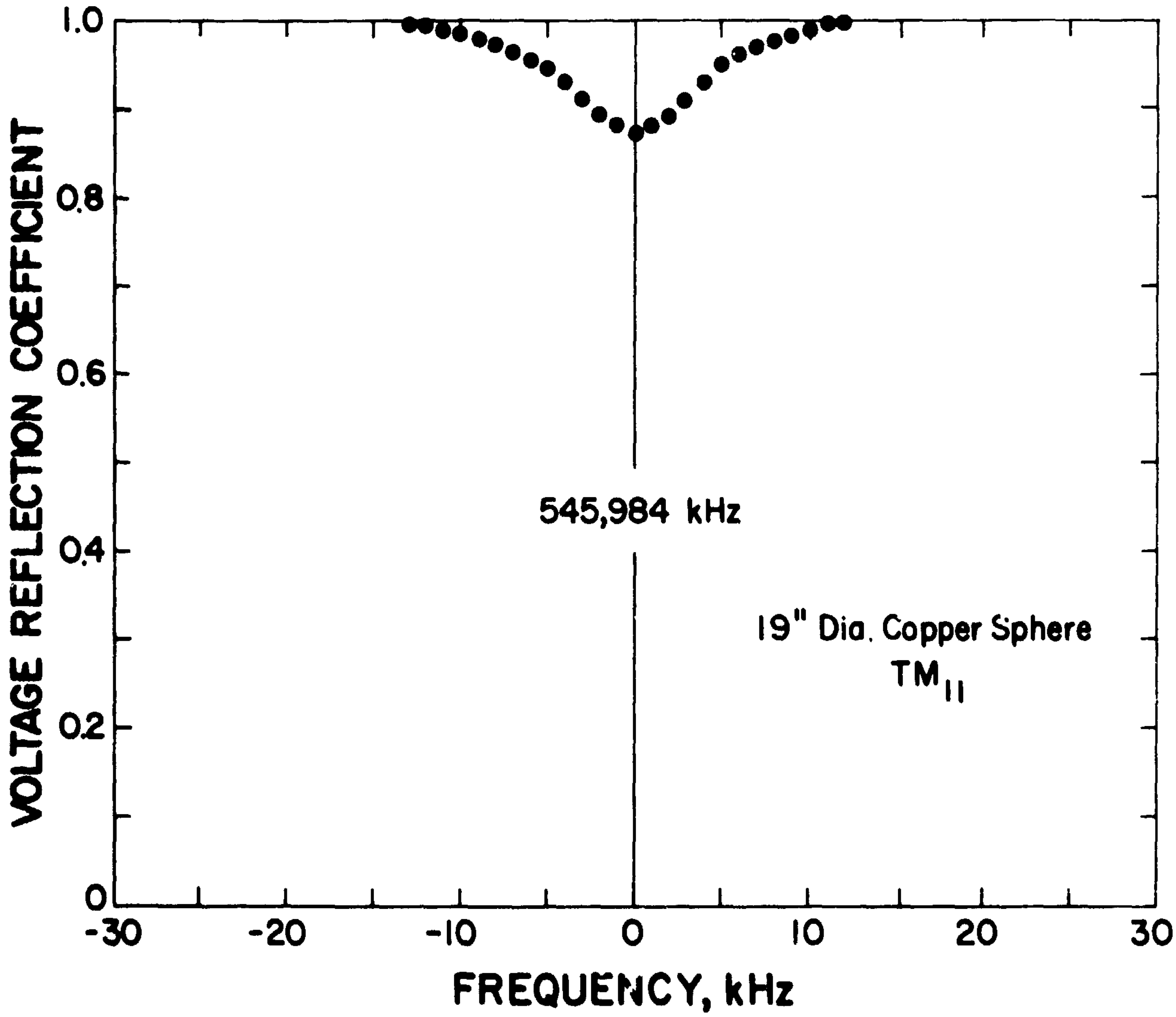

Figure C1. Frequency response of the copper spherical vessel for the TM_{011} mode.

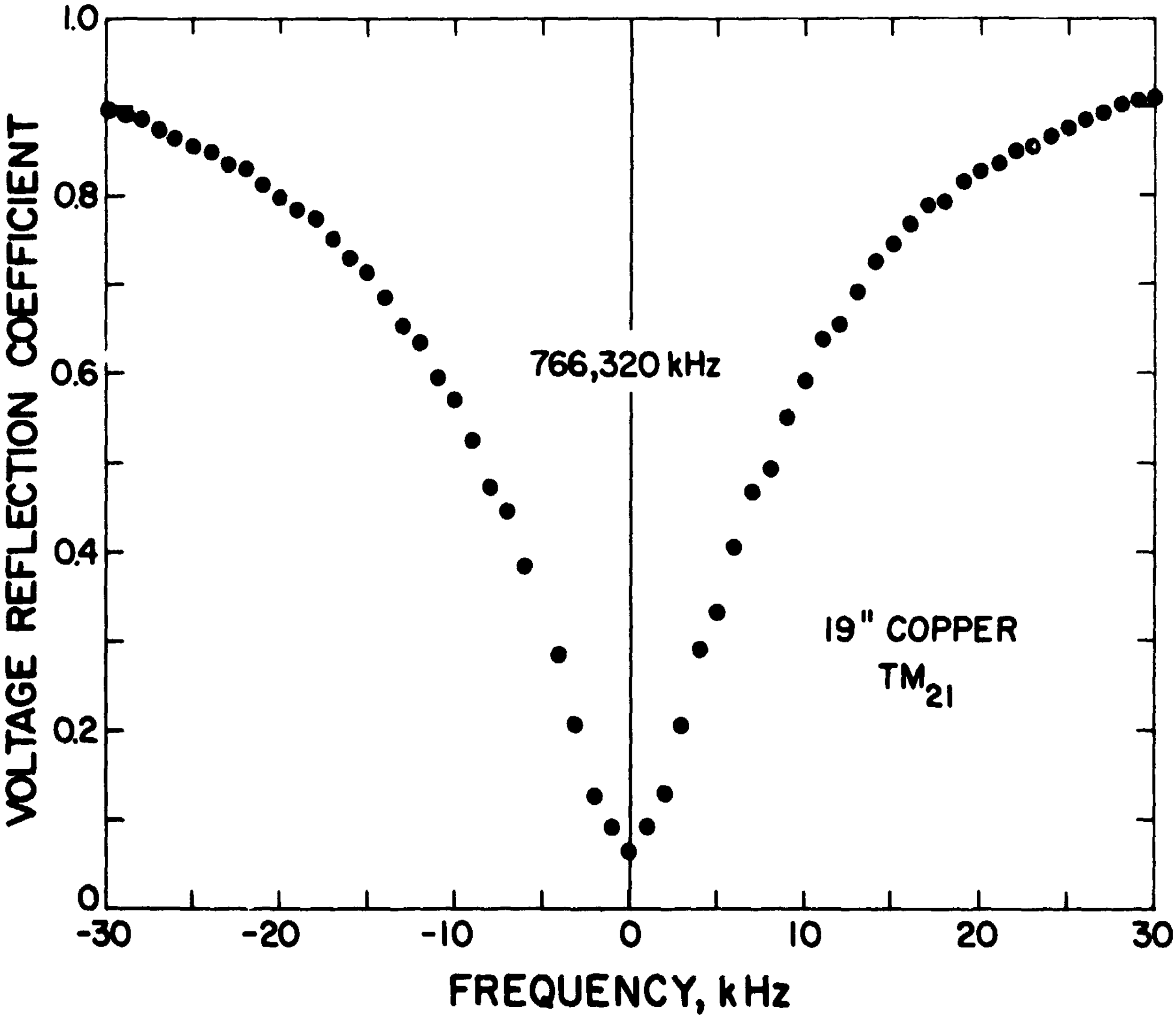

Figure C2. Frequency response of the copper spherical vessel for the TM_{021} mode.

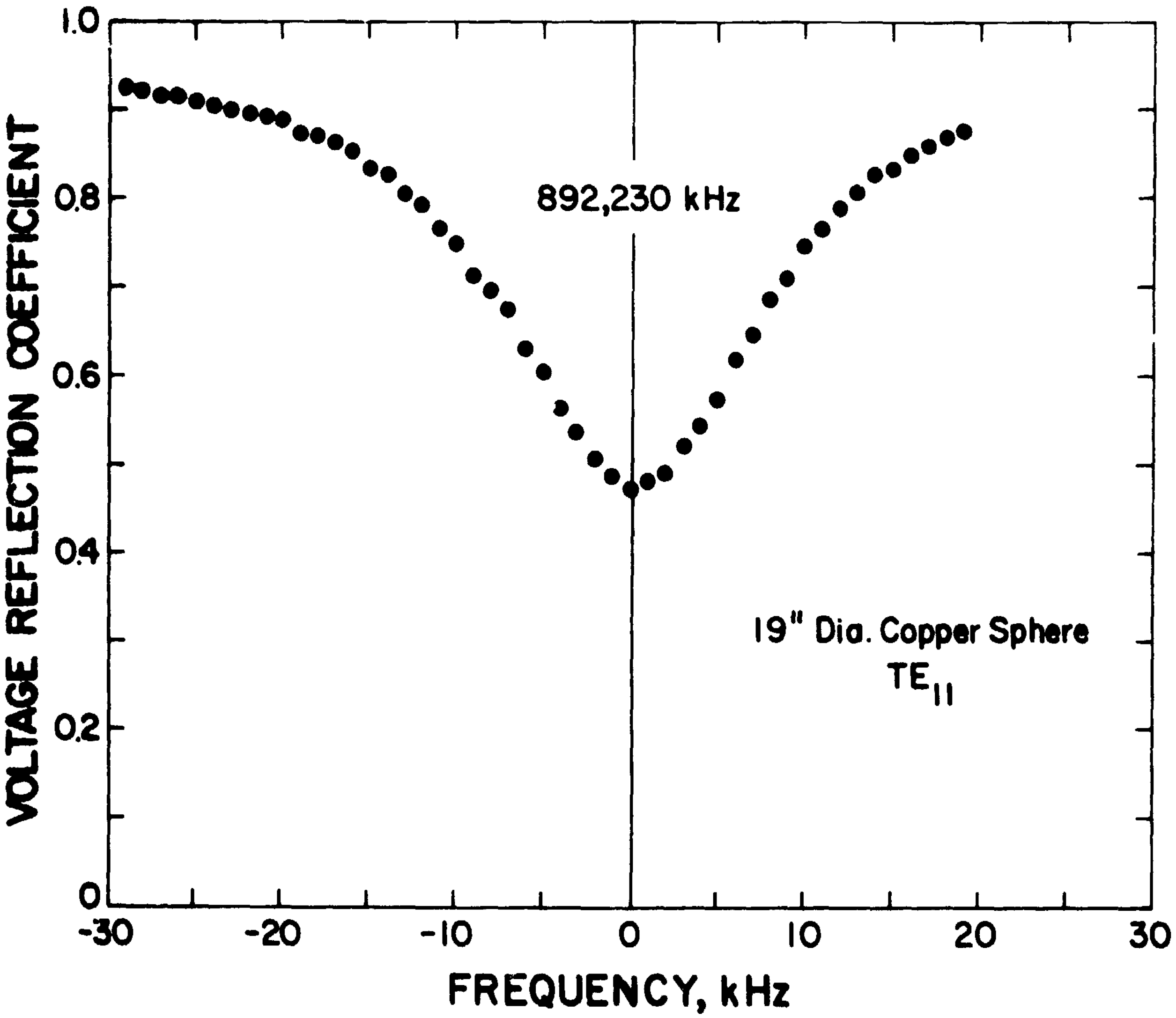

Figure C3. Frequency response of the copper spherical vessel for the TE_{11} mode.

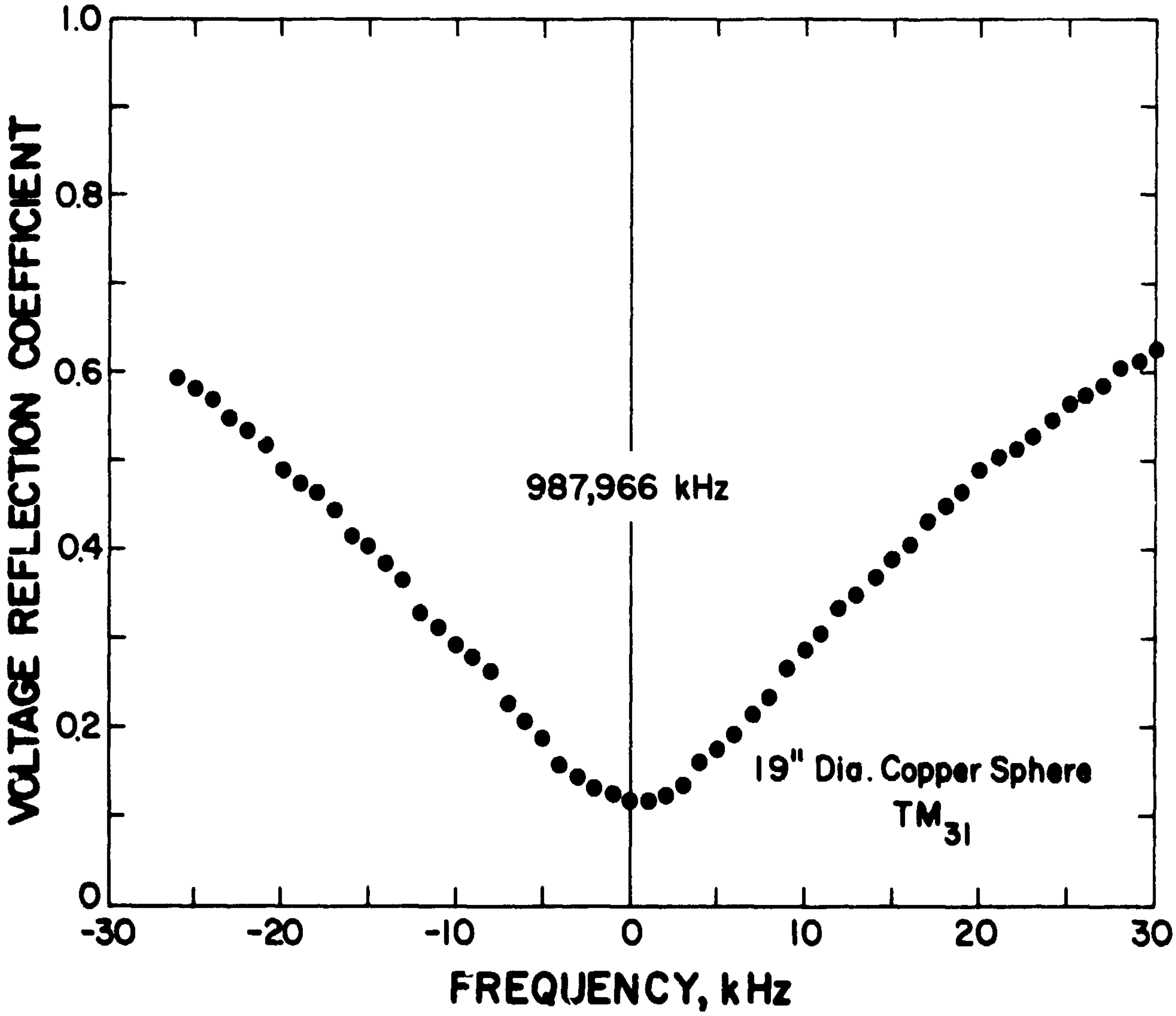

Figure C4. Frequency response of the copper spherical vessel for the TM_{031} mode.

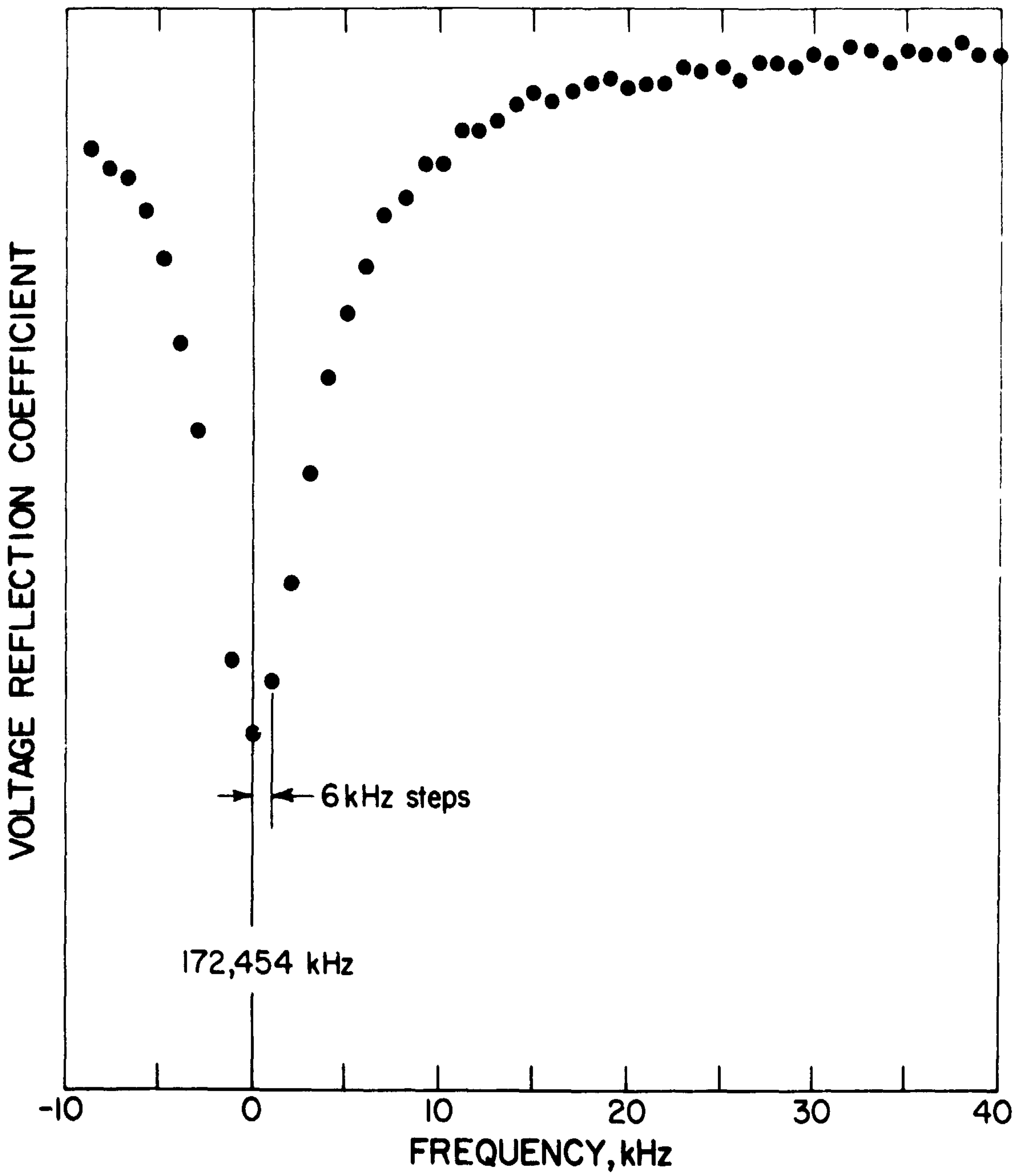

Figure C5. Frequency response of the 60 inch diameter stainless steel sphere - TM_{011} mode.

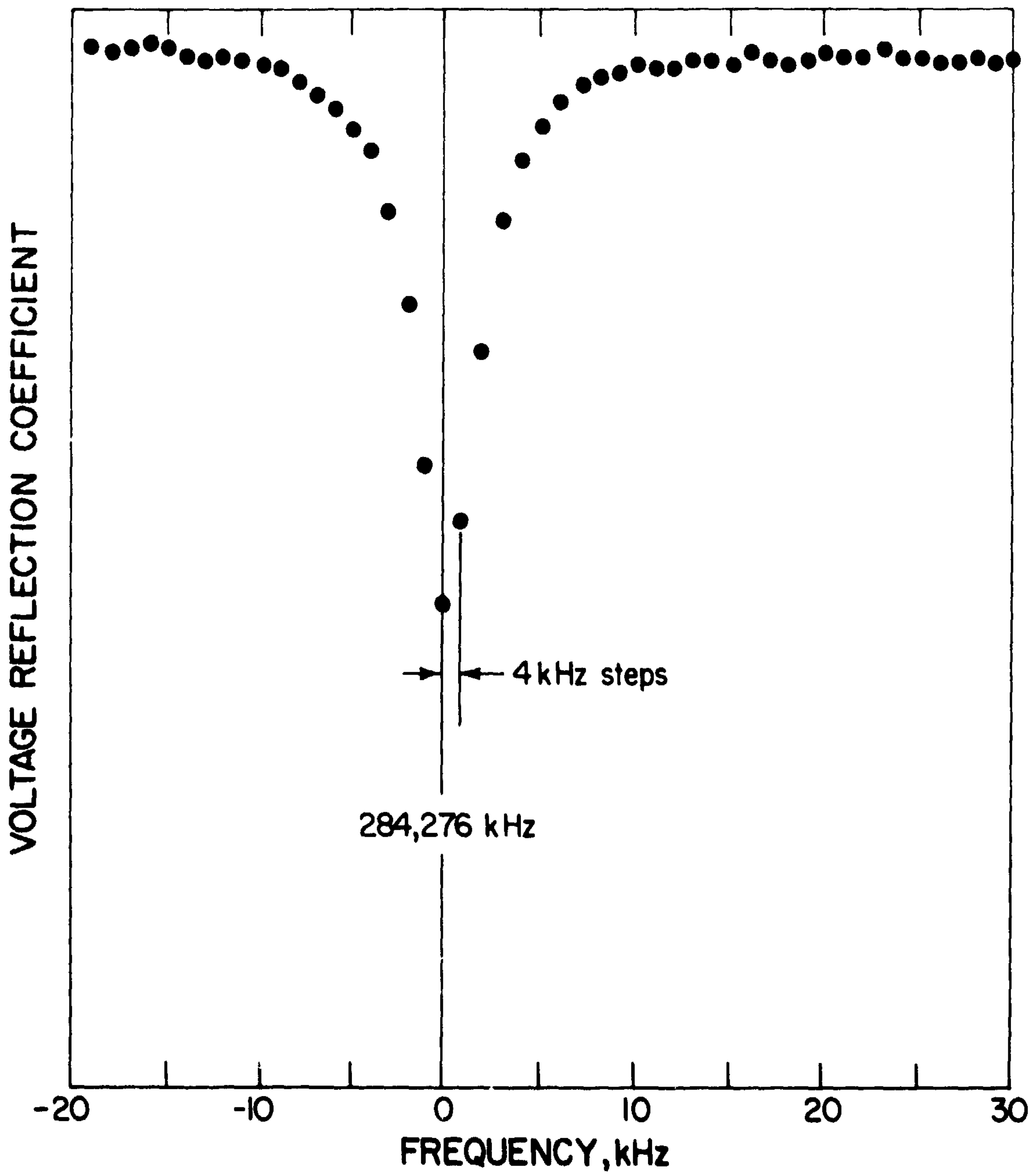

Figure C6. Frequency response of the 60 inch diameter stainless steel sphere - TE_{011} mode.

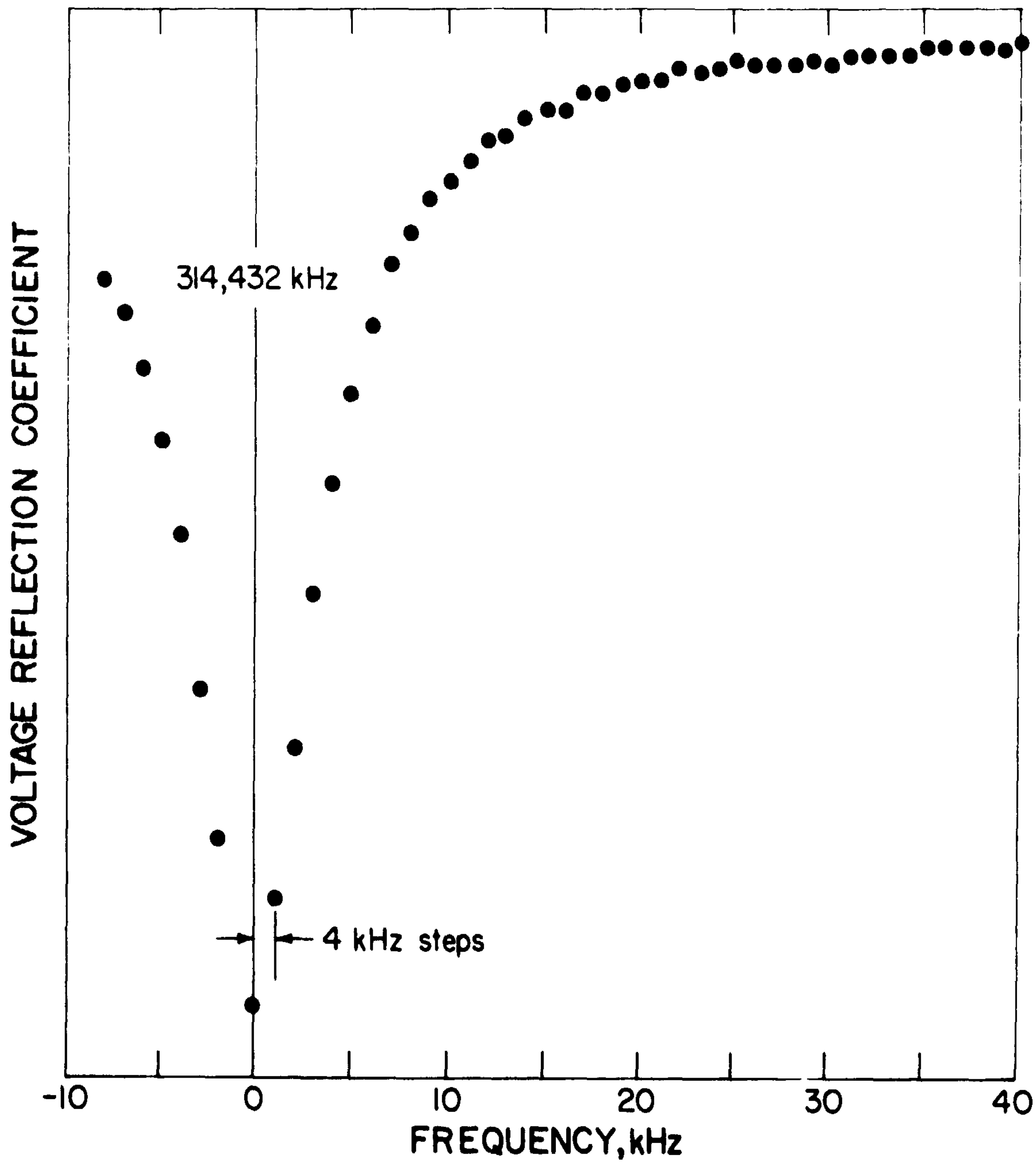

Figure C7. Frequency response of the 60 inch diameter stainless steel sphere - TM_{031} mode.

APPENDIX D

DATA REDUCTION FROM THE MAGNETIC TAPE UNIT

The magnetic tape unit stores the information coming from the data acquisition system described in Appendix B. Each data run lasts about ten seconds; during this time the system records about 25 independent measurements for each mode or about 375 data points in all (counting 3 antennas and 5 modes for each antenna). The data reduction processes the raw tape, finds the average and standard deviation of the 25 data points for each mode and punches these numbers on to standard data cards along with other identification codes. Data from other sources are also punched on these cards i. e., mass, pressure and temperatures. The cards are then ready for plotting routines, and other types of data analysis.

I. Program DMPMODES

Since the tape recorder in the laboratory is a continuous write recorder and not a sequential recorder, the letter D is hard-wired to the output whenever there is no data being recorded. Most of the tape is, in fact, dummy data. DMPMODES accomplishes many functions. It takes the data from the magnetic tape made in the laboratory, deletes all D's and other non-essential characters, sorts the 12 character data by antenna, lists this data and writes this data on a second magnetic tape.

Essentially, the program works as follows. A tape record is read into array M. A pointer, KNT, moves down the array. If the word in M(KNT) is all D's, KNT is incremented. When a word that is not all D's comes along, the character: (or 15 octal) is searched for. When a: is found, it and the characters surrounding it are placed into the first two locations of the array IW. Thinking of these two 8 byte words as one 16 byte word, it should look like $d_1d_2r_1r_2a{:}t_1t_2t_3t_4t_5t_6$

DDDD, where all subscripted letters are integers, and D's are dummy data. d_1d_2 is the data code selected from the recorder front panel. r_1r_2 is the run code, also selected from the front panel. a_1 is the antenna code. t_1-t_6 are the data. If this 16 byte "word" is not correct, that is, if an alpha character appears where an integer is supposed to be, the data point is rejected and the program starts searching for the next data point. If the data point appears to be all right, it is decoded, and the data is printed under the appropriate antenna column. Also, the 16 byte "word" is written on a second magnetic tape, thus saving later programs from having to re-sort the mass of characters on the input tape.

II. Program AVMODES

Basically, this program takes data from the second magnetic tape, sorts it by antenna and mode, finds the average time and standard deviation for each mode for each antenna, lists these averages and standard deviations, and punches on standard data cards the averages and standard deviations, along with the date, date code, run code, antenna number, mode number, and the number of points used to calculate the average and standard deviation. The input magentic tape is essentially a sequence of the magnetic tapes written by DMPMODES. The tape has all the data from all the days of running the experiment. Each day is separated from the others by an end of file marker, and each run is separated from other runs by an inter-record gap. The first record of each file contains the date of the run.

The program works as follows. The first record is read into the first 10 words of array M. The date of the run is extracted from these ten words and stored into the variable IDATE. Each of the other records in the file are read into the array M, one at a time. Every two words of the array M are the same as in the 16 byte "word" described above in the discussion of DMPMODES. This 16 byte word is decoded, or broken up, into the date code, IDC; the run code, IRC; the antenna code, IA; the colon character, ICOL; and the time data, ITIME. The time is checked to see which mode, if any, it belongs to. The point is then used to calculate the average and standard deviation of that particular mode of that particular antenna. Note that for each record on the tape, or run, there is a possible total of 15 of these averages and standard deviations to be printed and punched (corresponding to three antennas with five modes each). The punch card output is used for graph routines and other data analysis programs.

III. The following pages give a listing of these programs which are being used on the CDC 3800 computer.

```
      PROGRAM DMPMODES
      DIMENSION MSG(3),IW(8),IHZ(3),IHZSQ(3),T(3),TSQ(3),K(3),IOA(5000)
      COMMON M(32765)
    1 FORMAT(I5)
    2 FORMAT(*1RECORD *,I5,* LONGER THAN 32764, SOME LOST.*)
    3 FORMAT(8R1)
    4 FORMAT(2I2,I1,R1,I6,4X)
    5 FORMAT(*1*,57X,*TAPE RECORD NUMBER *,I3,3A8/*8*
     151X,*DATE CODE9   *,I2,5X,*RUN CODE9   *,I2/
     255X,*ANTENNA IDENTIFICATION CODE*/33X,*0*,32X,*1*,32X,*2*/)
    6 FORMAT(31X,I6)
    7 FORMAT(64X,I6)
    8 FORMAT(97X,I6)
    9 FORMAT(*0AVG*,27X,F9.2,2(23X,F9.2)/* SIGMA*,23X,E12.6,2(21X,E12.6)
     1/1X,I4,* SCANS DELETED IN THIS RECORD.*)
      NRUNO=999
      CALL Q9OVER
      CALL IOHCHECK
      NREC=0
      READ 1,NSKIP
      IF(EOF,60)10,103
  103 DO 105 I=1,NSKIP
      BUFFERIN(1,0)(M,M)
  104 IF(UNIT,1)104,105
  105 CONTINUE
   10 BUFFERIN(1,0)(M,M(32765))
      IF(NREC.EQ.0.OR.KOA.EQ.1)GO TO 115
      BUFFEROUT(2,1)(IOA,IOA(KOA-1))
  115 KOA=1
      MSG(1)=MSG(2)=MSG(3)=8H
      KNT=0
      IHZ(1)=IHZ(2)=IHZ(3)=0
      K(1)=K(2)=K(3)=0
      IHZSQ(1)=IHZSQ(2)=IHZSQ(3)=0
      NREC=NREC+1
      IDROP=-1
      LINE=75
      KCODE=0
  117 IF(UNIT,2)117,11
   11 IF(UNIT,1)11,15,99,13
   13 MSG(1)=8H CONTAIN
      MSG(2)=8HS PARITY
      MSG(3)=8H ERRORS
   15 L=LENGTHF(1)
      IF(L.GT.4)GO TO 195
      NREC=NREC-1
      GO TO 10
  195 IF(L.LT.32764)GO TO 198
      PRINT 2,NREC
  198 IDROP=IDROP+1
  205 KNT=KNT+1
```

```
      IF(KCODE.EQ.1)KNT=KNT+1
      KCODE=0
   20 IF(KNT.GT.L-2)23,24
   23 DO 242 I=1,3
      FI=K(I)
      T(I)=IHZ(I)
      T(I)=T(I)/FI
      IF(K(I).GT.1)GO TO 241
      TSQ(I)=0.
      GO TO 242
  241 TSQ(I)=IHZSQ(I)
      TSQ(I)=SQRT(ABS((FI*TSQ(I)-T(I)**2)/FI/(FI-1.)))
  242 CONTINUE
      PRINT 9,(T(I),I=1,3),(TSQ(I),I=1,3),IDROP
      GO TO 10
   24 IF(M(KNT).EQ.8HDDDDDDDD)GO TO 27
      DECODE(8,3,M(KNT))IW
   25 DO 26 I=1,8
      IF(IW(I).NE.15B)GO TO 26
      NSH=I-6
      IF(NSH)29,37,30
   26 CONTINUE
   27 KNT=KNT+1
      GO TO 20
   29 KNT=KNT-1
      NSH=NSH+8
      KCODE=1
   30 MSK1=2**(6*NSH)
      MMN1=MSK1-1
      MSK2=2**((8-NSH)*6)
      MMN2=MSK2-1
      DO 35 I=1,2
      IW(I)=M(KNT+I-1).AND.MMN2
      IW(I)=IW(I)*MSK1
      IC=M(KNT+I)/MSK2
   35 IW(I)=IW(I).OR.(IC.AND.MMN1)
      GO TO 40
   37 IW(1)=M(KNT)
      IW(2)=M(KNT+1)
   40 ITEST=IW(2).AND.7700000000B
      IF(ITEST.EQ.8H00D00000)GO TO 198
      ITEST=IW(1).AND.770000000000000B
      IF(ITEST.EQ.8HD0000000)IW(1)=IW(1).AND.77777777777777B
      DECODE(16,4,IW)ID,NRUN,NANT,IC,IDATA
      IF(IOHERR(0))198,43
```

```
43 IF(IC.NE.15B)GO TO 198
   IOA(KOA)=IW(1)
   IOA(KOA+1)=IW(2)
   KOA=KOA+2
   LINE=LINE+1
   IF(NRUN.EQ.NRUNO.AND.LINE.LE.67)GO TO 53
   PRINT 5,NREC,(MSG(I),I=1,3),ID,NRUN
   LINE=1
53 NANT=NANT+1
   K(NANT)=K(NANT)+1
   IHZ(NANT)=IHZ(NANT)+IDATA
   IHZSQ(NANT)=IHZSQ(NANT)+IDATA*IDATA
   NRUNO=NRUN
   GO TO (55,56,57)NANT
55 PRINT 6,IDATA
   GO TO 205
56 PRINT 7,IDATA
   GO TO 205
57 PRINT 8,IDATA
   GO TO 205
99 STOP
   END
```

```
      PROGRAM AVMODES
      DIMENSION M(5000),TIME(5,3),TIMESQ(5,3),KNT(5,3),MODE(5,2)
      DATA(((MODE(I,J),I=1,5),J=1,2)=1100,2900,4200,5100,6500,1655,3900,
     15100,6060,7800)
      CALL IOHCHECK
      NF=0
      READ 1,NFSKIP
    1 FORMAT(I5)
      IF(EOF,60)10,102
  102 DO 105 I=1,NFSKIP
  105 CALL SKIPFILE(1)
   10 BUFFERIN(1,1)(M,M(10))
      NREC=0
      NF=NF+1
   11 IF(UNIT,1)11,15,99,13
   13 PRINT 2,NREC,NF
    2 FORMAT(*0PARITY ERROR IN RECORD *,I3,* OF FILE *,I3)
   15 IDATE=M(1).AND.7777777777B
      IDATE=IDATE*1000000B
      M(2)=M(2)/10000000000B
      IDATE=IDATE.OR.(M(2).AND.777777B)
      PRINT 6
    6 FORMAT(1H1/)
   16 DO 17 J=1,3
      DO 17 I=1,5
      KNT(I,J)=0
      TIME(I,J)=0.
   17 TIMESQ(I,J)=0.
      BUFFERIN(1,1)(M,M(5000))
      NREC=NREC+1
   21 IF(UNIT,1)21,25,10,23
   23 PRINT 2,NREC,NF
   25 L=LENGTHF(1)
      DO 40 J=1,L,2
    3 FORMAT(2I2,I1,R1,I6,4X)
      DECODE(16,3,M(J))IDC,IRC,IA,ICOL,ITIME
      IF(IOHERR(0))40,26
   26 IF(ICOL.NE.15B)GO TO 40
      IF(IA.LT.0.OR.IA.GT.2)GO TO 40
      IAC=IA+1
      DO 30 I=1,5
      IF(ITIME.GT.MODE(I,2))GO TO 30
      IF(ITIME.GE.MODE(I,1))GO TO 32
      GO TO 40
   30 CONTINUE
      GO TO 40
   32 KNT(I,IAC)=KNT(I,IAC)+1
      PN=ITIME
      PN=PN/100.
      TIME(I,IAC)=TIME(I,IAC)+PN
      TIMESQ(I,IAC)=TIMESQ(I,IAC)+PN**2
   40 CONTINUE
   50 DO 55 J=1,3
      IA=J-1
```

```
      DO 55 I=1,5
      PN=KNT(I,J)
      IF(KNT(I,J).EQ.0)GO TO 55
      IF(KNT(I,J).GT.1)GO TO 52
      TIMESQ(I,J)=0.
      GO TO 53
   52 TIMESQ(I,J)=SQRT(ABS(PN*TIMESQ(I,J)-TIME(I,J)**2)/(PN*(PN-1.)))
   53 TIME(I,J)=TIME(I,J)/PN
      PUNCH 4,IDATE,IDC,IRC,IA,I,TIME(I,J),TIMESQ(I,J),KNT(I,J)
    4 FORMAT(A8,2I3,2I2,F7.3,E12.4,I5)
      PRINT 5,IDATE,IDC,IRC,IA,I,TIME(I,J),TIMESQ(I,J),KNT(I,J)
    5 FORMAT(1X,A8,2I3,2I2,F7.3,E12.4,I5)
   55 CONTINUE
      GO TO 16
   99 STOP
      END
```

APPENDIX E

UNIFORM DENSITY HYDROGEN DATA ANALYSIS AND ACCURACY STATEMENTS

The data analysis for uniform density hydrogen is based on 41 observations at tank pressures above 400 psi; the temperatures at the top of the tank were slightly lower than the bottom temperatures (the heater was at the bottom) indicating almost uniform temperature with a condition for convective mixing due to gravity; experimentally, these conditions were necessary to achieve a near uniform density within the experimental vessel.

The data for the TM_{011} mode, as plotted in Figure 6 of the main text, is expected to follow equation (6), i.e.,

$$M = \frac{V}{A}\left(\frac{f_{01}^2 - f_1^2}{f_{01}^2 + 2f_1^2}\right) \qquad \text{(E-1)}$$

Using equation (2), the expression for f_1 in the time domain

$$f_1 = f_0 + r(t_1 - t_0) \qquad \text{(E-2)}$$

it follows after a little algebra

$$t_1 - t_0 = \frac{f_{01}}{r}\sqrt{\frac{1 - \frac{AM}{V}}{1 + \frac{2AM}{V}}} - \frac{f_0}{r} \qquad \text{(E-3)}$$

or equivalently

$$\Delta t_1 = \Delta t_0 + \frac{f_{01}}{r}\left(\sqrt{\frac{1 - \frac{AM}{V}}{1 + \frac{2AM}{V}}} - 1\right) \tag{E-4}$$

where

$$\begin{aligned} \Delta t_1 &= t_1 - t_0 \\ \Delta t_0 &= \frac{f_{01} - f_0}{r} \end{aligned} \tag{E-5}$$

(Δt_0 is just the time interval at $M = 0$). The gauging function is then between Δt_1 and M; these quantities being related to three independent parameters Δt_0, $\frac{f_{01}}{r}$, $\frac{A}{V}$ through equation (E-4). These three parameters may be determined by fitting the data to (E-4) or, alternately, may be determined by separate physical measurement. For example, the sweep rate, r, can be determined from Δt_0, f_0 and f_{01} by

$$r = \frac{f_{01} - f_0}{\Delta t_0} \tag{E-6}$$

The measured values of these quantities were $f_{01} = 581.9$ MHz, $f_0 = 411$ MHz and $\Delta t_0 = 16.20$ milliseconds giving $r = 10.54$ MHz/msec. V can be calculated from the inside radius of the tank $R = 8.906$ inches (22.62 cm) giving $V = 4.85 \times 10^4\ cm^3$. A can be obtained from other experimental data; ref. 4 of the main text gives $A = 1.006\ cm^3/gm$. Table E-I gives the comparison between these values and the values obtained by a nonlinear least squares fit of the data to equation (E-4).*

* C. Daniel, F. S. Wood. Fitting Equations to Data, Wiley Interscience, N. Y. (1971) p. 320.

TABLE E-I

	Δt_0	$\frac{f_{01}}{r}$	$\frac{A}{V}$
Measured value	16.20 msec	55.15 msec	$9.42 \times 10^{-3} lb^{-1}$
Fitted value	16.19	52.88	9.44×10^{-3}
95% confidence limit (lower)	16.20	39.20	6.81×10^{-3}
95% confidence limit (upper)	16.20	66.50	12.21×10^{-3}

Although the confidence limits for the fitted values are relatively large, the actual fitted values are quite consistent with the independently determined values.

The semi-empirical gauge equation may then be given by

$$\Delta t_1 = 16.19 + 52.88 \left(\sqrt{\frac{1 - 9.44 \times 10^{-3} M}{1 + 2 \times 9.44 \times 10^{-3} M}} - 1 \right) \quad \text{(E-7)}$$

where Δt_1 is measured in milliseconds and M in pounds; it remains to determine the accuracy of the data with respect to this equation.

Table E-II gives the observed value of Δt_1 and the value of Δt_1 calculated from (E-7) for each of the observed mass values. The residuals are plotted in Figure E-1 as the Percent Full Scale Residual

TABLE E-II

Mass (lbs)	Δt_1(OBS)	Δt_1(CALC)	Residual	% Full Scale Residual
0.00	16.200	16.186	0.014	0.28%
0.20	16.018	16.037	-0.019	-0.38
0.44	15.839	15.859	-0.020	-0.41
0.52	15.820	15.799	0.021	0.43
0.73	15.631	15.644	-0.013	-0.26
0.84	15.550	15.564	-0.014	-0.29
0.94	15.460	15.483	-0.023	-0.47
1.00	15.500	15.446	0.054	1.10
1.15	15.340	15.337	0.003	0.06
1.15	15.329	15.337	-0.008	-0.16
1.16	15.326	15.330	-0.004	-0.08
1.42	15.163	15.141	0.022	0.45
1.42	15.160	15.141	0.019	0.38
1.54	15.034	15.054	-0.020	-0.41
1.54	15.029	15.054	-0.025	-0.51
1.56	15.029	15.039	-0.010	-0.20
1.57	15.019	15.032	-0.013	-0.26
1.58	15.030	15.025	0.005	0.10
1.81	14.842	14.859	-0.017	-0.35
2.06	14.674	14.687	-0.013	-0.26
1.85	14.841	14.831	0.010	0.20
2.11	14.670	14.645	0.025	0.51
2.43	14.415	14.417	-0.002	-0.04
2.45	14.413	14.403	0.010	0.20
2.82	14.180	14.142	0.038	0.78
3.33	13.820	13.786	0.034	0.69
3.70	13.557	13.530	0.027	0.55
4.23	13.141	13.167	-0.026	-0.53
4.25	13.136	13.154	-0.018	-0.38
4.71	12.815	12.856	-0.041	-0.83
5.19	12.501	12.520	-0.019	-0.39
5.20	12.518	12.514	0.004	0.08
5.62	12.221	12.235	-0.014	-0.28
5.63	12.222	12.228	-0.006	-0.12
5.68	12.212	12.195	0.017	0.35
6.43	11.679	11.703	-0.024	-0.49
6.44	11.686	11.697	-0.011	-0.22
6.51	11.680	11.651	0.029	0.59
6.77	11.480	11.483	-0.003	-0.06
6.79	11.480	11.470	0.010	0.20
7.08	11.304	11.283	0.021	0.43

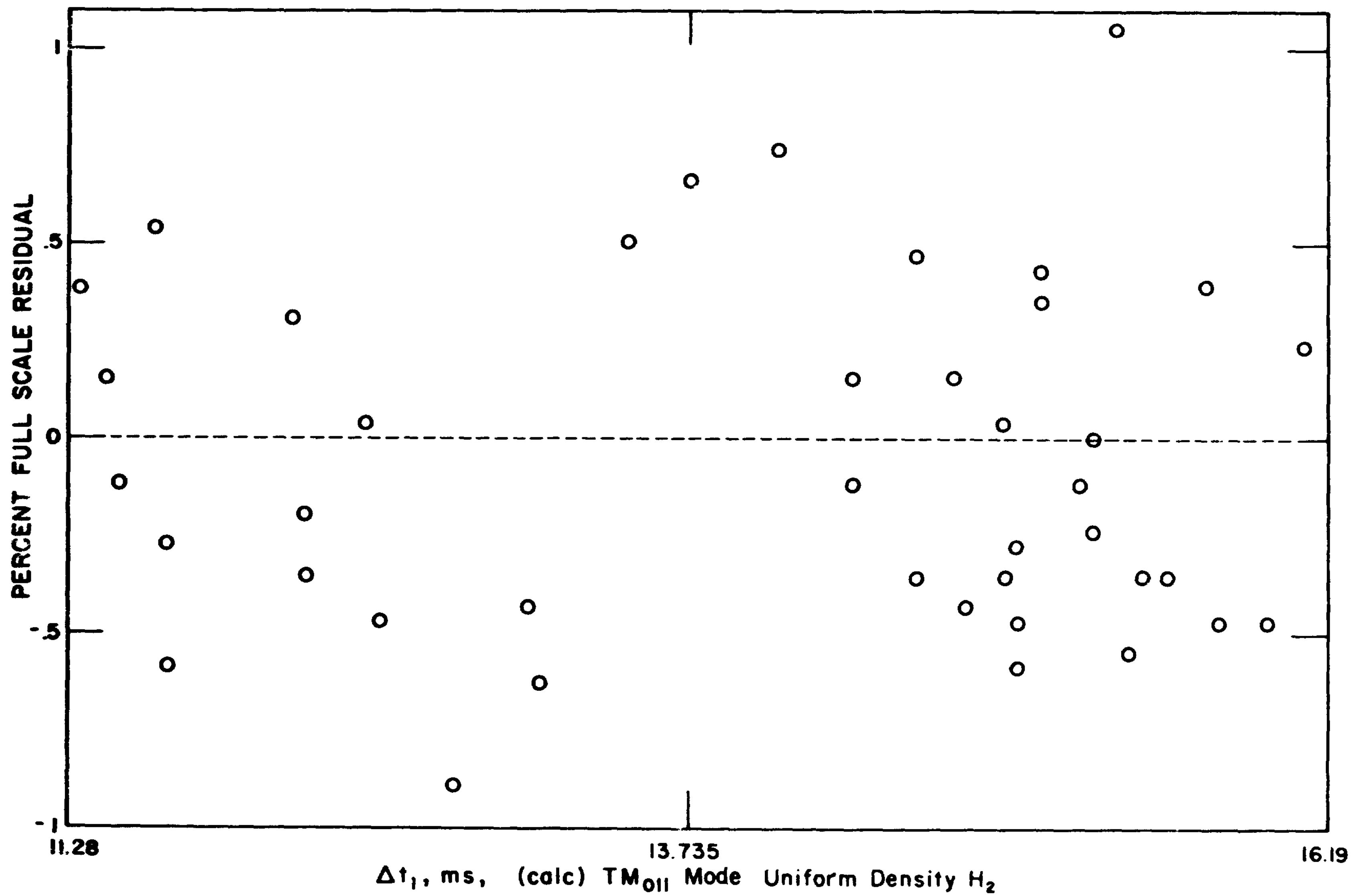

Figure E1. Residuals vs Δt_1

vs. Δt_1(calc); this graph shows a fairly random scatter of the data between -0.83% and 1.10% full scale.

The cumulative distribution of the residuals is plotted in Figure E-2 vs. the expected intervals in a normal distribution. The S-shaped trend of the data indicates that the frequency distribution is slightly flatter than the normal bell-shaped error function. This is probably due to the fact that the Δt_1 are really only measured to four significant figures, the most significant digit corresponding to 0.2%; this would cause a broadening of the frequency distribution on the order of $\pm$ 0.2%. The slope of the straight line through the tails of the curve gives an estimate of the standard deviation σ = 0.4%.* This gives a 3σ deviation (the 99.9% confidence interval) of 1.20%.

Operational Readout

As indicated in the main text, a quadratic fit will be easier to work with operationally and should give a sufficiently accurate gauging function. The quadratic equation

$$\Delta t_1 = 16.20 + AM + BM^2 \qquad \text{(E-8)}$$

was fitted to the data in Table II by solving (E-8) simultaneously for M = 6.77, Δt_1 = 11.48 and M = 2.43, Δt_1 = 14.415. The result is A = -0.7554 and B = 8.61×10^{-3}. The residuals for this fit range between -0.63 and 0.93 percent full scale, a slightly better fit than the theoretical curve. This analysis is tabulated in Table III.

* Chernov, H. and Lieberman, G. S., J. Amer. Statist. Assn. 49, 778-85 (1954).

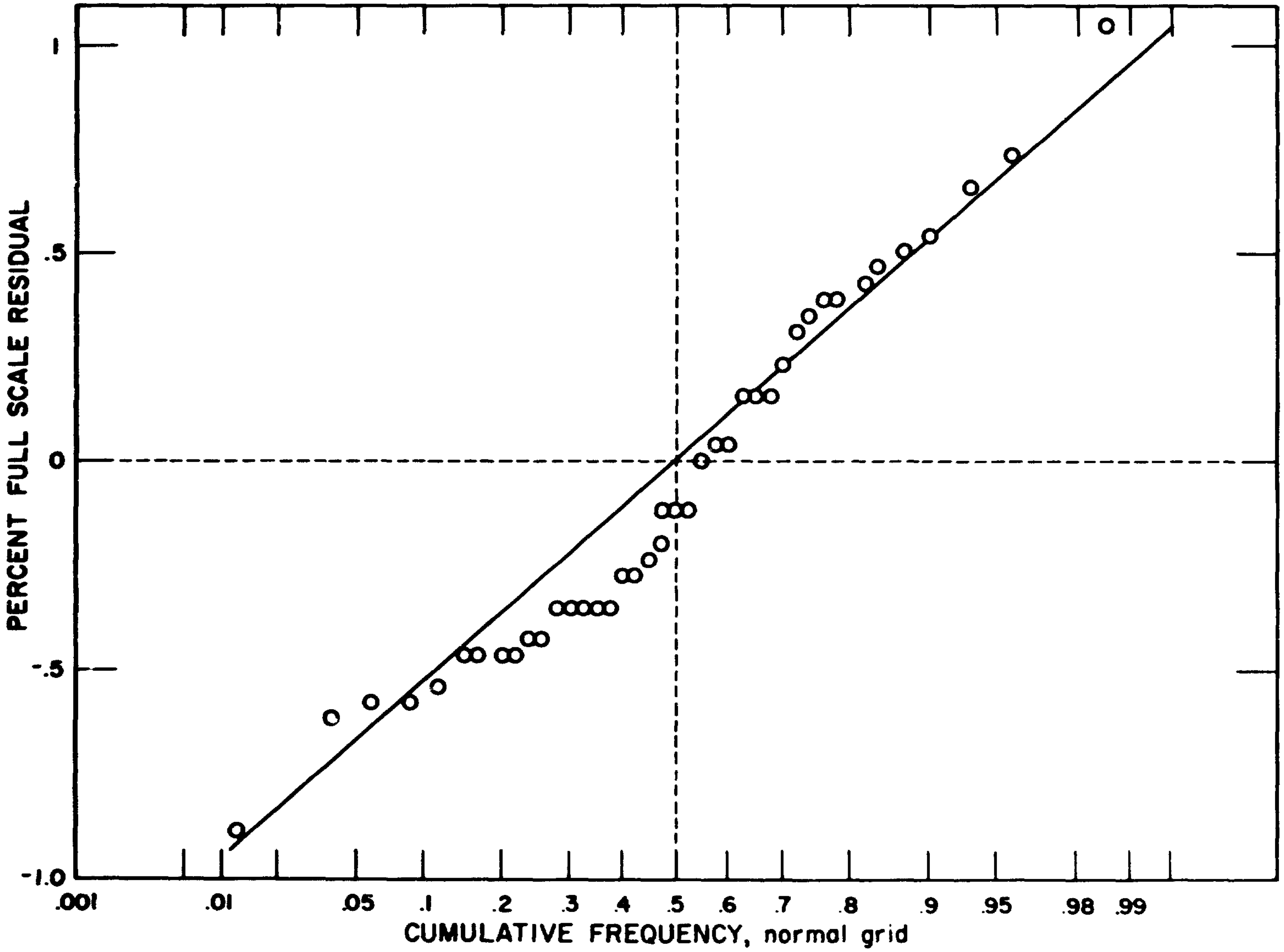

Figure E2. Cumulative Distribution of Residuals

TABLE E-III

Mass (lbs)	Δt_1(OBS)	Δt_1(CALC)	% Full Scale Residual
0.00	16.20	16.2	0.00%
0.2	16.018	16.049	0.63
0.44	15.839	15.869	0.62
0.52	15.82	15.809	0.21
0.73	15.631	15.653	-0.45
0.84	15.55	15.571	-0.44
0.94	15.46	15.497	-0.77
1.00	15.50	15.453	0.93
1.15	15.340	15.342	-0.05
1.15	15.329	15.342	-0.30
1.16	15.326	15.335	-0.19
1.42	15.163	15.144	0.37
1.42	15.160	15.144	0.31
1.54	15.034	15.057	-0.47
1.54	15.029	15.057	-0.57
1.56	15.029	15.042	-0.28
1.57	15.019	15.035	-0.33
1.58	15.03	15.027	0.04
1.82	14.842	14.853	-0.24
2.06	14.674	14.680	-0.13
2.11	14.67	14.644	0.52
2.43	14.415	14.415	0.01
2.45	14.413	14.400	0.25
2.82	14.180	14.138	0.85
3.33	13.820	13.780	0.82
3.7	13.557	13.522	0.70
4.23	13.141	13.158	-0.36
4.25	13.136	13.145	-0.19
5.19	12.501	12.511	-0.21
4.71	12.815	12.833	-0.37
5.2	12.518	12.504	0.27
5.62	12.221	12.226	-0.12
5.63	12.222	12.220	0.04
5.68	12.212	12.187	0.51
6.43	11.679	11.698	-0.40
6.44	11.688	11.692	-0.09
6.51	11.68	11.647	0.67
6.77	11.480	11.480	-0.01
6.79	11.480	11.467	0.25
7.08	11.304	11.283	0.42

APPENDIX F

TOTAL MASS GAUGING IN A SPHERICAL RESONANT CAVITY

Introduction

When a closed metal container is excited by an RF antenna probe inserted through a hole in the container, theoretically there are an infinite number of excitation frequencies for which the container is strongly coupled to the antenna; this means that energy can flow more freely between the antenna and the container at these resonant frequencies. The resonant frequencies correspond to standing wave patterns in the cavity which are called resonant modes. The wave pattern of the mode which occurs at the lowest possible resonant frequency is called the fundamental mode. This mode and the modes of the next few higher frequencies are called lower order modes.

When the cavity is uniformly filled with a fluid, the resonant frequency changes because the velocity of propagation of the resonant standing wave, $c = 1/\sqrt{\mu\epsilon}$, depends on the dielectric constant, ϵ, and the magnetic permeability, μ, of the fluid. For example, in a spherical resonant cavity uniformly filled, the resonant frequencies, f_{np}, are given by

$$f_{np} = \frac{u_{np}}{2\pi b\sqrt{\mu\epsilon}} \qquad \text{(F-1)}$$

where b is the radius of the sphere, and n and p are subscripts which label the different modes (these will be explained in detail). The u_{np} are eigenvalues of the modes and are obtained in the process of finding solutions to Maxwells equations. The resonant frequencies can then be related to total mass by using the Clausius-Mossotti relation

$$P\rho = \frac{\epsilon - 1}{\epsilon + 2} \qquad \text{(F-2)}$$

where P is the polarizability of the fluid which is a slowly varying function of the fluid density, ρ.

If the cavity is uniformly filled with a liquid the eigenvalues, u_{np}, are just numbers independent of the fluid within the cavity and there is therefore a simple relationship between resonant frequency and total mass. However, if the container is only partially filled with liquid, the rest of the cavity being a vacuum or a gas, then the values of u_{np} will depend on μ and ϵ of the liquid, the μ_o and ϵ_o of the gas, and the geometry which the liquid takes within the cavity; the resonant frequency, then, is no longer an unambiguous function of mass but depends on the liquid geometry as well. This is because the standing wave patterns are distorted because of the boundary conditions at the liquid-gas interface. However, the resonant frequency of each partially filled mode does lie between the completely empty and completely full values

$$\frac{u_{np}}{2\pi b\sqrt{\mu\epsilon}} < f_{np} < \frac{u_{np}}{2\pi b\sqrt{\mu_o \epsilon_o}}, \qquad \text{(F-3)}$$

and varies continuously between these values as the cavity is filled. This suggests that the resonant frequency at least approximately indicates total mass independent of geometry.

The purpose of this note is to investigate the geometry effects for a spherical cavity with spherical symmetry of the liquid gas interface. This geometry is similar to a "zero-g" formation with the liquid clinging to the walls and a gas bubble in the middle of the cavity. The reason for choosing this geometry is that it is one of the few examples of a partially filled cavity for which the Maxwell Equations can be solved in closed form. Even though this gometry is particularly simple, it does give a reasonable indication of the uncertainty which may be involved when the geometry is not known. Numerical examples are calculated for cases in which the liquid is hydrogen or nitrogen.

From a practical point of view, the spherical cavity is an ideal container geometry for this method of mass gauging. The reason for this is that the spherical symmetry of the cavity wall creates a degeneracy in the modes. That is, there are a number of standing wave patterns which have the same resonant frequency. This results in the fact that the distinct resonant frequencies of the lower order modes are widely separated and minimizes the effect of mode crossing in a partially filled cavity. Mode crossing occurs when, for a particular liquid geometry, the resonant frequency of a higher mode falls below that of a lower mode. For example, if the liquid is nitrogen, mode crossing between the first two modes is impossible and for the next few higher modes is quite unlikely; this is established from the table of eigenvalues, Table 1 on page F-12 and the inequalities expressed in (F-3).

The relative independence of the lower order modes suggests that they can each be monitored independently. Since each mode has its own geometry in the standing wave pattern, it seems reasonable that the modes themselves may be used to at least partially determine the fluid geometry. (Mathematically the problem reduces to this: Given some of the eigenvalues of a boundary value problem, how closely can the eigenfunctions be approximated.) In fact, it will be shown that for the spherical symmetry considered in this analysis, that for a liquid of unknown density, both the location of the liquid-gas interface and the density (hence the total mass) can be determined uniquely if and only if five modes are monitored simultaneously. The reason for this is that each mode determines exactly one independent relation between the resonant frequency of that mode and the five unknown parameters ϵ, μ, ϵ_o, μ_o, and a, where r = a is the liquid-gas interface. For most applications it is sufficient to assume that $\epsilon_o \approx \mu_o \approx \mu \approx 1$, leaving only two unknowns, namely ϵ and a. In this case, two modes will uniquely determine the total mass.

Solutions for Maxwells Equations in Spherical Coordinates

When the cavity is resonating at an angular frequency, ω, the time phase of the electromagnetic field is the same at all points within the cavity. Hence, for a loss free cavity the electric and magnetic fields can be written as the real parts of $Ee^{i\omega t}$ and $He^{i\omega t}$, respectively, where E and H are vectors which depend only on the spacial coordinates. The source free Maxwell Equations can then be written

$$
\begin{aligned}
\text{curl } E &= -i\omega\mu H \\
\text{curl } H &= i\omega\epsilon E \\
\text{div } \epsilon E &= 0 \\
\text{div } \mu H &= 0.
\end{aligned}
\qquad (F\text{-}4)
$$

It should be emphasized at this point that only two assumptions have been made, the cavity is loss free and it is source free; in practice these are usually very good assumptions for calculating resonant frequencies. A third assumption which we will now make, may have to be justified more carefully in any given situation: we assume that there are two regions within the cavity, each of which have uniform density. The technical advantage of this assumption is that derivatives of μ and ϵ are not involved; the equation (F-4) can be solved in each region where μ and ϵ are constant and the boundary conditions are then modified to include the liquid-gas interface. The boundary conditions can be written

$$\left\{\epsilon E \cdot n,\ \mu H \cdot n,\ Exn \text{ and } Hxn \text{ continuous at each boundary point}\right\} \qquad (F\text{-}5)$$

where n is the unit normal vector to the surface at that point. Since div E = 0 and div H = 0, both E and H can be expressed in terms of vector potentials G and F,

$$E = \text{curl } F$$
$$H = \text{curl } G \qquad \text{(F-6)}$$

where the Maxwell Equations impose consistency conditions between G and F. Two independent solutions may be obtained by choosing a coordinate direction, say $\hat{r}$, the unit vector in the radial direction and finding fields which are perpendicular to $\hat{r}$. If E is perpendicular to $\hat{r}$ we say we have a TE (transverse electric) mode. This situation may be assured if F is chosen to be

$$F = f\hat{r} \qquad \text{(F-7)}$$

where f is a scalar function of the spatial coordinates. In this case we have from (F-4) and (F-7)

$$E = \text{curl } f\hat{r}$$
$$H = -\frac{1}{i\omega\mu} \text{curl curl } f\hat{r}. \qquad \text{(F-8)}$$

If H is perpendicular to r we say we have a TM (transverse magnetic) mode. This situation may be assured if G is chosen to be

$$G = g\hat{r} \qquad \text{(F-9)}$$

where g is a scalar function of the spacial coordinates. In this case we have from (F-4) and (F-9)

$$E = \frac{1}{i\omega\epsilon} \text{curl curl } g\hat{r}$$
$$H = \text{curl } g\hat{r}. \qquad \text{(F-10)}$$

The general solution for E and H may be obtained by a superposition of (F-8) and (F-10)

$$E = \text{curl } f\hat{r} + \frac{1}{i\omega\epsilon} \text{curl curl } g\hat{r}$$

$$H = \text{curl } g\hat{r} - \frac{1}{i\omega\mu} \text{curl curl } f\hat{r} . \tag{F-11}$$

To find equations which f and g satisfy, we consider the TE and TM modes separately. For the TM mode (F-10) and (F-4) imply that

$$\text{curl } E = - i\omega\mu \text{ curl } g\hat{r}$$

or

$$\text{curl } (E + i\omega\mu g\hat{r}) = 0 . \tag{F-12}$$

This last relation is satisfied only if

$$E + i\omega\mu g\hat{r} = \text{grad } \varphi \tag{F-13}$$

for some scalar function φ. Substituting (F-13) into the second of equation (F-4) we have

$$\text{curl curl } g\hat{r} = \omega^2\mu\epsilon\, g\hat{r} + i\omega\epsilon \text{ grad } \varphi . \tag{F-14}$$

Using the vector equation

$$\text{curl curl } g\hat{r} = \nabla^2 g\hat{r} - \text{grad } (\nabla \cdot g\hat{r}) \tag{F-15}$$

and

$$\omega^2\mu\epsilon = k^2$$

we find that g satisfies the following equations

$$(\nabla^2 + k^2)\, g\hat{r} = 0$$

$$\nabla \cdot g\hat{r} = - i\omega\epsilon\varphi . \tag{F-16}$$

A similar argument for the TE mode shows that f satisfies the following equation

$$(\nabla^2 + k^2)\, f\hat{r} = 0$$

$$\nabla \cdot f\hat{r} = i\omega\mu\nabla\psi . \tag{F-17}$$

Equations (A-16) and (A-17) are equivalent to the scalar Helmholtz equations for g/r and f/r with standard solutions given by*

$$B_n(kr)\, L_n^m(\theta, \varphi)\ , \qquad \text{(F-18)}$$

where the $L_n^m(\theta, \varphi)$ are spherical harmonics and the $B_n(kr)$ satisfy the differential equation

$$\left[\frac{d^2}{dr^2} + k^2 - \frac{n(n+1)}{r^2}\right] B_n(kr) = 0\ . \qquad \text{(F-19)}$$

The general solution of equation (F-19) can be given as a linear combination of $j_n(kr)$ and $y_n(kr)$ which are the Spherical Bessel Functions of order n of the first and second kind respectively.**

$$B_n(kr) = C_n kr j_n(kr) + D_n kr y_n(kr) \qquad \text{(F-20)}$$

where C_n and D_n are constants. The general solutions for f and g may be written as an infinite series

$$f = \sum_{n,m}^{\infty} \left(C'_{nm} kr j_n(kr) + D'_{nm} kr y_n(kr)\right) L_n^m(\theta, \varphi)$$

$$g = \sum_{n,m}^{\infty} \left(C_{nm} kr j_n(kr) + D_{nm} kr y_n(kr)\right) L_n^m(\theta, \varphi)\ . \qquad \text{(F-21)}$$

The constants C_{nm}, D_{nm}, C'_{nm}, and D'_{nm} may be evaluated by substituting (F-21) into (F-11) and applying the boundary conditions (F-5). Equation (F-21) can be viewed as an infinite superposition of modes.

*See R. F. Harrington, Time Harmonic Electromagnetic Fields, McGraw Hill (1961).

**See M. Abrahamowitz and I. A. Stegun, NBS Handbook of Mathematical Functions, p. 437.

TM Modes Under Spherical Symmetry

The TM modes are obtained by setting $f = 0$. If the liquid has spherical symmetry the boundary conditions may be satisfied by using only one value each for n and m in equation (F-21) and thus the series for g contains at most two non-vanishing terms:

$$g = \left(C_{nm} kr j_n(kr) + D_{nm} kr y_n(kr)\right) L_n^{m}(\theta, \varphi). \tag{F-22}$$

Using equations (F-11) and (F-16) along with (F-22), the components of the electric and magnetic fields may be written as follows:

$$\begin{aligned}
E_r &= \frac{-1}{i\omega\epsilon}\left(\frac{\partial^2}{\partial r^2} + k^2\right) g = \frac{n(n+1)}{i\omega\epsilon r^2}\, g \\
E_\theta &= \frac{-1}{i\omega\epsilon r}\frac{\partial^2}{\partial r\partial\theta}\, g \\
E_\varphi &= \frac{-1}{i\omega\epsilon r\sin\theta}\frac{\partial^2}{\partial r\partial\varphi}\, g \\
H_r &= 0 \\
H_\theta &= -\frac{1}{r\sin\theta}\frac{\partial g}{\partial\varphi} \\
H_\varphi &= \frac{1}{r}\frac{\partial g}{\partial\theta}.
\end{aligned} \tag{F-25}$$

The boundary conditions are applied by letting the container walls exist at $r = b$ and the liquid-gas interface at $r = a \leq b$ (if $a = 0$ the container is full and if $a = b$ the container is empty.). The conditions $\mu H\cdot n$ and $H x n$ continuous at $r = a$ and $r = b$ imply continuity of H_θ and H_φ and hence that g is continuous at $r = a$ and $r = b$. This is compatible with the continuity of $\epsilon E\cdot n$. The condition $E x n$ continuous implies that E_θ and E_φ is continuous and hence that $\frac{1}{\epsilon}\frac{\partial}{\partial r} g$ is continuous at $r = a$ and $r = b$. In summary the boundary conditions are completely specified by

$$g \text{ continuous at } r = a \text{ and } r = b \tag{F-26}$$

$$\frac{1}{\epsilon}\frac{\partial}{\partial r} g \text{ continuous at } r = a \text{ and } r = b. \tag{F-27}$$

Since the $L_n^m(\theta, \varphi)$ are independent both of radial position and fluid properties, the condition (F-26) is equivalent to

$$k_o a j_n(k_o a) = C_{nm} ka j_n(ka) + D_{nm} ka y_n(ka) \tag{F-28}$$

and

$$g(b) = C_{nm} kb j_n(kb) + D_{nm} kb y_n(kb) \tag{F-29}$$

where the coefficient of $y_n(k_o a)$ in equation (F-22) is zero because g must be finite at $r = 0$. (Here, $k_o = \omega\sqrt{\epsilon_o \mu_o}$ applies to the region in the gas and $k = \omega\sqrt{\epsilon\mu}$ applies to the region in the liquid.) Likewise condition (F-27) is equivalent to

$$\frac{1}{\epsilon_o}\frac{\partial}{\partial a}\left[k_o a j_n(k_o a)\right] = \frac{1}{\epsilon}\frac{\partial}{\partial a}\left[D_{nm} ka j_n(ka) + D_{nm} ka y_n(ka)\right] \tag{F-30}$$

and

$$0 = \frac{1}{\epsilon}\frac{\partial}{\partial b}\left[C_{nm} kb j_n(kb) + D_{nm} kb y_n(kb)\right]. \tag{F-31}$$

Equations (F-28), (F-30), and (F-31) are three independent relations in the eight variables, C_{nm}, D_{nm}, a, ω, ϵ, μ, ϵ_o, and μ_o. The inhomogeneous equations (F-28) and (F-30) can be solved uniquely for C_{nm} and D_{nm} and these values are substituted in equation (F-31) which then becomes a homogeneous relation in six variables a, ω, ϵ, μ, ϵ_o, and μ_o. We will denote this relation by

$$F_n(\omega, a, \epsilon, \mu, \epsilon_o, \mu_o) = 0 \tag{F-32}$$

or sometimes more simply by $F_n(\omega, \text{etc.}) = 0$. For a given set of values for a, ϵ, μ, ϵ_o, and μ_o (which is determined by conditions in the container), it can be shown that F_n plotted as a function of ω is oscillatory and hence there are an infinite number of solutions to equation (F-32). The solution for the p^{th} zero of equation (F-32) is called ω_{np} and the field pattern obtained by substituting ω_{np} and the values for C_{nm} and D_{nm} into equations (F-22) and (F-25) is called the TM_{mnp} mode where

$$n = 1, 2, 3, \ldots\ldots$$

$$p = 1, 2, 3, \ldots\ldots$$

$$m = 0, \pm 1, \pm 2, \ldots\ldots \pm n.$$

(The range on m comes from the properties of the spherical harmonics.) Since ω_{np} is independent of m, we see that there are a number of modes corresponding to the same ω_{np}. This number is called the degeneracy of ω_{np}. For example, the fundamental frequency ω_{11} corresponds to three modes, TM_{011}, TM_{-111}, and TM_{111} and hence has degeneracy 3. Sometimes the first subscript is dropped and the three modes are collectively referred to as the TM_{11} mode (which is an abuse of the term "mode").

We now discuss the conditions under which the resonant frequencies ω_{np} can determine the total mass. The total mass M is a function of three of the above variables, a, ϵ_o, and ϵ. If the resonant frequencies, ω_{np}, of the modes are known, then we have the following relations in the five variables a, ϵ_o, μ_o, ϵ, and μ

$$\begin{aligned} 0 &= F_1(\omega_{11}, \text{ etc.}) = F_1(\omega_{12}, \text{ etc.}) = \ldots\ldots \\ &= F_2(\omega_{21}, \text{ etc.}) = F_2(\omega_{22}, \text{ etc.}) = \ldots\ldots \\ &\quad \vdots \qquad\qquad\qquad \vdots \qquad\qquad\qquad \vdots \\ &= F_n(\omega_{np}, \text{ etc.}) \end{aligned} \qquad \text{(F-33)}$$

where each of the $F_n(\omega_{np}$, etc.) is a relation determined by measuring the resonant frequency of a TM_{mnp} mode. Since there are five variables, it is clear that at least five different modes are necessary to completely determine the total mass. From the properties of the Spherical Bessel Functions it can be shown that each of the above relations is also independent; therefore, five modes are also sufficient to determine the total mass. If further assumptions are made, fewer modes may be sufficient. For example, for most liquids $\mu \approx \mu_o \approx 1$ reduces the number of necessary modes to 3; if it is further assumed that $\epsilon_o \approx 1$, then the number of necessary modes is two; finally if in addition ϵ is known, then only one resonant frequency is necessary to determine the total mass.

Alternately, it may be that the interface, $r = a$, is known and ϵ (hence the density) is unknown; if $\epsilon_o \approx \mu_o \approx \mu \approx 1$, then the density and hence the total mass may be determined by a single resonant frequency. As a limiting case of this situation, the case $a = 0$ indicates a completely full cavity and the resonant frequencies are given by

$$\omega_{np} = \frac{u_{np}}{b\sqrt{\epsilon\mu}} \tag{F-34}$$

where u_{np} is the p^{th} zero of equation (F-32) considered as a function of the quantity kb. (The quantities u_{np} are also known as eigenvalues of the TM_{np} "mode".) The measured frequency f_{np} is given by $f_{np} = \frac{\omega_{np}}{2\pi}$. The calculated values for u_{np} in the case $a = 0$ are listed in Table 1 in increasing order for the lowest ten modes. (Table 1 also includes results of a similar analysis for the TE modes.) The resonant frequencies f_{np} also plotted in Table 1 are for the specific case of a 48-cm diameter empty container.

We see from Table 1 that the resonant frequencies of the lower order modes are widely spaced. This is primarily due to the degeneracy and makes it feasible to simultaneously monitor several of the lower order modes.

Table F-I.

Modes	Eigenvalues	Degeneracy	Frequency (48 cm dia. Sphere)
TM_{11}	u_{11} = 2.744	3	f_{11} 0.543 GHz
TM_{21}	u_{21} = 3.870	5	f_{21} 0.766
TE_{11}	u'_{11} = 4.493	3	f'_{11} 0.889
TM_{31}	u_{31} = 4.973	7	f_{31} = 0.984
TE_{21}	u'_{21} = 5.763	5	f'_{21} = 1.140
TM_{41}	u_{41} = 6.062	9	f_{41} = 1.200
TM_{12}	u_{12} = 6.117	3	f_{12} = 1.210
TE_{31}	u'_{31} = 6.998	7	f'_{31} = 1.384
TM_{51}	u_{51} = 7.140	11	f_{51} = 1.413
TM_{22}	u_{22} = 7.443	5	f_{22} = 1.472

Examples Using Hydrogen and Nitrogen

Equation (F-32) was solved for the four lowest order modes using the FORTRAN program listed in Table 2.* For given values of a, ϵ, μ, ϵ_o, and μ_o, the program finds the zeros of $F_n(\omega, \text{etc.})$ plotted as a function of kb where

$$kb = \omega\sqrt{\mu\epsilon}\, b.$$

The p^{th} zero is

$$u_{np} = \omega_{np}\sqrt{\mu\epsilon}\, b.$$

The computer plots the quantity αu_{np} vs. $\bar{\rho}$ which is essentially resonant frequency, f_{np}, vs. total mass M. Here,

$$\alpha = \sqrt{\frac{\epsilon_o\mu_o}{\epsilon\mu}}.$$

*Written by A. E. Hiester.

Table F-II.

```
      PROGRAM PLOT3
      DIMENSION IFILM(13),ITITLE(13),X(100),Y(100),AL(3),RHO(3)
      DATA (IFILM=24HART HIESTER, X3474            )
      A(N,U,F,AL)=(1./AL*PJ(N,AL*F*U)*YPP(N,F*U)-AL**2*PPJ(N,AL*F*U)*YP(
     1N,F*U))/(PJ(N,F*U)*YPP(N,F*U)-PPJ(N,F*U)*YP(N,F*U))
      B(N,U,F,AL)=(AL**2*PJ(N,F*U)*PPJ(N,AL*F*U)-1./AL*PPJ(N,F*U)*PJ(N,A
     1L*F*U))/(PJ(N,F*U)*YPP(N,F*U)-PPJ(N,F*U)*YP(N,F*U))
      FUN(N,U,F,AL)=A(N,U,F,AL)*PJ(N,U)-B(N,U,F,AL)*YP(N,U)
    1 FORMAT(3F10.0)
    2 FORMAT(*U*,I2,5H      )
    3 FORMAT(1H1,10X,2A8//9X,11HALPHA * UNP,10X,*RHOBAR*//)
    4 FORMAT(9X,F9.5,10X,F10.7)
    5 FORMAT(*OU NOT FOUND IN 100 ITERATIONS*//1X,6E22.8)
    6 FORMAT(5H$1* U,I2,1H )
      P=1.
      ITITLE(1)=8H RESONAN
      ITITLE(2)=8HT FREQUE
      ITITLE(3)=8HNCY VS M
      ITITLE(4)=8HASS - H2
      ITITLE(7)=8HR$9HOBAR
      ITITLE(10)=8H      $1
      ITITLE(11)=8HA$9LPHA
      ITITLE(5)=ITITLE(6)=ITITLE(8)=ITITLE(9)=ITITLE(13)=8H
      READ 1,(AL(I),I=1,3)
      READ 1,(RHO(I),I=1,3)
      CALL GRAPH(1,1,3,IFILM,0,6)
      DO 60 N=1,4
      ID=P
      ID=ID+10*N
      ENCODE(8,2,IFILM)ID
      ENCODE(8,6,ITITLE(12))ID
      DO 55 I=1,3
      GO TO (7,8,9),I
    7 LTYP=8HTP SOLID
      GO TO 95
    8 LTYP=8HTP LIQ
      GO TO 95
    9 LTYP=8HNBP LIQ
   95 PRINT 3,IFILM(1),LTYP
      LINE=0
      DO 50 J=1,99
      RHOBAR=J
      RHOBAR=RHOBAR/100.*RHO(I)
      F=(1.-RHOBAR/RHO(I))**(1./3.)
      UB=7.5
      US=2.5
      FUS=FUN(N,US,F,AL(I))
      FUB=FUN(N,UB,F,AL(I))
      IT=0
   10 UM=(UB-US)/2.+US
      IT=IT+1
      IF(IT.LE.100)GO TO 15
      PRINT 5,US,FUS,UM,FUM,UB,FUB
      STOP
```

Table F-II. (Continued)

```
15 FUM=FUN(N,UM,F,AL(I))
   IF(ABS(FUM).LT..00001)GO TO 45
   IF(FUM.GT.0..AND.FUS.GT.0..OR.FUM.LT.0..AND.FUS.LT.0.)GO TO 20
   UB=UM
   FUB=FUM
   GO TO 10
20 US=UM
   FUS=FUM
   GO TO 10
45 X(J)=RHOBAR
   Y(J)=AL(I)*UM
   LINE=LINE+1
   IF(LINE.NE.51)GO TO 50
   LINE=0
   PRINT 3,IFILM(1),LTYP
50 PRINT 4,Y(J),X(J)
   IF(I.NE.1)GO TO 53
   CALL LGRAPH(X,Y,99,ITITLE,IFILM)
   CALL CPGRAPH(X(99),Y(99),1,,,I+4)
   GO TO 55
53 CALL CLGRAPH(X,Y,99)
   CALL CPGRAPH(X(99),Y(99),1,,,I+4)
55 CONTINUE
   IFILM(1)=8H$9, $1TP
   IFILM(2)=8H SOLID'/
   IFILM(3)=8H$1+ TP L
   IFILM(4)=8HIQUID'/$
   IFILM(5)=8H1* NBP L
   IFILM(6)=8HIQUID
   CALL COMGRAPH(.75,.75,6,IFILM)
   CALL SKIPFRM
60 CONTINUE
   STOP
   END

   FUNCTION SY(N,Z)
   Y1(Z)=-COS(Z)/Z
   Y2(Z)=-COS(Z)/Z**2-SIN(Z)/Z
   Y3(Z)=(-3./Z**3+1./Z)*COS(Z)-3./Z**2*SIN(Z)
   GO TO (10,20,30,40,50)N+1
10 SY=Y1(Z)
   RETURN
20 SY=Y2(Z)
   RETURN
30 SY=Y3(Z)
   RETURN
40 SY=5./Z*Y3(Z)-Y2(Z)
   RETURN
50 SY=7./Z*(5./Z*Y3(Z)-Y2(Z))-Y3(Z)
   RETURN
   END

   FUNCTION SJ(N,Z)
   J1(Z)=SIN(Z)/Z
```

Table F-II. (Continued)

```
      J2(Z)=SIN(Z)/Z**2-COS(Z)/Z
      J3(Z)=(3./Z**3-1./Z)*SIN(Z)-3./Z**2*COS(Z)
      GO TO (10,20,30,40,50)N+1
   10 SJ=J1(Z)
      RETURN
   20 SJ=J2(Z)
      RETURN
   30 SJ=J3(Z)
      RETURN
   40 SJ=5./Z*J3(Z)-J2(Z)
      RETURN
   50 SJ=7./Z*(5./Z*J3(Z)-J2(Z))-J3(Z)
      RETURN
      END

      FUNCTION PJ(N,Z)
      FN=N
      PJ=Z*SJ(N-1,Z)-FN*SJ(N,Z)
      RETURN
      END

      FUNCTION YP(N,Z)
      FN=N
      YP=Z*SY(N-1,Z)-FN*SY(N,Z)
      RETURN
      END

      FUNCTION PPJ(N,Z)
      FN=N
      PPJ=(FN*(FN+1.))/Z*SJ(N,Z)
      RETURN
      END

      FUNCTION YPP(N,Z)
      FN=N
      YPP=(FN*(FN+1.))/Z*SY(N,Z)
      RETURN
      END
```

$$f_{np} = \frac{\alpha u_{np}}{2\pi b\sqrt{\epsilon_o \mu_o}} ,$$

and

$$M = \bar{\delta} V$$

where V is the volume of the tank in cm^3. The results may then be applied to spheres of any size and to any dielectric fluid.

We have assumed that $\mu = \mu_o = \epsilon_o = 1$ and plotted the results for three different densities corresponding to solid hydrogen, triple point liquid, and normal boiling point liquid; this corresponds to about 22 percent range in density. The results for the first four modes are shown in figures A1, A2, A3, and A4. It is seen that the uncertainty in total mass is smaller for higher modes. Qualitatively this is because the field patterns are spread more uniformly throughout the cavity for the higher modes. For example, the uncertainty in mass vs. αu_{41} (or f_{41}) is less than 5 percent over most of the range. This is to be compared with a density change of 22 percent indicating that the resonant mode has a tendency to integrate over the mass of the liquid rather than the volume.

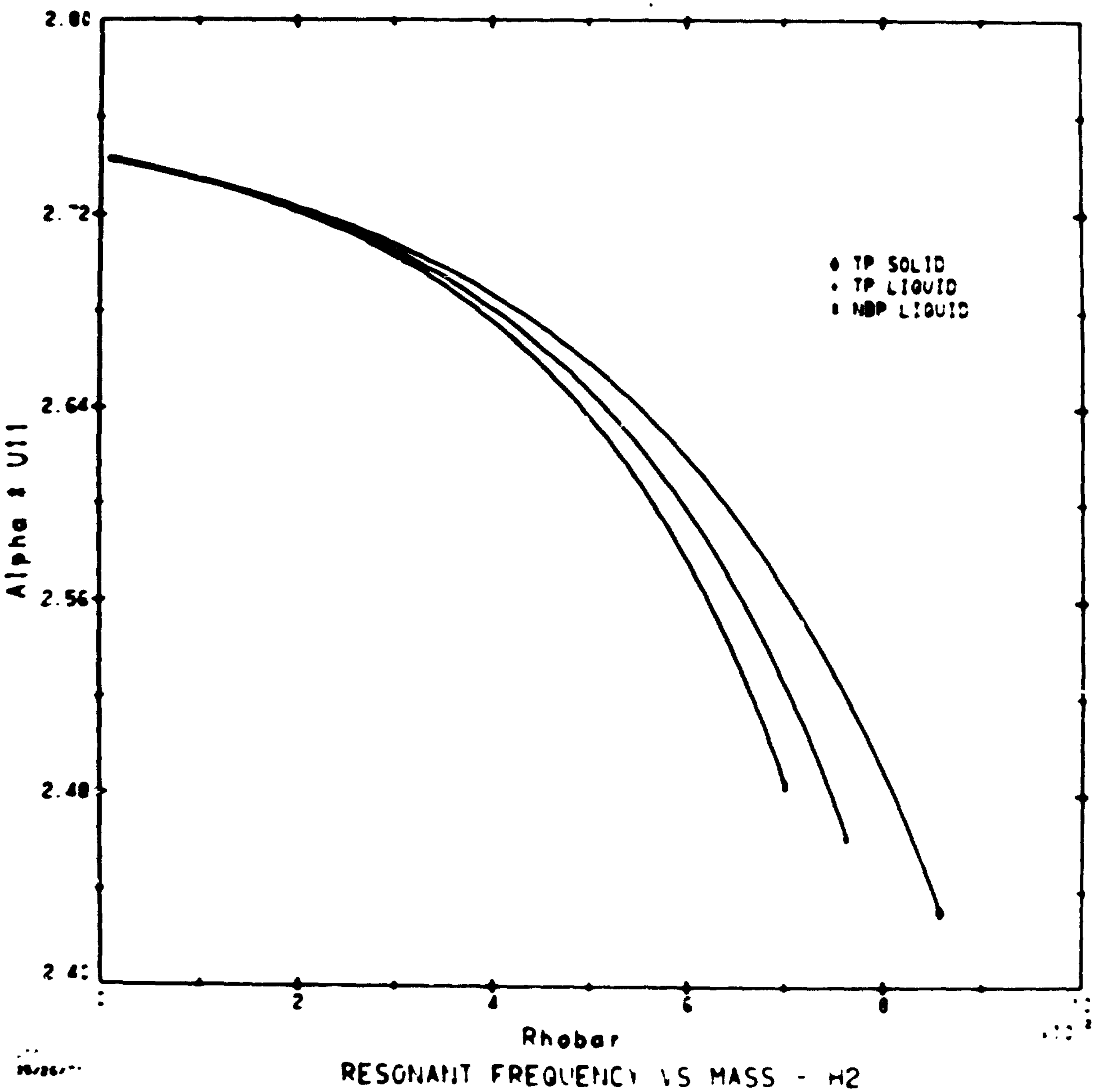

Figure F1. Resonant Frequency vs. Mass, TM_{m11} Mode.

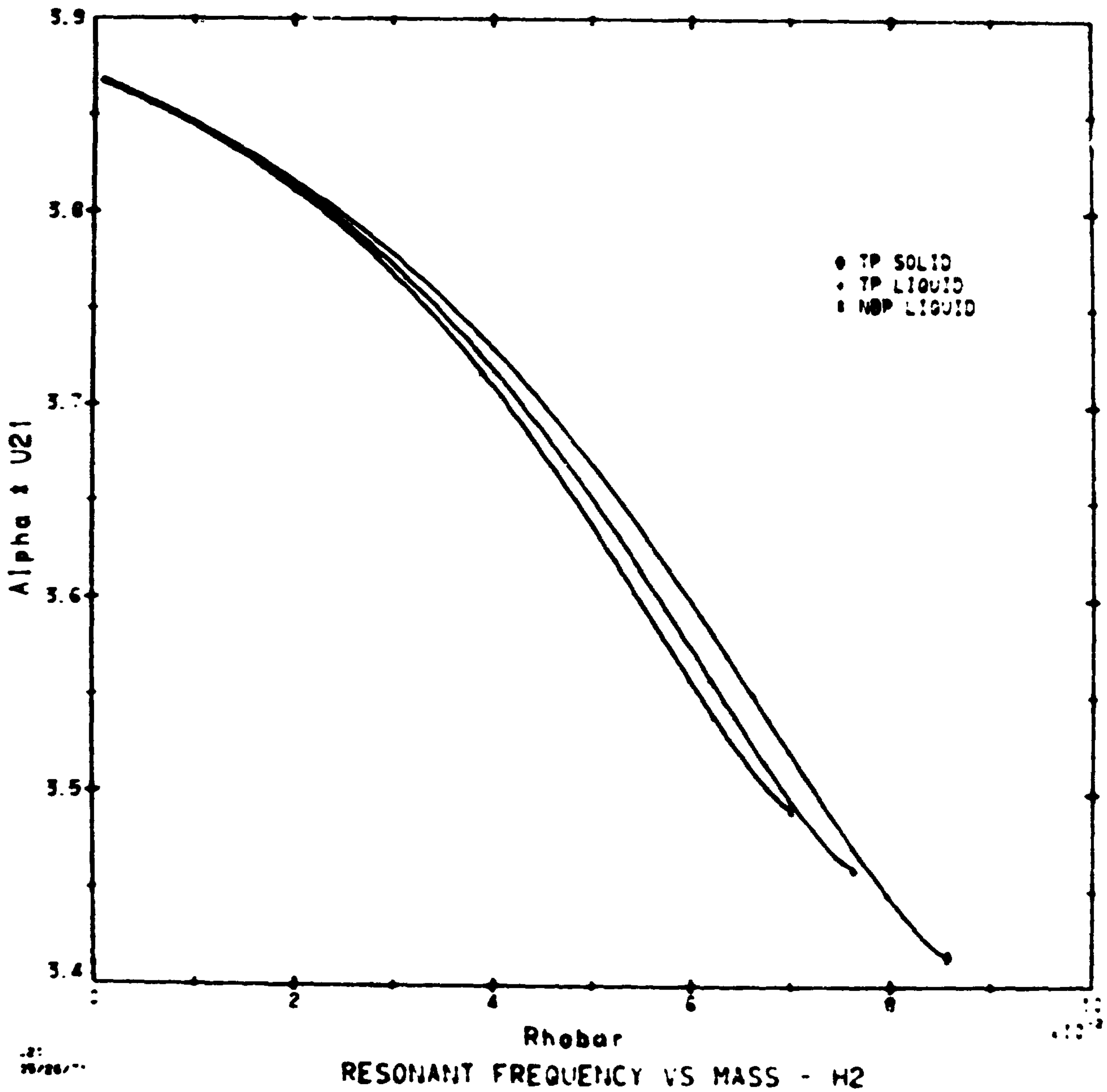

Figure F2. Resonant Frequency vs. Mass, TM_{m21} Mode.

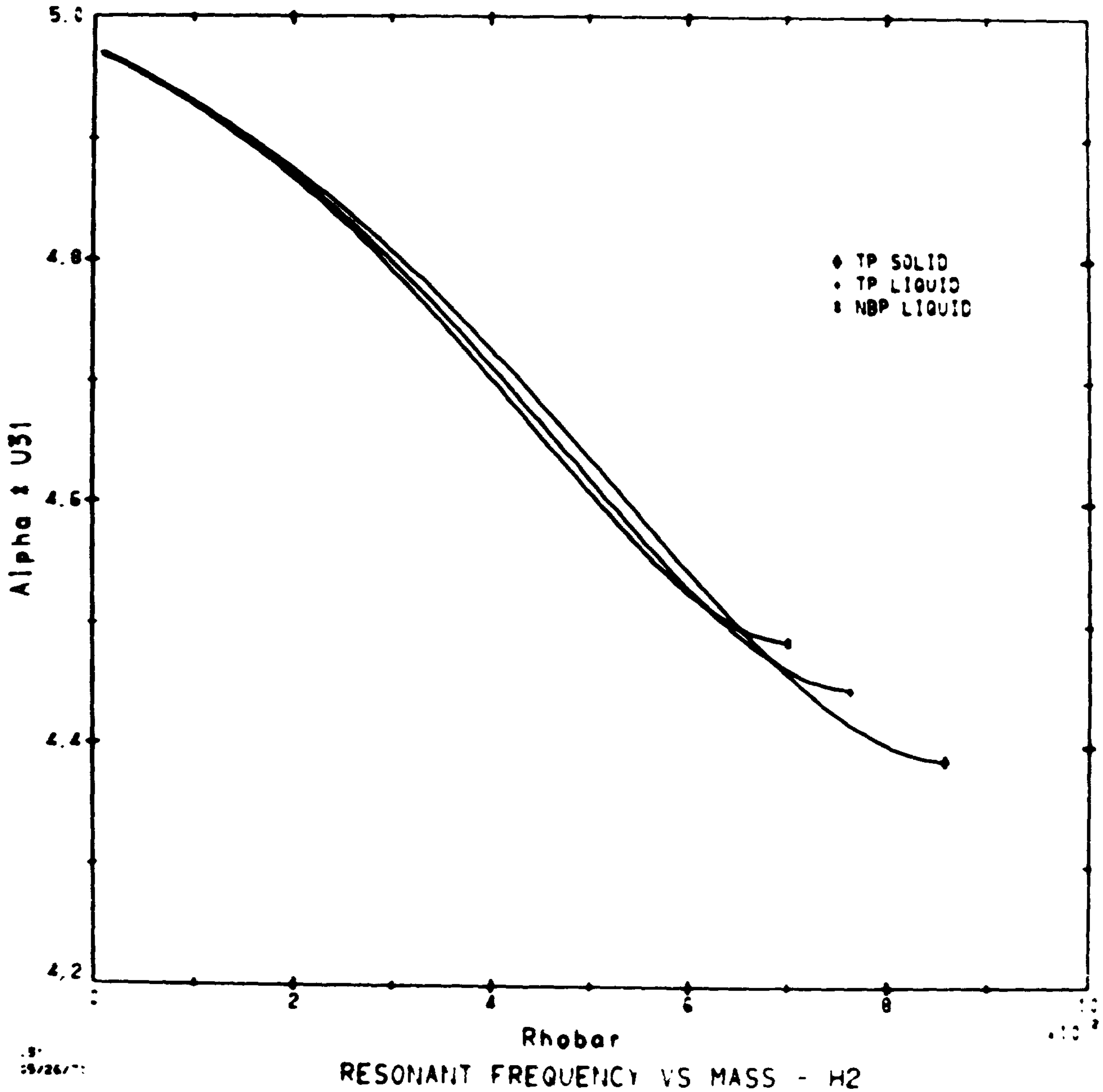

Figure F3. Resonant Frequency vs. Mass, TM_{m31} Mode.

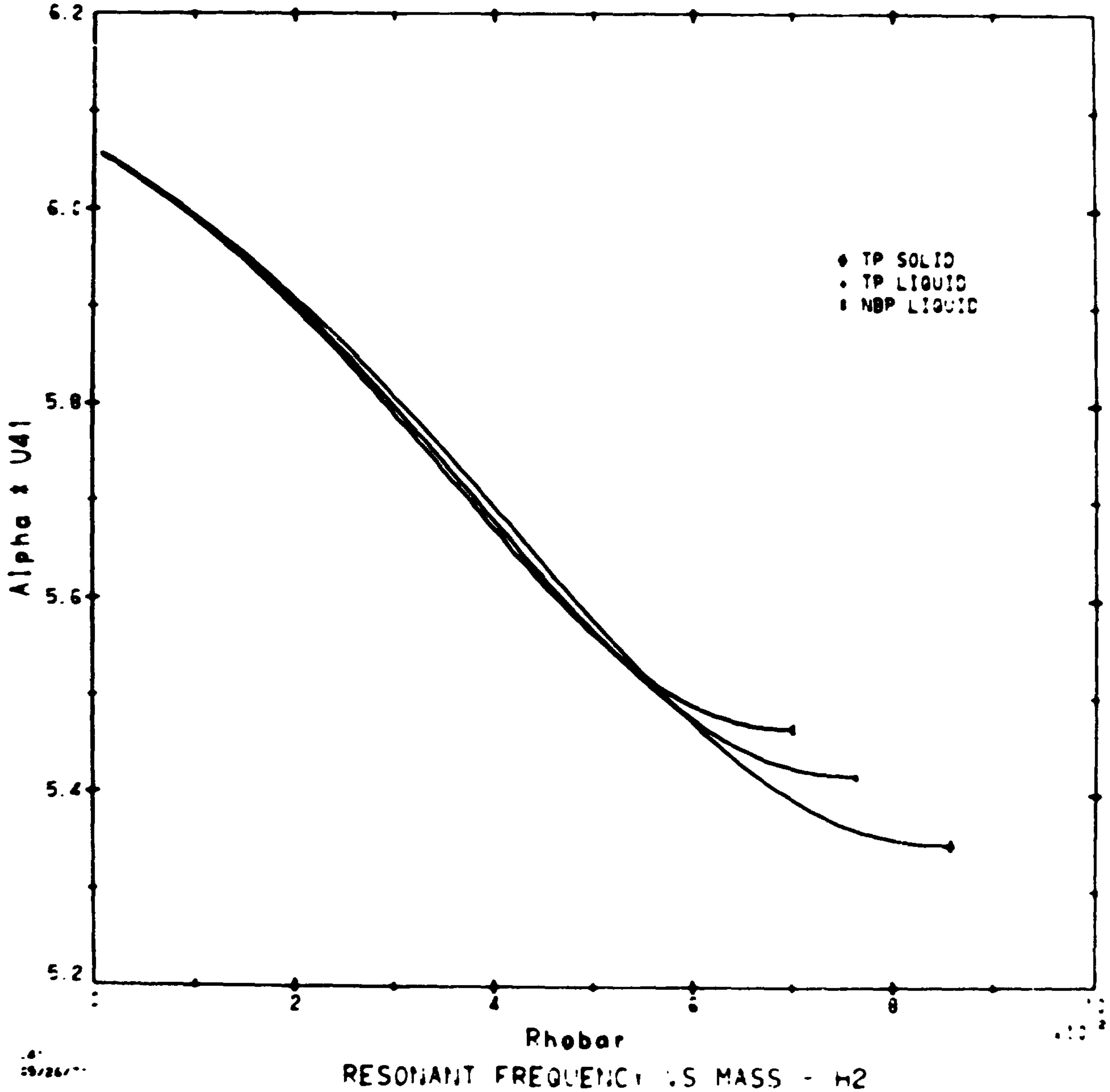

Figure F4. Resonant Frequency vs. Mass, TM_{m41} Mode.

APPENDIX G

APPROXIMATE METHODS FOR AN INHOMOGENEOUS DIELECTRIC

Introduction

The problem is to compute resonant frequencies of a microwave cavity containing an inhomogeneous but isotropic dielectric. We suppose the cavity wall is a perfect conductor, the dielectric dissipates no power, and the dielectric has uniform magnetic permeability. Mathematically, we are dealing with the boundary value problem posed by Maxwell's equations[1] in the absence of sources and with the electric vector everywhere normal to the wall of the cavity. For a Fourier component $Ee^{j\omega t}$ of electric field with (angular) frequency ω, the boundary value problem is

$$\nabla X E = -j\omega\mu H$$

$$\nabla X H = j\omega\epsilon E \qquad (1)$$

E normal to boundary.

We will use the subscripts 0, 1 to denote quantities pertaining to the corresponding mode for a cavity containing a uniform dielectric of permittivity ϵ_0 or ϵ_1, respectively. We assume that the permittivity ϵ is piecewise continuous and satisfies $\epsilon_0 \leq \epsilon \leq \epsilon_1$. Also we assume that $\epsilon_1 - \epsilon_0$ is small enough so that the set of modes for the permittivities ϵ_0, ϵ, ϵ_1 are at most slightly different from each other in shape and can be put in one-to-one correspondence. For convenience we will regard ϵ_0 as the permittivity of free space.

[1] We use the technique, notation, and units (MKSA) of Wolfgang K. H. Panofsky and Melba Phillips, Classical Electricity and Magnetism, Addison-Wesley, 1955.

The resonant frequency ω_0 of any mode in the empty cavity may be computed[2] from a standard solution of Maxwell's equations. The resonant frequency ω of the corresponding mode when the cavity is partially filled with dielectric is lower, and we wish to estimate its value without further extensive calculations. We prefer estimating techniques which are insenstitive to the spatial distribution of dielectric material in the cavity and which do not require further computation of electromagnetic field strengths.

The first method considered is adapted from a technique of approximation due to Rayleigh. Two approximations of this type are formed, and it is shown that one is always at least as large as the other. Then the larger is shown to be always at least as large as the true value of ω. Finally, a refinement of the last method is described, known as the Rayleigh-Ritz method. This first group of methods gives upper bounds for the true resonance frequency. The lower Rayleigh estimate has not been proved to be a lower bound. But the difference between the upper and lower Rayleigh estimates is within 10 percent of the difference between the empty and full cavity resonant frequencies, in the case of liquid nitrogen in a sphere in a steady uniform gravitational field (See Figure G1). One should bear in mind that the upper Rayleigh estimate has been proved an upper bound <u>only</u> for the fundamental (TM_{011}) mode.

The moment methods improve on the Rayleigh methods in two ways. First, they provide lower bounds as well as upper bounds; and second, they are easier to apply to higher modes. The first order moment method yields a lower bound for the fundamental mode which is comparable to the lower Rayleigh estimate, and an upper bound which is identical to the upper Rayleigh estimate. Higher moments have not yet been computed.

[2] See Appendix F, Table I.

The Green's function was investigated as a tool for obtaining lower bounds. The resonance frequencies of the cavity are eigenvalues of a certain linear operator L. The Green's function is used to compute a norm for L^{-1}. Preliminary results are inconclusive as to its value, and careful estimates must be made with an automatic computer.

Rayleigh Methods

The Rayleigh method[3] of equating "potential" and "kinetic" energies in the perturbed field suggests the following heuristic procedure. We suppose that $E = a\,E_0$ for some number a independent of position and compute the magnetic field from equations (1):

$$H = \frac{\nabla X E}{-j\omega\mu} = \frac{a\nabla X E_0}{-j\omega\mu} = \frac{a(-j\omega_0\mu H_0)}{-j\omega\mu} = a\,\frac{\omega_0}{\omega}\,H_0.$$

Then we eliminate a by equating the time-average electric and magnetic field energies[4].

$$\int \frac{1}{2}\,\epsilon E^2 \approx \int \frac{1}{2}\,\mu H^2$$

$$a^2 \int \epsilon E_0 \approx a^2 \int \mu\,\frac{\omega_0{}^2}{\omega}\,H_0^2\ .$$

But $\int \epsilon_0 E_0{}^2 = \int \mu H_0{}^2$, so we conclude that ω^2 is approximately equal to

$$\underline{\omega}^2 = \omega_0^2\ \frac{\int E_0{}^2}{\int K\,E_0{}^2} \qquad (2)$$

where $K = \epsilon/\epsilon_0$ is the dielectric constant. Notice that the ratio b of H to H_0 is also independent of position, as a is.

[3] G. Temple and W. G. Bickley, Rayleigh's Principle, Dover, 1956, pp. 1-24.

[4] All integrals are volume integrals over the region of the cavity, unless otherwise specified.

But if we suppose $H = bH_0$ for some number $\underline{b}$ independent of position, equations (1) lead to

$$E = b \frac{\omega_0 \epsilon_0}{\omega \epsilon} E_0$$

and the ratio of E to E_0 is now dependent on position because ϵ is. A computation like that of the preceding paragraph shows that ω^2 is approximately equal to

$$\overline{\omega}^2 = \omega_0^2 \frac{\int \frac{1}{K} E_0^2}{\int E_0^2} . \tag{3}$$

We show (Theorem 1) that $\omega_1 < \underline{\omega} \le \overline{\omega} \le \omega_0$ for every mode and (Theorem 2) that $\omega_1 \le \omega \le \overline{\omega}$ for the fundamental mode. The remainder of this Appendix describes ways to compute lower bounds for ω in the fundamental mode.

The electric field E for any solution of (1) for a given ϵ and ω is an eigenfunction of the differential operator

$$L = \frac{1}{\mu\epsilon} \nabla \times \nabla \times$$

corresponding to the eigenvalue ω^2. Let S be the spherical cavity including the inside region and also the boundary surface. Let Δ be the set of all vector functions on S having continuous derivatives of all orders. Then Δ is a pre-Hilbert space with respect to the inner product

$$(F, G) = \int F \cdot G ,$$

and we will denote by Θ the Hilbert space which is the $(,)$ - completion of Δ. It is easy to show that L maps Δ into Θ, and so L^{-1} is well-defined on $L\Delta$. But L^{-1} is bounded (Theorem 3) and $L\Delta$ is dense so that L^{-1} has a unique continuous extension to Θ which we also denote L^{-1}.

Now L is symmetric[5] in the sense that

$$(LF, G) = (F, LG)$$

for every F, G in Δ and <u>positive</u> in the sense that $(LF, F) > 0$ for every F in D. The same is true for L_1, L_0, and the inverses of all three operators. Moreover we have easily

$$(E_0, LE_0) \le (E_0, L_0 E_0)$$

$$(E_1, L^{-1} E_1) \le (E_1, L_1^{-1} E_1) .$$

Now observe that

$$L_0 - \omega_0^2 = \frac{\epsilon_1}{\epsilon_0}\left(L_1 - \omega_0^2 \frac{\epsilon_0}{\epsilon_1}\right) ,$$

so that E_0, E_1 belong to the same eigenspace of L_0. But we have agreed[6] that E_0, E, E_1 shall correspond to exactly the same mode. This means that E_1 is a scalar multiple of E_0 and

$$\frac{(E_1, E_1)}{(E_1, L^{-1} E_1)} = \frac{(E_0, E_0)}{(E_0, L^{-1} E_0)} .$$

<u>Theorem 1</u>: $\omega_1 \le \underline{\omega} \le \overline{\omega} \le \omega_0$.

<u>Proof</u>:

$$\omega_1^2 = \frac{(E_1, E_1)}{(E_1, \omega_1^{-2} E_1)} = \frac{(E_1, E_1)}{(E_1, L_1^{-1} E_1)}$$

$$\le \frac{(E_1, E_1)}{(E_1, L^{-1} E_1)} \quad \frac{(E_0, E_0)}{(E_0, L^{-1} E_0)} = \frac{(E_0, E_0)}{(E_0, K L_0^{-1} E_0)}$$

$$= \frac{(E_0, E_0)}{(E_0, K\omega_0^{-2} E_0)} = \underline{\omega}^2 .$$

---

[5] D. A. Taggart and F. W. Schott, "Ferrite-Filled Cavity Resonator," <u>Applied Science Research</u> <u>25</u>, November 1971, page 38.

[6] See the penultimate sentence of the first paragraph of the introduction.

Also $$\omega_0^2 = \frac{(E_0, L_0 E_0)}{(E_0, E_0)} \geq \frac{(E_0, L E_0)}{(E_0, E_0)} = \frac{(E_0, \frac{1}{K} L_0 E_0)}{(E_0, E_0)}$$

$$= \frac{(E_0, \frac{1}{K} \omega_0^2 E)}{(E_0, E_0)} = \bar{\omega}^2 .$$

Finally, we prove $\underline{\omega} \leq \bar{\omega}$ using the Schwartz inequality:

$$(E_0, E_0)^2 = (\sqrt{K} E_0, \frac{1}{\sqrt{K}} E_0)^2 \leq \| \sqrt{K} E_0 \|^2 \cdot \| \frac{1}{\sqrt{K}} E_0 \|^2$$

so that $$\frac{(E_0, E_0)}{(\sqrt{K} E_0, \sqrt{K} E_0)} \leq \frac{(\frac{1}{\sqrt{K}} E_0, \frac{1}{\sqrt{K}} E_0)}{(E_0, E_0)} .$$

Theorem 2. If ω is the lowest resonant frequency, $\omega_1 \leq \omega \leq \bar{\omega}$.

Proof. Because ω^2 is minimal for L and E_0 belongs to D, we have

$$(E_0, (L - \omega^2) E_0) \geq 0 \quad \text{which implies} \quad \omega^2 \leq \frac{(E_0, L E_0)}{(E_0, E_0)} = \bar{\omega}^2 .$$

Similarly, we have ω_1^{-2} maximal for L_1^{-1} and

$$(E_1, (L_1^{-1} - \omega_1^{-2}) E_1) \leq 0$$

so $$\omega_1^2 \leq \frac{(E_1, E_1)}{(E_1, L^{-1} E_1)} = \underline{\omega}^2 .$$

Remark. The result $\omega \leq \bar{\omega}$ is often called Rayleigh's principle.

Figures G1 through G5 show how $\underline{\omega}/\omega_0$ and $\bar{\omega}/\omega_0$ vary as a spherical cavity is filled with liquid nitrogen in the presence of a steady gravitational field.[7] Preliminary data indicate that the true value lies between these two estimates for the fundamental mode.

The Rayleigh-Ritz method is a refinement of the foregoing which also produces an upper bound for ω. We will consider here only the case of the fundamental mode. The force of Therorem 2 is that

$$\omega^2 < \frac{(F, LF)}{(F, F)}$$

when F is any continuous vector field on the cavity which is normal to the walls and twice differentiable in the interior. Theorem 2 states this for the case in which F is the electric field of the fundamental mode for an empty cavity. We now consider the case in which F is a finite sum

$$F = \sum_{n=1}^{N} C_n \; F_n$$

Where F_n is the electric field of the n th mode in an empty cavity, $\|F_n\| = 1$, C_n is a complex number to be determined later, and N is a positive integer. The preceding inequality then leads to

$$\omega^2 \le \frac{\sum_{n=1}^{N} \sum_{n=1}^{N} C_n \bar{C}_n \omega_n^2 \left(F_n, \frac{1}{K} F_n\right)}{\sum_{n=1}^{N} |C_n|^2}$$

where ω_n is the angular resonant frequency of the nth mode in the empty cavity. Then

[7] These results have been calculated numerically by techniques described in Appendix H.

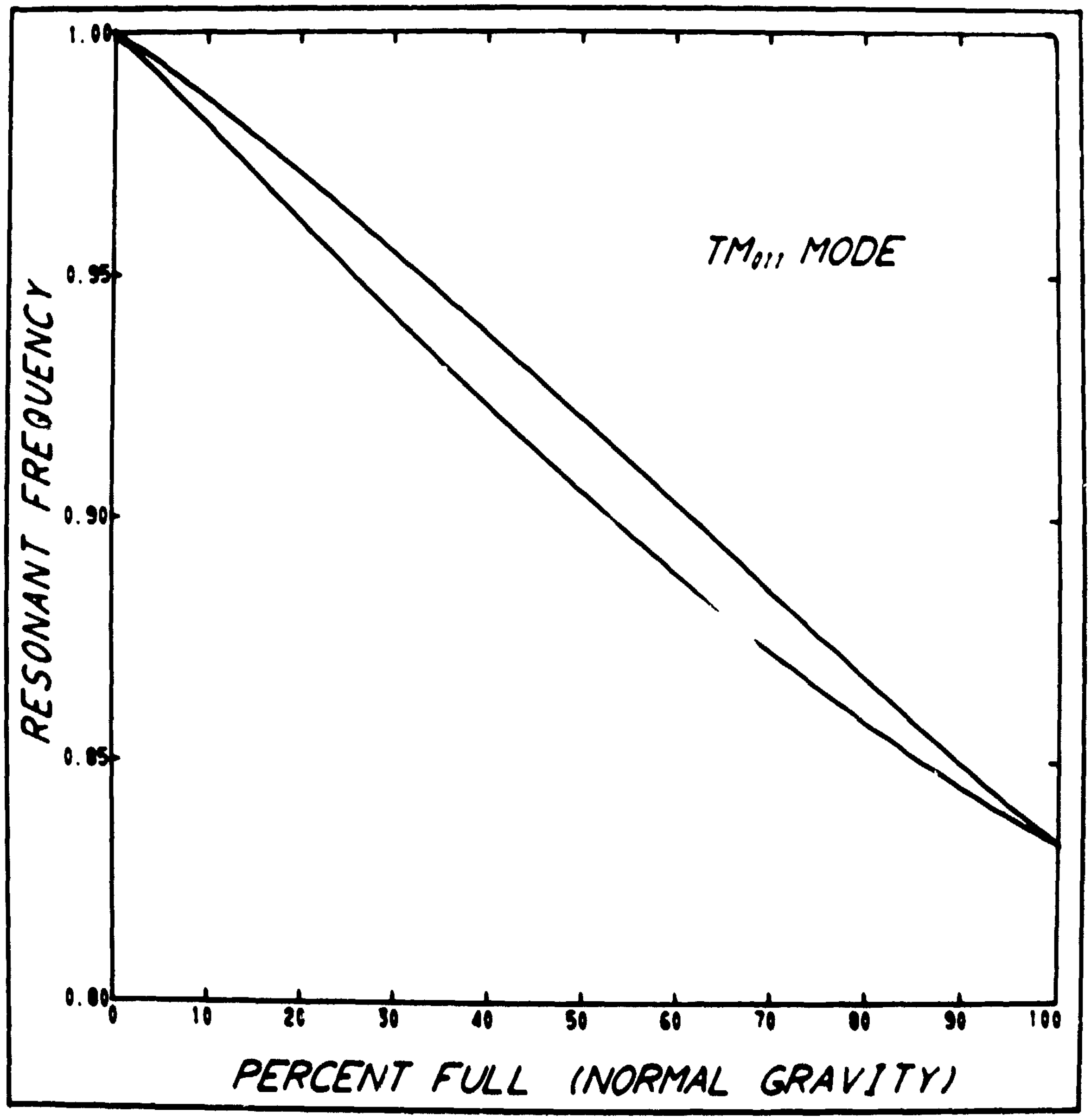

Figure G1

Upper and lower Rayleigh approximations to the normalized frequency ω/ω_0 as a function of fill fraction, for the TM_{011} mode using liquid nitrogen.

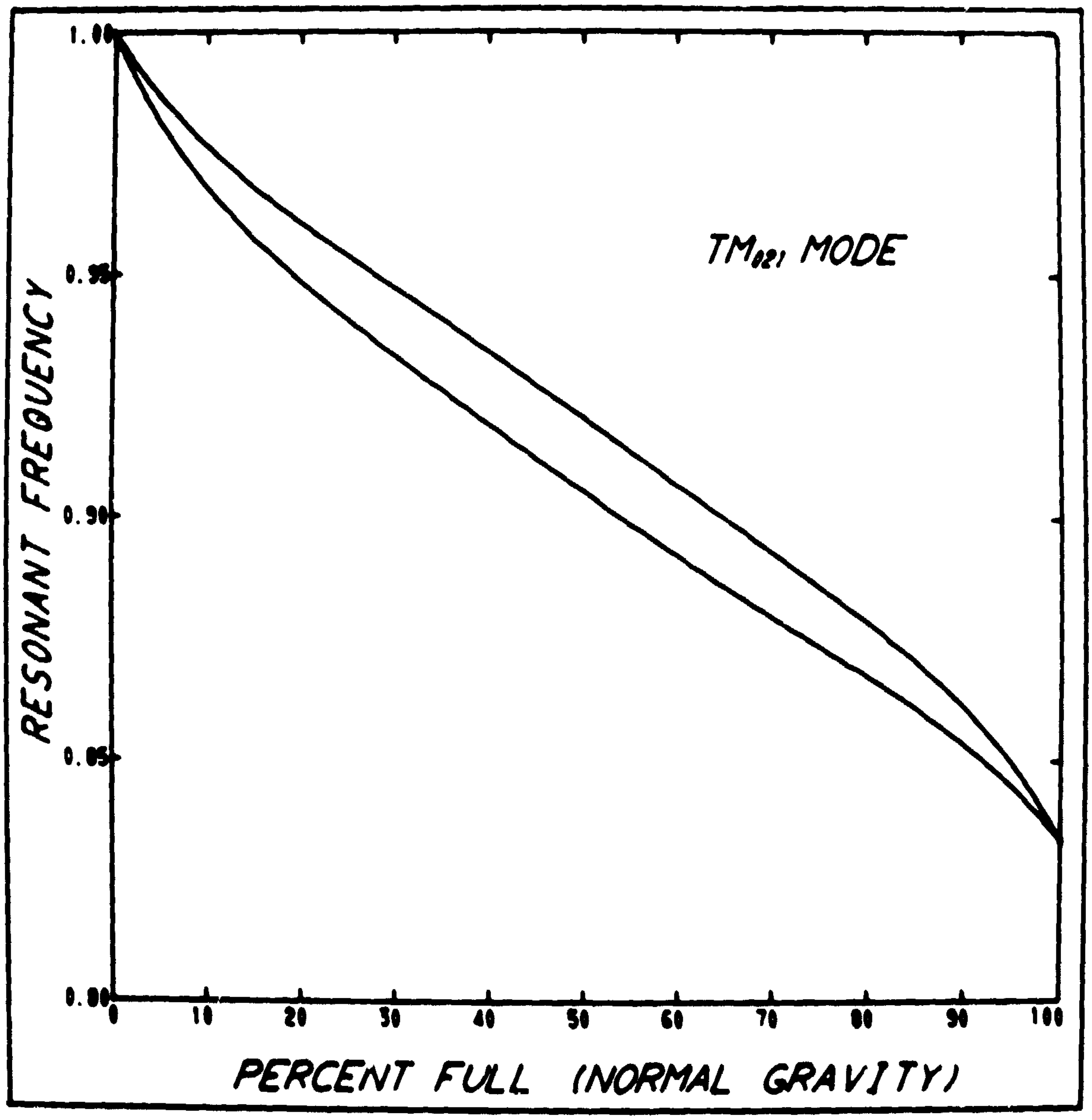

Figure G2

Upper and lower Rayleigh approximations to the normalized frequency ω/ω_0 as a function of fill fraction, for the TM_{021} mode using liquid nitrogen.

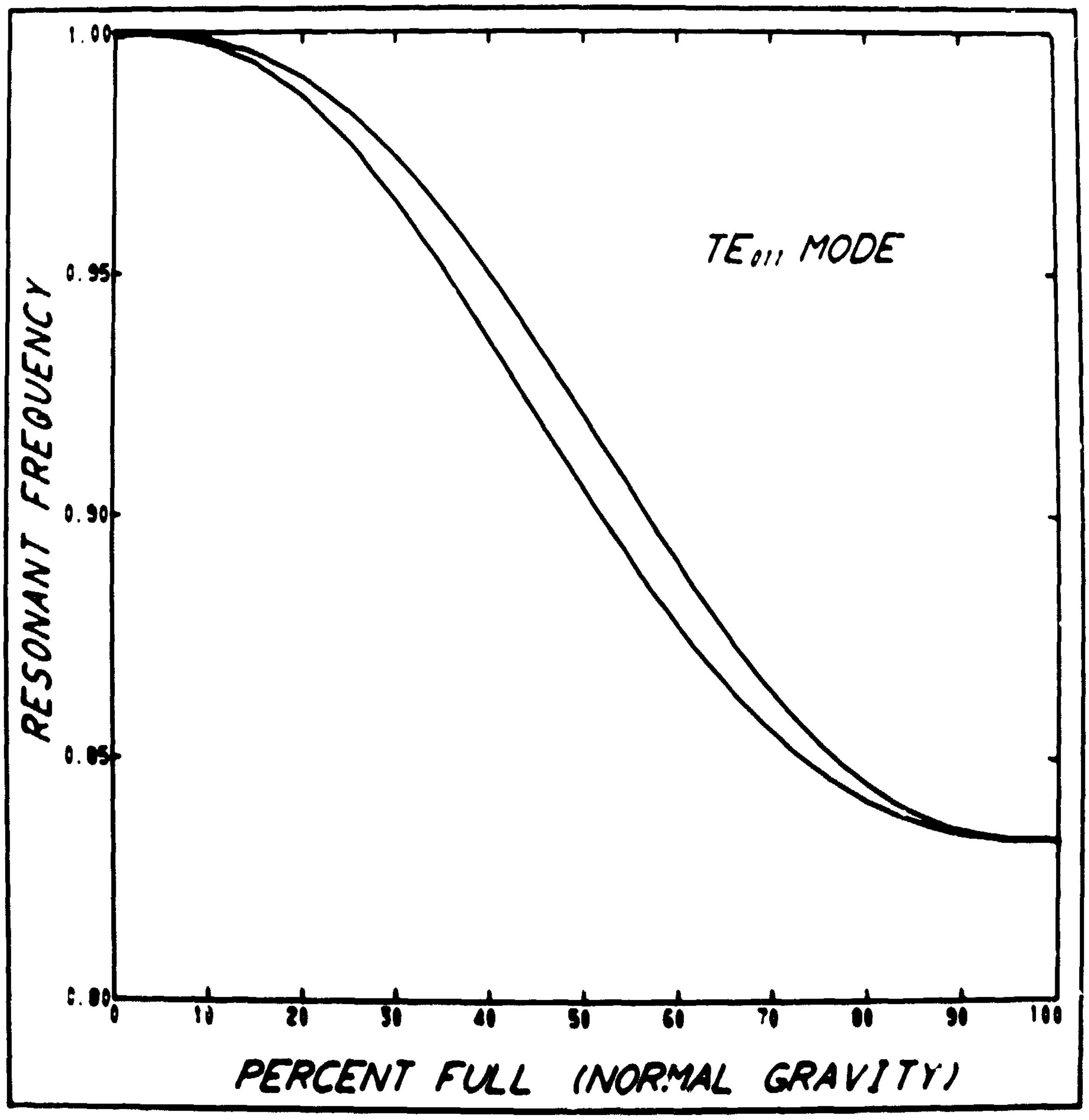

Figure G3

Upper and lower Rayleigh approximations to the normalized frequency ω/ω_0 as a function of fill fraction, for the TE_{011} mode using liquid nitrogen.

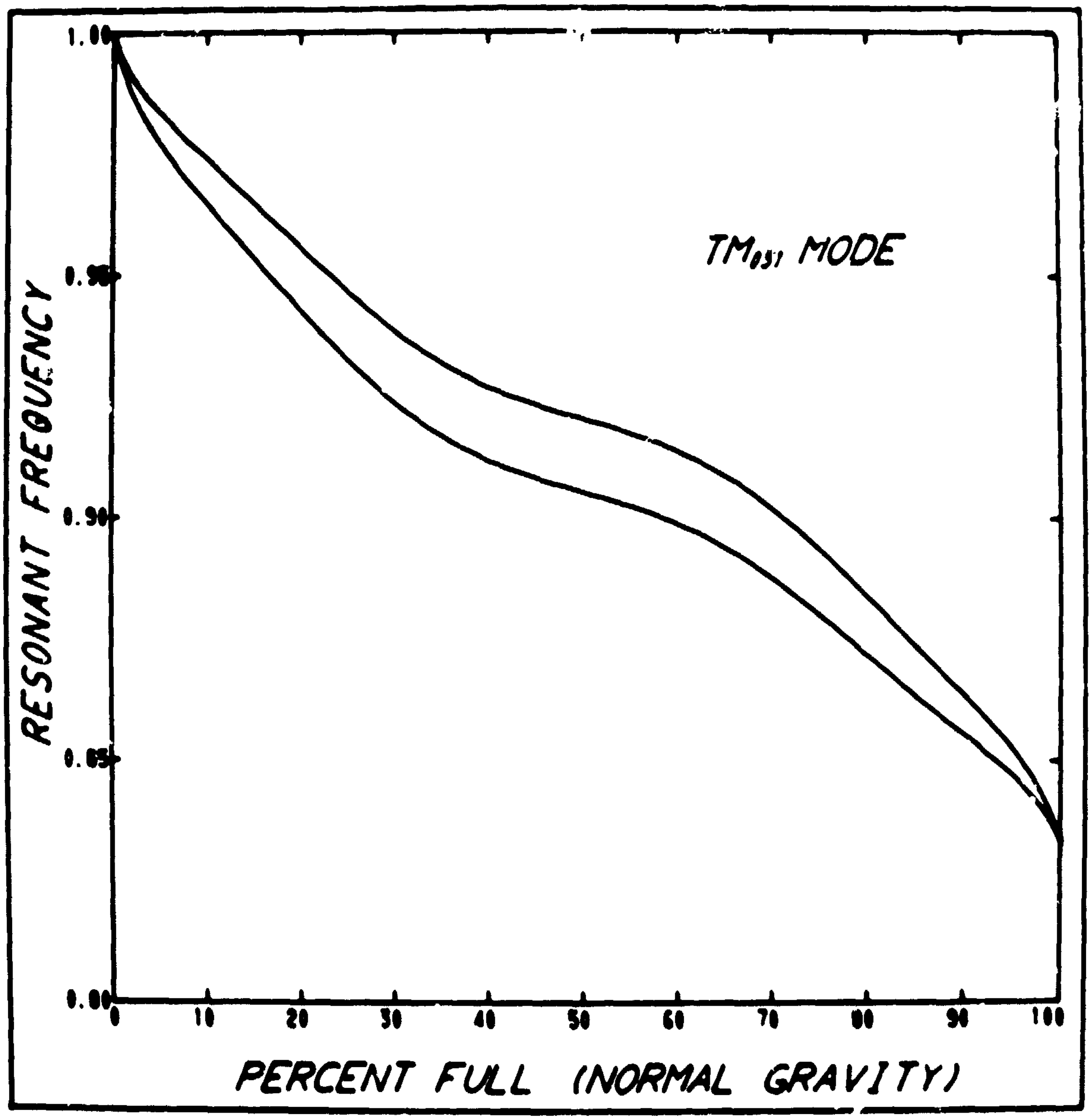

Figure G4

Upper and lower Rayleigh approximations to the normalized frequency ω/ω_0 as a function of fill fraction, for the TM$_{031}$ mode using liquid nitrogen.

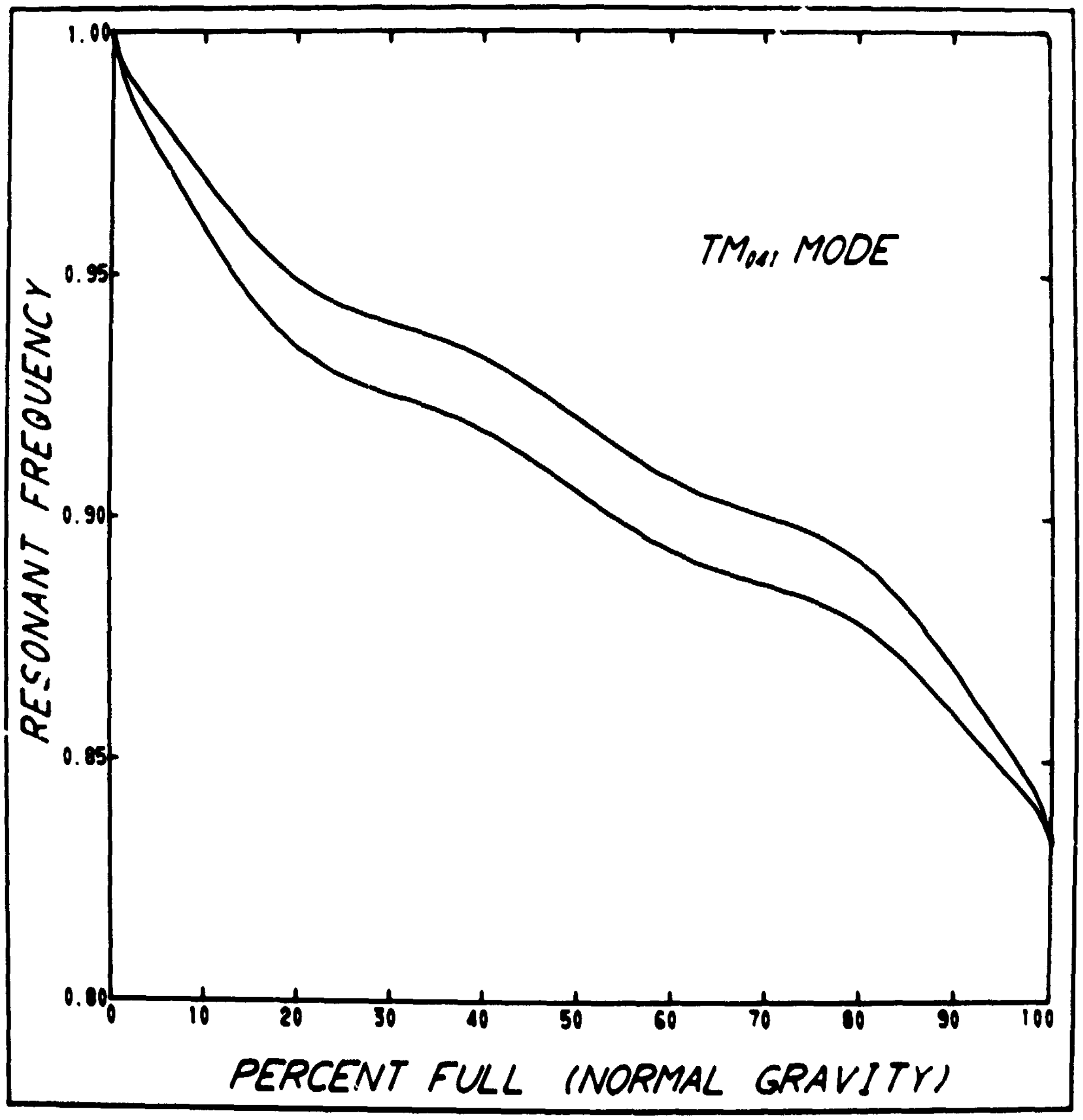

Figure G5

Upper and lower Rayleigh approximations to the normalized frequency ω/ω_0 as a function of fill fraction, for the TM_{041} mode using liquid nitrogen.

$$\omega^2 \leq \min \sum_{m=1}^{N} \sum_{n=1}^{N} C_m \bar{C}_n \; \omega_n^2 \; (F_m, \frac{1}{K} F_n)$$

where the minimum is taken over all choices of $C_1, C_2, \ldots, C_N$ for which

$$\sum_{n=1}^{N} | C_n |^2 = 1$$

This is easily solved by Lagrange's method of multipliers, because the coefficients $(F_m, \frac{1}{K} F_n)$ can be computed from results already obtained for the lower modes in the empty cavity. We propose not only to estimate ω this way, but also to investigate the way this estimate depends on K.

The Moment Method

The moment method was pioneered by Temple[8], elucidated by Kato[9] and generalized to higher order by Stackgold[10]. It derives its name from the set of numbers

$$m_n = \frac{(L^n E_0, E_0)}{(E_0, E_0)} \quad , \; n = 1, 2, 3, \ldots$$

called moments of the operator L with respect to the vector function E_0. Stackgold[11] showed that

---

[8] G. Temple, "The Theory of Rayleigh's Principle as Applied to Continuous Systems," Proceedings of the Royal Society of London, vol 119 (1928), p. 276-293.

[9] Tosio Kato, "On the Upper and Lower Bounds of Eigenvalues," Journal of the Physical Society of Japan, vol 4 (1949), pp. 334-339.

[10] Ivar Stackgold, The Use of Moments in Estimating the Spectrum, Department of the Navy, O. N. R. London Branch, August 1968, pp. 1-19, Accession Number A0839570.

[11] Lynn Taylor Wells, Extensions, Generalization, and Clarifications of Lower Bound Methods Applied to Eigenvalue Problems of Continuous Elastic Systems, Dissertation for the PhD at Ohio State Univ. (1970), pp. 66ff.

$$m_n - \frac{m_{2n} - m_n^2}{b^n - m_n} \le \omega^{2n} < m_n + \frac{m_{2n} - m_n^2}{m_n - a^n}$$

where ω is the angular resonant frequency of some empty cavity mode whose electric field is E_0. (The numbers a, b will be defined shortly.) For our purposes it will be convenient to normalize the moments as follows:

$$M_n = \frac{m_n}{\omega_0^{2n}} = \frac{(L^n E_0, E_0)}{\omega_0^{2n}(E_0, E_0)}$$

so that the inequality becomes

$$M_n - \frac{M_{2n} - M_n^2}{\left(\frac{b}{\omega_0^2}\right)^n - M_n} \le \left(\frac{\omega}{\omega_0}\right)^{2n} \le M_n + \frac{M_{2n} - M_n^2}{M_n - \left(\frac{a}{\omega_0^2}\right)^n} .$$

The real numbers a, b are chosen as far apart as possible consistent with the condition that ω^2 be the only spectral point of L which lies strictly between a, b. Then for the fundamental mode the best choice of a is $-\infty$ and the best choice of b is the angular resonant frequency of the first harmonic <u>if</u> it were known. This leads to the simplification

$$M_n - \frac{M_{2n} - M_n^2}{(\gamma_n^2 - 1)M_n} \le \left(\frac{\omega}{\omega_0}\right)^{2n} \le M_n$$

for the fundamental mode, where

$$\gamma_n^2 = \left(\frac{b}{\omega_0^2}\right)^n \frac{1}{M_n} .$$

Thus for the simplest estimate (n=1) the upper bound is the upper Rayleigh estimate

$$M_1 = \frac{(\frac{1}{K} L_0 E_0, E_0)}{\omega_0^2 (E_0, E_0)} = \frac{\int \frac{1}{K} E_0^2}{\int E_0^2} = \left(\frac{\bar{\omega}}{\omega_0}\right)^2 ,$$

and

$$\gamma_1^2 = \frac{b}{\bar{\omega}^2} .$$

For this simplest estimate we also need a value for

$$M_2 = \frac{(LE_0, LE_0)}{\omega_0^4 (E_0, E_0)} = \frac{(\frac{1}{K} L_0 E_0, \frac{1}{K} L_0 E_0)}{\omega_0^4 (E_0, E_0)} = \frac{\int \frac{1}{K^2} E_0^2}{\int E_0^2} .$$

Consider the special case of a spherical cavity half-full of liquid dielectric with the fundamental mode symmetrically oriented across the interface. Then

$$\int_{\text{LIQUID}} E_0^2 = \int_{\text{GAS}} E_0^2$$

so that for $n = 1, 2$

$$M_n = \frac{\frac{1}{K_1^n} \int_{\text{LIQUID}} E_0^2 + \int_{\text{GAS}} E_0^2}{\int E_0^2} = \frac{1}{2} \left(\frac{1}{K_1^n} + 1\right).$$

Then if the liquid is nitrogen ($K_1 = 1.44$),

$M_1 = 0.8472$ and $M_2 = 0.7411$.

The data indicate the resonant frequencies of the lowest two modes have the ratio

$$\frac{700 \text{ MHz}}{510 \text{ MHz}} = 1.37$$

so

$$\gamma_1 = \frac{\sqrt{b}}{\omega_0}\frac{1}{\sqrt{M_1}} \le \frac{1.37}{\sqrt{0.8472}} = 1.488 .$$

Hence our best possible estimate of this type is

$$\left(\frac{\bar{\omega}}{\omega_0}\right)^2 = 0.847 \ge \left(\frac{\omega}{\omega_0}\right)^2 \ge 0.847 - \frac{0.7411 - 0.7178}{(1.488^2-1)0.8472}$$

$$= 0.847 \frac{.0233}{1.028}$$

$$= 0.824$$

$$\bar{\omega}/\omega_0 = 0.920 \ge \omega/\omega_0 \ge 0.908 \ge 0.906 = \underline{\omega}/\omega_0 .$$

If $\gamma_1 = 1.3$ we obtain $\omega/\omega_0 \ge 0.902$ and if $\gamma_1 = 1.2$, $\omega/\omega_0 \ge 0.886$ (see Fig. G6). Oddly enough, the upper bound does not improve as n increases from 1 to 2:

$$\sqrt{M_1} = .920 \qquad \text{and} \qquad \sqrt{M_2} = .928.$$

Calculating the lower bound corresponding to n = 2 is much more difficult because

$$M_4 = \frac{(L^4 E_0, E_0)}{\omega_0^8 (E_0, E_0)} = \frac{(L^3 E_0, L E_0)}{\omega_0^8 (E_0, E_0}$$

involves calculating higher powers of L operating on E_0.

The principle disadvantage of this class of methods is that it requires approximate knowledge of the next eigenvalue higher than the one being estimated. That is, we must estimate b or γ_n. But the above results for a spherical cavity suggest that the lower Rayleigh estimate is indeed a lower bound for the fundamental mode. This hypothesis should be investigated for a spherically symmetric distribution of dielectric material.

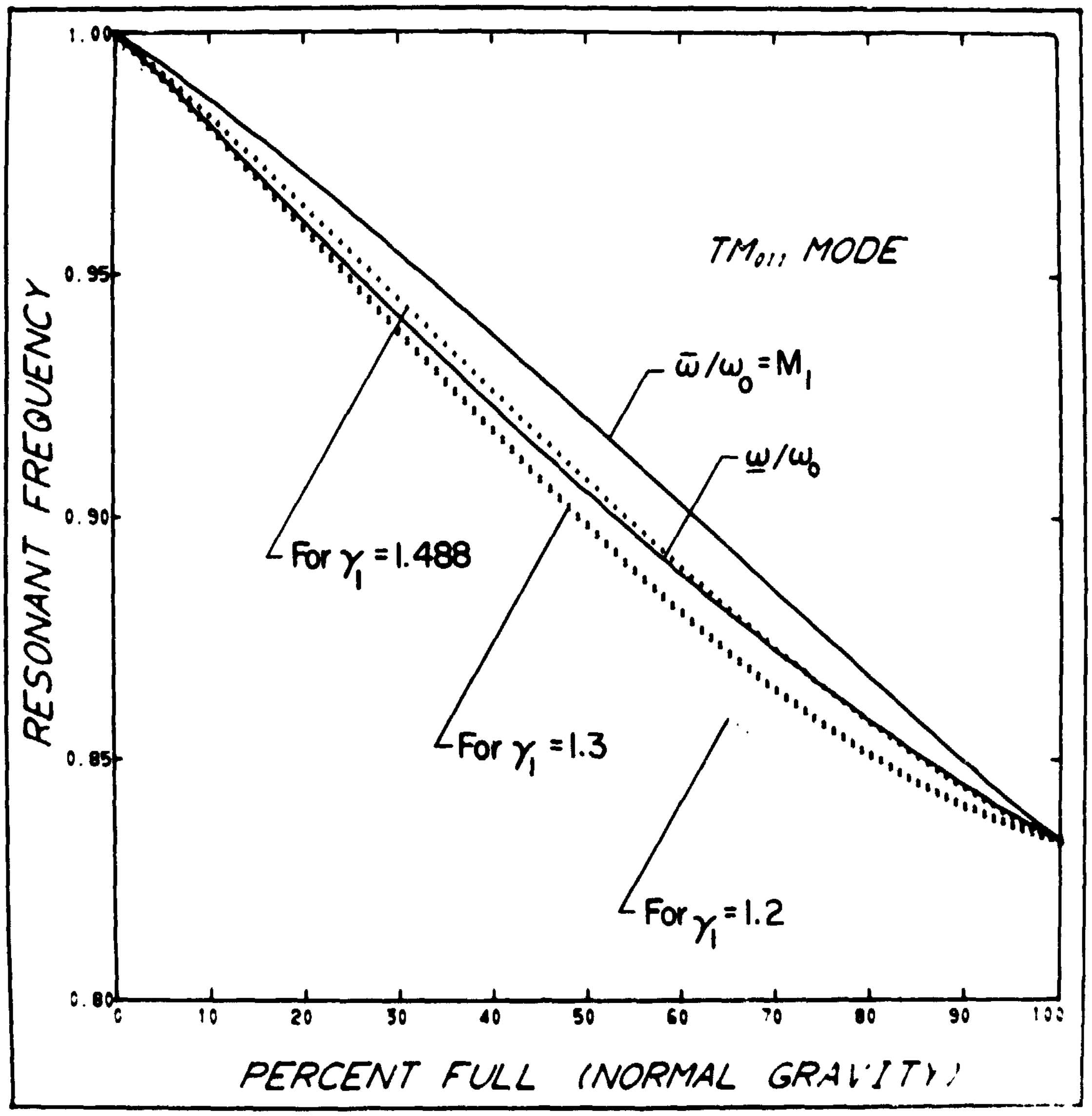

Figure G6 (Compare Figure G1)

Lower bounds for ω/ω_0 from the first order method of moments, using three different values of γ_1. The solid lines are the Rayleigh upper and lower approximations.

Lemma. For any cavity V of diameter D

$$\int_V \frac{d^3 R'}{(4\pi)^2 \, |R - R'|^2} \le \frac{D}{4\pi} \qquad (R \epsilon V),$$

and for a spherical cavity V of diameter D,

$$\int_V \frac{d^3 R'}{(4\pi)^2 \, |R - R'|^2} \le \frac{D}{4\pi} \left(\frac{1 + \sqrt{2}}{4} \right) \qquad (R \epsilon V).$$

Proof. Make a change of variable

$$S = R' - R.$$

Since $R \epsilon V$, the point $S = 0$ always belongs to the cavity. Then (for any shape of cavity) as R^1 varies over the cavity, S varies over a region which is the cavity translated by the vector -R. So regardless of R the region of integration is contained in a sphere of radius D about -R. Hence

$$\int_{V-R} \frac{d^3 S}{(4\pi)^2 \, |S|^2} \le \frac{1}{4\pi} \int_0^D \frac{s^2 \, ds}{s^2} \int_0^{4\pi} \frac{d\omega}{4\pi} = \frac{D}{4\pi}$$

where ω denotes solid angle.

In the spherical case, refer to Figure G7, which is a cross-sectional view of the region of integration. If the R'-origin (marked by the vector -R) is eccentric from the S-origin by a distance aD, then the cavity will be wholly contained in a pair of hemispheres centered at the S-origin and having radii $(\frac{1}{2} + a)$ D and bD, where $a^2 + b^2 = (1/2)^2$. Then we have

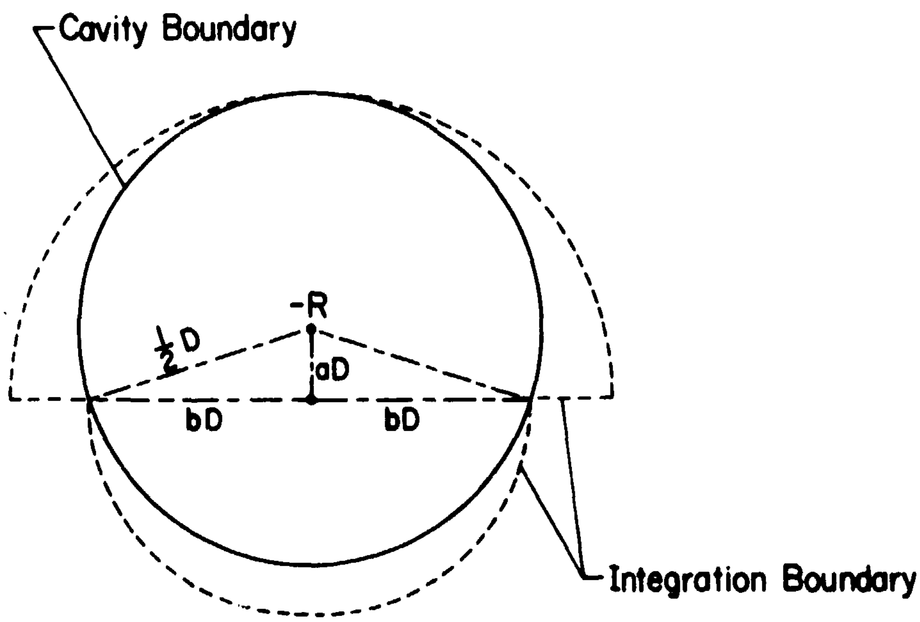

Figure G7

A cross-sectional view of the region of S - integration for the Lemma. The R′- origin is marked by the vector -R, and is eccentric from the S - origin by a distance aD.

$$\int_{V-R} \frac{d^3 S}{(4\pi)^2 |S|^2} \le \frac{1}{4\pi} \int_0^{(\frac{1}{2}+a)D} \frac{s^2 ds}{s^2} \int_0^{2\pi} \frac{d\Omega}{4\pi} + \frac{1}{4\pi} \int_0^{bD} \frac{s^2 ds}{s^2} \int_{2\pi}^{4\pi} \frac{d\Omega}{4\pi}$$

$$= \frac{1}{4\pi} \cdot (\frac{1}{2}+a) D \cdot \frac{1}{2} + \frac{1}{4\pi} \cdot bD \cdot \frac{1}{2}$$

$$= \frac{D}{8\pi} (\frac{1}{2} + a + b)$$

$$= \frac{D}{16\pi} (1 + 2a + 2b)$$

where $(2a)^2 + (2b)^2 = 1$. Let $2a = \cos\theta$, $2b = \sin\theta$ and maximize $f(\theta) = 1 + \sin\theta + \cos\theta$. Since $f'(\theta) = \cos\theta - \sin\theta$ we have the maximum of $f(\frac{\pi}{4}) = 1 + \sqrt{2}$ and the lemma is proved.

Theorem 3. L^{-1} is bounded on LD and is extended by the operator M, where

$$MF(R) = \int \frac{\mu\epsilon(R')F(R')d^3 R'}{4\pi |R-R'|}$$

Furthermore, M is bounded and

$$\|L^{-1}\| \le \|M\| \le \frac{1}{c^2} \left[\int K^2(R') \left\| \frac{1}{4\pi|R-R'|} \right\|_R^2 d^3 R'\right]^{1/2} \le \frac{\|K\|}{c^2} \sqrt{\frac{D}{4\pi}}$$

regardless of the distribution of ϵ or the shape of the cavity. Here c is the speed of light and D is the greatest distance between any two points in the cavity, $K = \epsilon/\epsilon_0$, and $\|K\| [\int K^2 d^3 R']^{1/2}$.

Proof. First we compute LM using the identity

$\nabla \times \nabla \times = \nabla\nabla \cdot - \nabla^2$ and the fact that

$$-\nabla^2 M\Gamma(R) = -\int \frac{\mu\varepsilon(R')F(R')}{4\pi} \nabla^2 \left(\frac{1}{|R - R'|} \right) d^3 R'$$

$$= -\int \frac{\mu\varepsilon(R')F(R')}{4\pi} \left[-4\pi\, \delta(R-R') \right] d^3 R'$$

$$= \mu\varepsilon(R)F(R),$$

where δ is the Dirac distribution.

Represent the mth Cartesian component of F by F_m, set $g(R, R') = \frac{1}{4\pi |R-R'|}$, and show differentiation by subscripts, referring to primed coordinates. Then we have the following identity in Cartesian tensors:

$$(\mu\varepsilon F_m \; g,_n),_m = (\mu\varepsilon F_m),_m g,_n + \mu\varepsilon F_m \; g,_{nm} .$$

Now integrate both sides over the cavity volume in primed coordinates and apply the divergence theorem to the left hand side to obtain

$$\int \mu\varepsilon F_m g,_n d^2 R' = \int (\mu\varepsilon F_m),_m g,_n d^3 R' + \int \mu\varepsilon F_m g,_{nm} d^3 R' .$$

The left hand side vanishes if the surface of integration is described just outside the (lossless) cavity. The result expressed in vector notation is

$$0 = \int (\nabla' \cdot \mu\varepsilon F)\, \nabla' g \; d^3 R' + \int \mu\varepsilon \; F \cdot \nabla' \nabla' g \;\; d^3 R'$$

where ∇' is the nabla operating on primed coordinates.

Using this last result it is easy to show that

$$\nabla\nabla \cdot MF(R) = \int \mu\varepsilon F\cdot\nabla\nabla g$$
$$- \int \mu\varepsilon F\cdot\nabla'\nabla' g$$
$$= - \int (\nabla' \cdot\mu\varepsilon F)\nabla' g \ ,$$

and it follows that

$$\nabla x\nabla xMF(R) = \mu\varepsilon F - \int (\nabla'\cdot\mu\varepsilon F)\nabla' g$$

or $$LMF(R) = F - \frac{1}{\varepsilon} \int (\nabla' \cdot\varepsilon F)\nabla' g \ .$$

We see that for every G in D,

$$\nabla' \cdot\varepsilon LG(R') = \nabla' \cdot \frac{1}{\mu} \nabla' x\nabla' xG(R') - 0,$$

whence LMLG = LG. But the boundary value problem for L has a unique solution, so L has a trivial kernel and L^{-1} exists. Thus

$$MLG = G,$$

where G is arbitrary in D. This shows that M extends L^{-1}.

Since M extends L^{-1}, it will have at least as large a norm, and it now suffices to compute the norm of M.

$$\|MF(R)\|_{*} \le \int \mu\varepsilon(R')|F(R')| \left\| \frac{1}{4\pi|R-R'|} \right\|_{*} d^3R'$$

$$\le \left[\int \mu^2\varepsilon^2(R') \left\|\frac{1}{4\pi|R-R'|}\right\|_{*}^{2} d^3R'\right]^{1/2} \left[\int |F(R')|^2 d^3R'\right]^{1/2}$$

implies the first inequality asserted for $\|M\|$. The weaker bound on $\|M\|$ comes from an estimate of

$$\left\| \frac{1}{4\pi\,|R-R'|} \right\|^2 = \frac{1}{(4\pi)^2} \int \frac{d^3 R}{(R-R')^2} \le \frac{D}{4\pi}$$

which leads easily to the second bound on $\|M\|$ stated in the theorem.

Corollary. Suppose $\epsilon = \epsilon_1 > \epsilon_0$ for a fraction α of the volume of the cavity and $\epsilon = \epsilon_0$ for the remainder. Then the crude estimate of the theorem takes the form

$$\|M\| \le \frac{D^2}{c^2} \left[\frac{1 + \alpha\,(K_1^2 - 1)}{24} \right]^{1/2}$$

Proof.

$$\|K\|^2 = \int_{\epsilon=\epsilon_1} K_1^2 + \int_{\epsilon=\epsilon_0} 1^2$$

$$= [\alpha\, K_1^2 + (1-\alpha)]\,\frac{\pi}{6}\, D^3 ,$$

so $$\frac{D\,\|K\|^2}{4\pi} = D^4 \left[\frac{\alpha\, K_1^2 + (1-\alpha)}{24} \right] ,$$

and the conclusion follows.

Theorem 4. For the fundamental mode,

$$\omega \ge \frac{1}{\|L^{-n}\|^{1/2n}} \ge \frac{1}{\|M^n\|^{1/2n}}$$

for every positive integer n.

Proof.

$$\omega^{2n} = \frac{(E, E)}{(L^{-n} E, E)} ,$$

but $(L^{-n} E, E) \le \|L^{-n} E\| \cdot \|E\| \le \|L^{-n}\| \cdot \|E\|^2 \le \|M^n\|\ \|E\|^2$

by the Schwartz inequality and Theorem 3 above.

Thus $\omega^{2n} \geq \frac{1}{\|L^{-n}\|} \geq \frac{1}{\|M^n\|}$ and the assertion follows.

Remark. Since $\lim_n \|L^{-n}\|^{1/n}$ is the spectral radius of L^{-1}, the reader may think the case n = 1 sufficient. But the more general estimate is given in the hope that it may facilitate computation.

Corollary.

$$\omega \geq \frac{c}{D} \left[\frac{24}{1+\alpha(K_1^2-1)}\right]^{1/4}$$

Proof. Immediate from the corrollary to Theorem 3.

Application. For an empty spherical cavity 48 cm in diameter (any shape) $\alpha=0$ and D=0.48 meter, so

$$\frac{\omega}{2\pi} > \frac{\sqrt[4]{24} \times 300 \times 10^6 \text{ meter/sec}}{2\pi \times 0.48 \text{ meter}} = 220 \text{ MHz.}$$

But theoretical calculations[12] give an exact theoretical value of 543 MHz. and experimental verification using liquid nitrogen at atmospheric pressure gives 546 MHz. So our crude bound is quite crude. But we hope for a better result when

$$\left\| \frac{1}{4\pi |R-R'|} \right\|$$

is calculated accurately as a function of R'.

---

[12] See Appendix F, Table I.

A somewhat different group of techniques is associated with higher powers of M.

$$M^n F(R) = \int \cdots \int \frac{\mu^n \epsilon^n K(R_1) \ldots K(R_n) F(R_n) d^3 R_1 \ldots d^3 R_n}{4\pi |R - R_1| 4\pi | R_1 - R_2 | \ldots 4\pi | R_{n-1} - R_n |}$$

$$|M^n F(R)| \leq \int \cdots \int \mu^n \epsilon^n \frac{1}{4\pi | R - R_1 |} \cdot \frac{K(R_1) \ldots K(R_n) | F(R_n) | d^3 R_1 \ldots d^3 R_n}{4\pi | R_1 - R_2 | \ldots 4\pi | R_{n-1} - R_n |}$$

$$\leq \mu^n \epsilon^n I_n^{1/2}(K) \left[\int \cdots \int F^2 (R_n) d^3 R_1 \ldots d^3 R_n \right]^{1/2}$$

where $$I_n(K) = \int \cdots \int \left| \frac{1}{4\pi | R - R_1 |} \right|^2 \frac{K^2(R_1) \ldots K^2(R_n) d^3 R_1 \ldots d^3 R_n}{(4\pi)^2 | R_1 - R_2 |^2 \ldots (4\pi)^2 | R_{n-1} - R_n |^2} .$$

Continuing, we have for a sphere of diameter D

$$\| M^n F(R) \|_R \leq \frac{1}{c^{2n}} I_n^{1/2}(K) \left[\int d^3 R_1 \right]^{\frac{n-1}{2}} \left[\int F^2 (R_n) d^3 R_n \right]^{1/2} .$$

If we call the last integral $\| F \|^2$, then for a sphere of diameter D

$$\| M^n \| \leq \frac{1}{c^{2n}} I_n^{1/2}(K) \left[\frac{\pi D^3}{6} \right]^{\frac{n-1}{2}}$$

$$1 > \| M^n \|^{-\frac{1}{2n}} \geq c \, I_n^{-\frac{1}{4n}} (K) \left[\frac{6}{\pi D^3} \right]^{\frac{n-1}{4n}}$$

$$1 > c \left(\frac{6}{\pi D^3} \right)^{\frac{1}{4}} \lim_n I_n^{-\frac{1}{4n}} (K) .$$

To estimate I_n, observe that (Lemma to Theorem 3) for a spherical cavity of diameter D,

$$\int \frac{K^2(R_n)d^3R_n}{(4\pi)^2(R_{n-1}-R_n)^2} \leq \frac{K_1^2 D}{4\pi}\left(\frac{1+\sqrt{2}}{4}\right)$$

$$\int \frac{K^2(R_{n-1})K^2(R_n)d^3R_{n-1}d^3R_n}{(4\pi)^2(R_{n-1}-R_n)^2(4\pi)^2(R_{n-1}-R_n)^2}$$

$$\leq \frac{K_1^2 D}{4\pi}\left(\frac{1+\sqrt{2}}{4}\right)\int \frac{d^3R_{n-1}}{(4\pi)^2(R_{n-1}-R_n)^2} \leq \left[\frac{K_1^2 D}{4\pi}\left(\frac{1+\sqrt{2}}{4}\right)\right]^2$$

$$I_n(K) \leq \left[\frac{K_1^2 D}{4\pi}\left(\frac{1+\sqrt{2}}{4}\right)\right]^{n-1}\int \left\|\frac{1}{4\pi|R-R_1|}\right\|_R^2 K(R_1)d^3R_1$$

$$\lim_n I_n^{1/n}(K) \leq \frac{K_1^2 D}{4\pi}\left(\frac{1+\sqrt{2}}{4}\right)$$

$$\omega \geq c\left[\frac{6}{\pi D^3}\cdot\frac{4\pi}{K_1^2 D}\left(\frac{4}{1+\sqrt{2}}\right)\right]^{1/4} = \frac{C}{(D/2)\sqrt{K_1}}\left(\frac{6}{1+\sqrt{2}}\right)^{1/4}$$

$$\frac{\omega}{2\pi} \geq \frac{c}{\pi D\sqrt{K_1}}\left(\frac{6}{1+\sqrt{2}}\right)^{1/4} = \frac{300\times 10^6}{3.14(.48)1.2}\times 1.254 = 208\text{ MHz}.$$

And replacing K_1 by 1 as an approximation for K in the estimate of I increases the answer by only a factor of 1.2 to the value 250 MHz. This suggests the crudeness of the estimate is due primarily to the way I was evaluated. Alternatively, set

$$J_n(K) = \int\cdots\int \frac{d^3R_1\ldots d^3R_n}{(4\pi)^2(R_1-R_2)^2\ldots(4\pi)^2(R_{n-1}-R_n)^2}$$

and observe that for a sphere of diameter D (see Lemma).

$$I_n(K) \le \frac{D}{4\pi}\left(\frac{1+\sqrt{2}}{4}\right) K_1^{2n} \; J_n(K)$$

$$\ge c\left[\frac{D}{4\pi}\left(\frac{1+\sqrt{2}}{4}\right)\right]^{-\frac{1}{4n}} K_1^{-1/2} \, J_n^{-\frac{1}{4n}}(K) \left[\frac{6}{\pi D^3}\right]^{\frac{n-1}{4n}}$$

$$\frac{\mu}{2\pi} \ge \frac{c}{2\pi\sqrt{K_1}}\left(\frac{6}{\pi D^3}\right)^{1/4} \lim_n J_n^{-\frac{1}{4n}}(K) \; .$$

One final approach in this vein is only heuristic at this point. The formula for $M^n F(R)$ is an integral whose integrand is overwhelmingly important when the variables

$$R, \; R_1, \; R_2, \; \ldots, \; R_n$$

have all nearly the same value. This suggests the approximation

$$M^n F(R) \approx \mu^n \epsilon_0^n K^n(R) F(R) W_n(R)$$

where $W_n(R) = \int \cdots \int \dfrac{d^3 R_1 \ldots d^3 R_n}{4\pi|R-R_1|\,4\pi|R_1-R_2|\ldots 4\pi|R_{n-1}-R_n|}$.

This strictly positive function can be estimated by the technique of the lemma:

$$\int_V \frac{d^3 R^1}{4\pi\,|R - R^1|} = \int_{R+V} \frac{d^3 S}{4\pi S}$$

$$\leq \int_o^{(\frac{1}{2}+a)D} |S|\, d|S| \int_o^{2\pi} \frac{d\Omega}{4\pi} + \int_o^{bD} |S|\, d|S| \int_{2\pi}^{4\pi} \frac{d\Omega}{4\pi}$$

$$= \frac{1}{2}\left(\frac{1}{2} + a\right)^2 D^2 \cdot \frac{1}{2} + \frac{1}{2} b^2 D^2 \cdot \frac{1}{2}$$

$$= \frac{1}{4} D^2 \left[\left(\frac{1}{2} + a\right)^2 + b^2\right]$$

$$= \frac{1}{4} D^2 \left[\frac{1}{4} + a + a^2 + b^2\right]$$

$$= \frac{1}{4} D^2 \left[\frac{1}{4} + a + \frac{1}{4}\right]$$

$$\leq \left(\frac{D}{2}\right)^2$$

because $a \leq \frac{1}{2}$.

Therefore $W_n(R) \leq \left(\frac{D}{2}\right)^{2n}$.

And since

$$\omega^{2n} = \frac{(E, E)}{(M^n E, E)} \approx \frac{(E, E)}{(c^{-2n} \; K^n W_n E, E)}$$

$$\omega \approx \frac{c\,(E, E)^{1/2n}}{(K^n W_n E, E)^{1/2n}}$$

But for a two phase system

$$(K^n W_n E, E)^{1/n} \le \left[K_1^n \int_{LIQUID} W_n E^2 + \int_{GAS} W_n E^2 \right] \to K_1^{1/2}$$

$$\le \left[K_1^n \left(\frac{D}{2}\right)^{2n} \int_{LIQUID} E^2 + \left(\frac{D}{2}\right)^{2n} \int_{GAS} E^2 \right]^{1/2n}$$

and this upper bound approaches $K_1^{1/2} \left(\frac{D}{2}\right)$ as n increases without bound. Hence

$$\omega \ge \frac{c}{(D/2)\sqrt{K_1}} \quad .$$

So for an empty cavity

$$\frac{\omega}{2\pi} = \frac{300 \times 10^6}{2\pi(0.24)1.2} = 166 \text{ MHz}.$$

Whether the validity of this approach can be established is unknown, and even if it can be, there seems less likelihood of getting a good estimate for $W_n(R)$ than for $J_n(K)$.

Recommendations for Further Study

1. Compute the Rayleigh estimates for several of the lower modes in the case of a spherically symmetric distribution of liquid.

2. Compute the bounds

$$M_n - \frac{M_{2n} - M_n^2}{\left(\frac{b}{\omega_0^2}\right)^n - M_n} \le \left(\frac{\omega}{\omega_0}\right)^2 \le M_n + \frac{M_{2n} - M_n^2}{M_n - \left(\frac{a}{\omega_0^2}\right)^n}$$

for n = 1, 2 in several of the lower modes for both normal gravity fill and spherically symmetric distributions of liquid.

3. Investigate the Green's function method by computing $\| M \|$, $J_n(K)$, $W_n(K)$ accurately.

APPENDIX H

NUMERICAL ANALYSIS OF THE SPHERICAL CAVITY FOR THE LOWEST ORDER MODES

Electric Field Contours

Equation (F-22) was used to generate the graphs plotted by subroutine TMTEPLOT. These are plots of the electric field contours, $|E(r, \theta)| = |E|$, for the TM_{011}, TM_{021}, TM_{031}, TM_{041}, and TE_{011} modes. Choosing C_{n1} as imaginary (n = 1, 2, 3, 4) in (F-22) the equations used in TMORTE for the TM modes became

$$g = z\, j_n(z)\, P_n\ (\cos\theta) \tag{H-1}$$

$$z = u_{n1} \frac{r}{b} \quad \text{for } n = 1,\ 2,\ 3,\ 4$$

and u_{n1} are the eigen values of the different modes. (The outside radius, b, is normalized to 1.0. P_n and j_n are the Legendre and spherical Bessel functions, respectively.) With

$$|E| \equiv \sqrt{E_r^2 + E_\theta^2 + E_\varphi^2}$$

being the magnitude of the electric field, and using (H-1), the components become

$$E_r = \frac{-n(n+1)}{r^2}\left[z\, j_n\ (z)\ P_n\ (\cos\theta)\right]$$

$$= \frac{-n(n+1)}{z}\left(u_{n1}\right)^2 j_n\ (z)\ P_n\ (\cos\theta)$$

Also

$$E_\theta = \frac{1}{r}\,\frac{\partial^2}{\partial r\,\partial \theta}\left[z\, j_n\,(z)\, P_n\,(\cos\theta)\right]$$

$$= \frac{1}{r}\,\frac{d}{d\theta}\left[P_n\,(\cos\theta)\right]\left\{z\, j_{n-1}\,(z) - n\, j_n\,(z)\right\}\frac{dz}{dr}$$

and

$$E_\varphi = 0.$$

The analygous equations for the TE modes are

$$f = u_{n1}\; j_n\,(z)\; P_n\,(\cos\theta)$$

The magnitude of the electric field becomes $|E| \equiv \sqrt{E_\varphi^2}.$

The components

$$E_r = E_\theta = 0$$

and

$$E_\varphi = u_{n1}\; j_n\,(z)\,\frac{d}{d\theta}\left[P_n\,(\cos\theta)\right].$$

The plots of $|E|$ for the first six modes are shown in figures 8 through 13 in the body of this report. Before plotting, $|E|$ was scaled by its largest value and normalized to 10. Hence, the contours are numbered 1, 2, . . . , 10.

Upper and Lower Raleigh Approximations for the Normal Fill Geometry.

The Resonant Frequency vs. Percent Full (Normal Gravity) graphs generated by subroutine LINPT were obtained numerically integrating $|E|^2$ over different portions of the resonating spherical cavity for the various modes. The graphs display the upper and lower

Rayleigh approximations for the true solution. Working in spherical coordinates, volume is a function of (r, θ, φ),

$$- \text{ie}, \quad V = f(r, \theta, \varphi).$$

However, assuming symmetry in the φ direction, $V = 2\pi\, g(r, \theta)$. Hence, the integrals for the different portions of the resonating cavity become

$$G\left[E(V_1)\right] = 2\pi \int_0^{\theta_k} \int_0^R |E|^2\, r^2 \sin\theta\, dr d\theta$$

$$+ 2\pi \int_{\theta_k}^{\pi} \int_0^{-H/\cos\beta} |E|^2\, r^2 \sin\beta\, dr\, d\beta$$

where

$$\frac{\pi}{2} \leq \beta \leq \theta_k \text{ (see figure H1 for } \theta_k)$$

and

$$F\left[E(V_{CF})\right] = 2\pi \int_{\theta_k}^{\pi} \int_{-H/\cos\beta}^{R} |E|^2\, r^2 \sin\beta\, dr\, d\beta.$$

G defines an integral of the field magnitude in the empty part (V_1) of the cavity and F defines an integral of the field magnitude in the part of the cavity containing fluid (V_{CF}). Figure H1 displays V_1 and V_{CF}. The upper and lower approximations were then computed by evaluating.

$$\sqrt{\frac{\frac{1}{K} F + G}{C}} \quad \text{and} \quad \sqrt{\frac{C}{KF + G}}$$

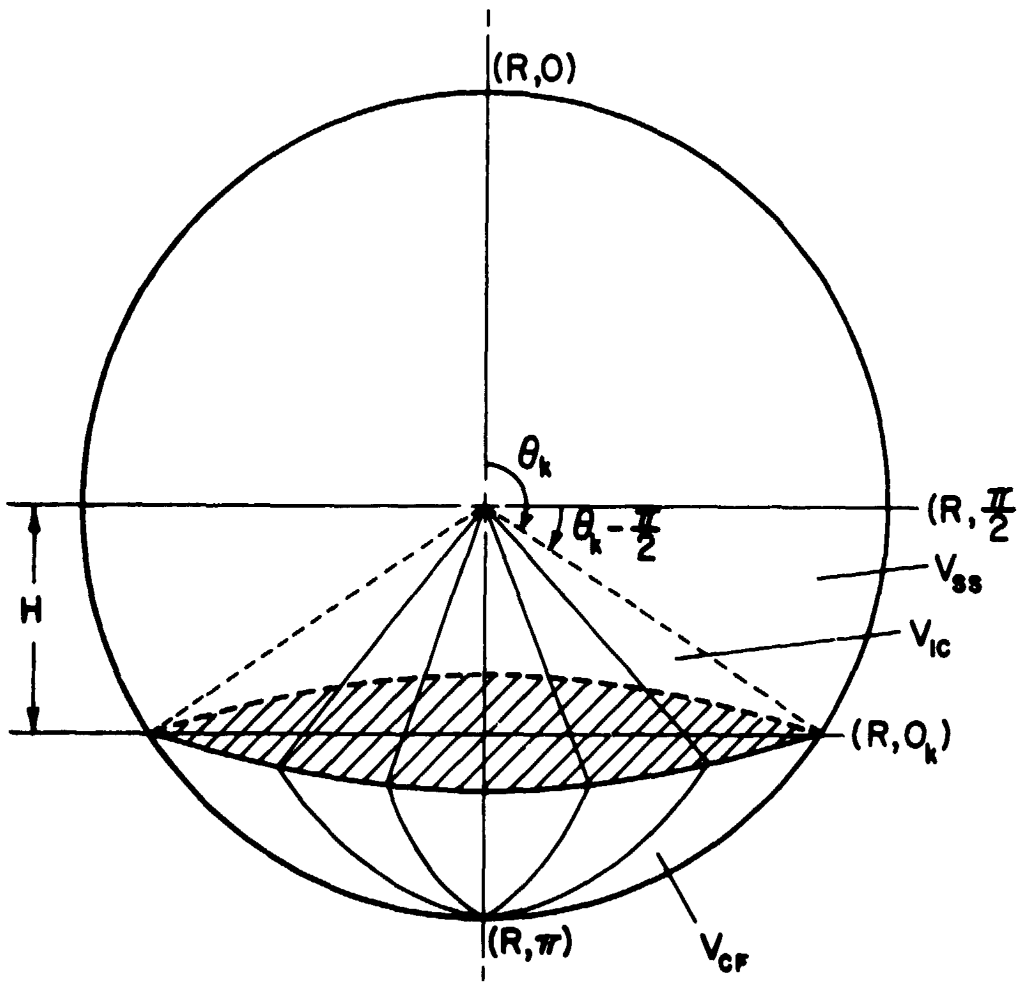

$$V_I = V_{SS} + V_{IC}$$

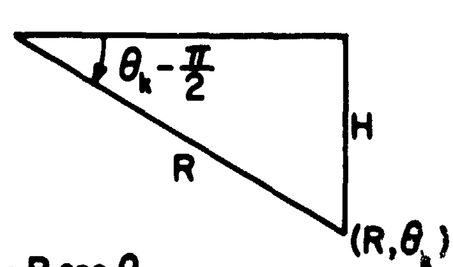

$$H = -R \cos \theta_k$$

Figure H1. Coordinate system for the normal fill geometry.

at steps of $\Delta V_{CF} = 1\%$. Here C = F + G and K is the dielectric constant of the fluid in the cavity.

Figures G1-G5 show the upper and lower Raleigh approximations for the first five spherical modes for the normal fill geometry.

Computer Routines

Ten computer routines were developed and coded in Fortran to calculate the magnitude of the electric fields ($|E(R, \theta)|$) and to integrate over the volume of the spherical cavity. These routines are as follows:

TMORTE, main program, calculates $|E|$ for the transverse magnetic or transverse electric modes;

BJ, PN, and DPN are three function routines called by TMORTE to evaluate spherical Bessel functions of the 1st kind and Legendre polynomials and their derivatives, respectively;

TMTEPLOT, subroutine called by TMORTE, plots $|E|$ for the transverse magnetic and transverse electric modes;

RCTOUR, subroutine called by TMTEPLOT, searches for specific contour values for TMTEPLOT to plot;

VOLUME, subroutine called by TMORTE, inegrates $|E|^2$ over the sphere to evaluate functions of the resonating frequency in the empty part and the full part of the spherical cavity;

RINTGL, subroutine called by VOLUME, performs that part of the integration along the radial lines, R, of the cavity;

LINPT, subroutine called by VOLUME, plots the upper and lower bounds of a Rayleigh approximation to the true solution for a Frequency vs. Percent Full graph;

INTRPL, subroutine called by VOLUME, interpolates between values of the percent full calculations to obtain required values.

A listing of the computer routines is given as follows:

```
      PROGRAM TMORTE                                                    TMT
C                                                                       TMT
      DIMENSION U(4), IFMT1(6), IFMT2(6), V(4)                          TMT
C                                                                       TMT
      COMMON /DATA/ EMAGN(109,181),IRLAB(3),ICLAB(19),MODE,DELTAR,DELTATTMT
     1,NRINC,NTINC,NRIP1,NTIP1,PI,JJ(181),ESCALE                        TMT
      COMMON /INDEX/ INDEX,EFSWT,GAMA1,GAMA2,GAMA3                      TMT
C                                                                       TMT
      DATA (U=2.744,3.870,4.973,6.062),(B=1.),(PI=3.14159265),(IRLAB=18HTMT
     1RADIAL DIRECTION  ),(ICLAB(1)=1H ),(ICLAB(2)=1HT),(ICLAB(3)=1HH),(TMT
     2ICLAB(4)=1HE),(ICLAB(5)=1HT),(ICLAB(6)=1HA),(ICLAB(7)=1H ),(ICLAB(TMT
     38)=1H ),(ICLAB(9)=1HD),(ICLAB(10)=1HI),(ICLAB(11)=1HR),(ICLAB(12)=TMT
     41HE),(ICLAB(13)=1HC),(ICLAB(14)=1HT),(ICLAB(15)=1HI),(ICLAB(16)=1HTMT
     50),(ICLAB(17)=1HN),(ICLAB(18)=1H ),(ICLAB(19)=1H ),(INCR=9),(INCT=TMT
     610),(V=4.493,5.763,6.998,0.0),(IFMT1=47H(8H1TM MODE,2H (,I2,1H)//5TMT
     77X,3A8/10X,13(I3,6X))),(IFMT2=25H(1X,A1,I3,1H0,2X,13E9.2/))      TMT
C                                                                       TMT
      INTEGER TMTE,EFSWT                                                TMT
      REAL KX                                                           TMT
C                                                                       TMT
C     ..............................................................TMT
C        ROUTINE TO CALCULATE COMPONENTS OF THE ELECTRIC FIELD OF THE   TMT
C        TRANSVERSE MAGNETIC MODE UNDER SPHERICAL SYMMETRY.  EQUATION   TMT
C        (A-22) OF NBS REPORT 9793 BECOMES                              TMT
C                                                                       TMT
C              G = P [COS(THETA)]  * Z * J (Z)                          TMT
C                   N                     N                             TMT
C                                                                       TMT
C        WHERE Z = U  R/B.                                              TMT
C                   N1                                                  TMT
C                                                                       TMT
C                                                                       TMT
C        ALSO CALCULATES COMPONENTS OF THE ELECTRIC FIELD FOR THE       TMT
C        TRANSVERSE ELECTRIC MODE UNDER SPHERICAL SYMMETRY.  THE        TMT
C        ANALYGOUS EQUATION OF (A-22) THEN IS                           TMT
C                                                                       TMT
C              F = P [COS(THETA)]  * K   * J (Z)                        TMT
C                   N                 N     N                           TMT
C                                                                       TMT
C        WHERE Z = K   R = V  R/B AND B IS THE RADIUS OF THE SPHERE.    TMT
C                   N1      N1                                          TMT
C     ..............................................................TMT
C                                                                       TMT
      R=1.0                                                             TMT
C      ASSIGN THETA THE VALUE 180 DEGREES (IN RADIANS)                  TMT
      THETA=PI                                                          TMT
C                                                                       TMT
    1 READ (60,19) TMTE,MODE,NRINC,NTINC,DFLDR,EFSWT,GAMA1,GAMA2,GAMA3  TMT
C                                                                       TMT
C        EFSWT = 1, CALCULATE E (AND NORMALIZE) EVERY TIME              TMT
C                2, CALCULATE E (AND NORMALIZE) AND WRITE E ON MAG TAPE TMT
C                   (LOG. UNIT NO. 1)                                   TMT
C                3, READ (NORMALIZED) E FROM MAG TAPE (LOG. UNIT NO. 1) TMT
C                                                                       TMT
```

```
      IF (EOF,60) 18,2
C
2     N=MODE/10
      ROTATE=DFLDR*PI/180.0
      IF (TMTE.EQ.2RTE) GO TO 3
C        TM MODE PARAMETERS
      INDEX=1
      UX=U(N)
      IFMT1(1)=8H(8H1TM M
      GO TO 4
C        TE MODE PARAMETERS
3     INDEX=2
      UX=V(N)
      IFMT1(1)=8H(8H1TE M
4     KX=UX/B
      INCR=9
      INCT=10
      IF (NRINC.NE.12) GO TO 5
      INCR=1
      INCT=1
5     DELTAR=R/NRINC
      NRIP1=NRINC+1
      DELTAT=THETA/NTINC
      NTIP1=NTINC+1
      DO 6 I=1,NTIP1
      JJ(I)=I-1
6     CONTINUE
      IF (EFSWT.EQ.3) GO TO 15
C
C     ---COMPONENTS OF THE ELECTRIC FIELD-----------------------------
      EMAX=0.0
      DO 12 IR=1,NRIP1
      R=(IR-1)*DELTAR
      Z=KX*R
      DZDR=KX
      DO 12 IT=1,NTIP1
      THETA=(IT-1)*DELTAT+ROTATE
      GO TO (7,10), INDEX
C        RADIAL (R) DIRECTION
7     IF (R.NE.0.0) GO TO 9
      IF (N.EQ.1) GO TO 8
      EMAGN(IR,IT)=0.0
      GO TO 12
8     EMAGN(IR,IT)=(2.0*KX*UX/(3.0*B))
      GO TO 11
9     ER=-N*(N+1)*(KX**2)*PN(COS(THETA),N)*BJ(Z,N)/Z
C
C        ANGULAR (THETA) DIRECTION
      ETHETA=DPN(COS(THETA),-SIN(THETA),N)*(DZDR/R)*(Z*BJ(Z,N-1)-N*BJ(Z,
     1N))
C
      EMAGN(IR,IT)=SQRT(ER**2+ETHETA**2)
      GO TO 11
C        TE MODE
```

```
10    EPHI=DPN(COS(THETA),-SIN(THETA),N)*KX*BJ(Z,N)
C        ER=ETHETA=0.0
      EMAGN(IR,IT)=ABS(EPHI)
11    IF (EMAGN(IR,IT).GT.EMAX) EMAX=EMAGN(IR,IT)
12    CONTINUE
C
      PRINT IFMT1, MODE,IRLAB,(JJ(J),J=1,NRIP1,INCR)
      DO 13 IT=1,NTIP1,INCT
      I=IT/10+1
      IF (INCT.EQ.1) I=IT
      PRINT IFMT2, ICLAB(I),JJ(I),(EMAGN(J,IT),J=1,NRIP1,INCR)
13    CONTINUE
C
C        SCALE E ACCORDING TO LARGEST VALUE AND NORMALIZE TO 10.0
      ESCALE=10.0/EMAX
      DO 14 IR=1,NRIP1
      DO 14 IT=1,NTIP1
      EMAGN(IR,IT)=EMAGN(IR,IT)*ESCALE
14    CONTINUE
      CALL TMTEPLOT
      IF (EFSWT.EQ.1) GO TO 16
      WRITE (1) ((EMAGN(IR,IT),IR=1,NRIP1),IT=1,NTIP1),ESCALE
      GO TO 16
C
15    READ (1) ((EMAGN(IR,IT),IR=1,NRIP1),IT=1,NTIP1),ESCALE
C
16    PRINT IFMT1, MODE,IRLAB,(JJ(J),J=1,NRIP1,INCR)
      DO 17 IT=1,NTIP1,INCT
      I=IT/10+1
      IF (INCT.EQ.1) I=IT
      PRINT IFMT2, ICLAB(I),JJ(I),(EMAGN(J,IT),J=1,NRIP1,INCR)
17    CONTINUE
      PRINT 20
C
      CALL VOLUME
      GO TO 1
C
18    PRINT 21
      CALL EXIT
C
19    FORMAT (R2,I3,2I5,F5.0,I5,3E10.3)
20    FORMAT (1H1)
21    FORMAT (///11H END OF JOB)
      END
      SUBROUTINE VOLUME
C
C        SPECIAL ROUTINE TO EVALUATE (FUNCTIONS OF) VOLUMES CUT FROM
C        A SPHERE BY A PLANE PERPENDICULAR TO THE VERTICAL AXIS OF
C        SYMMETRY.  HERE
C
C             V = F(R,THETA,PHI) = 2*PI*G(R,THETA).
C
      DIMENSION SVSSOE(1), SVSSE(180), SVICOE(1), SVICE(180), SVCFO(1),
     1SVCF(180), XTRA(3), SVCFOE(1), SVCFE(180), XTRAE(3), XO(1), X(30),
```

```
     2 Y0(1), Y(30), U(1-1), DEG(51), FVCF0(1), FVCF(30), GV10(1), GV1(3
     30), DFVCF(51), DGV1(51), Y1(101), Y2(101), Y1LB1(101), Y1LB2(101),
     4 Y1LB3(101)
C
      COMMON /DATA/ EMAGN(109,181),IRLAB(3),ICLAB(19),MODE,DELTAR,DELTAT
     1,NRINC,NTINC,NRIP1,NTIP1,PI,JJ(181),ESCALE
      COMMON /INDEX/ INDEX,EFSWT,GAMA1,GAMA2,GAMA3
C
      EQUIVALENCE (NRINC,NIR), (NRIP1,NIRP1), (NTINC,NIT), (NTIP1,NITP1)
     1,
      EQUIVALENCE (VOL,TVOLE)
C
      DATA (F38=0.375)
C
      D2R=PI/180.0
      TBX=PI
      RBX=1.0
      TPI38=2.0*PI*F38
      IPSWT=1
      TVOL=4.0*PI/3.0
C        RE-SCALE TO ORIGINAL EMAGN AND SQUARE
      RSCALE=1.0/ESCALE
      DO 1 IR=1,NRIP1
      DO 1 IT=1,NTIP1
      EMAGN(IR,IT)=(EMAGN(IR,IT)*RSCALE)**2
    1 CONTINUE
C
C        SET THE INITIAL AND TERMINAL VALUES FOR R AND THETA
      RA=0.0
      RB=1.0
      KTHETA=90
      TA=PI/2.0
      TB=PI
      XYZ=0.0
C
C        CALCULATE NECESSARY INDICES FOR A SIMPSONS 3/8THS INTEGRATION
      JB=(RA/RBX)*NIR+1.01
      JMAX=(RB/RBX)*NIR+0.01
      IB=(TA/TBX)*NIT+1.01
      IE=(TB/TBX)*NIT+0.01
      IEP1=IE+1
C
C        SOLVE FOR THE VOLUME OF THE SPHERICAL SEGMENT, 0.LE.THETA.LE.PI
      ISWT=1
      DO 2 I=1,91
      CALL RINTGL (ISWT,I,JB,JMAX,XYZ,VSSE)
      ISWT=3
      IM1=I-1
      SVSSE(IM1)=F38*VSSE*SIN(IM1*DELTAT)*DELTAT
    2 CONTINUE
      VALU=0.0
      DO 3 I=1,90,3
      VALU=VALU+SVSSE(I-1)+3.0*(SVSSE(I)+SVSSE(I+1)   SVSSE(I+2))
    3 CONTINUE
```

```
      VOLSSF=TPI38*VALU
      TVOLE=VOLSSE+VOLSSE
      IK=91
C
C        SOLVE FOR THE REMAINING VOLUMES, PI/2.L .THETA.LE.PI
      N=-1
      DO 10 NTHETA=KTHETA,IE,3
      N=N+1
      Y(30-N)=NTHETA
      H=-RB*COS(NTHETA*D2R)
      KTHP1=NTHETA+1
      IK= HP1
C
C        SOLVE FOR THE VOLUMES, NTHETA.LE.THETA.LL.PI
      DO 7 I=KTHP1,IEP1
      IM1=I-1
      TIM1=SIN(IM1*DELTAT)*DELTAT
      IF (NTHETA-90) 5,4,5
4     R=0.0
      GO TO 6
5     BETA=IM1*D2R
      R=-H/COS(BETA)
6     JE=(R/RBX)*NIR+0.01+0.6
C        VOLUME OF THE SPERICAL SEGMENT CONTAING FUEL
      CALL RINTGL (4,I,JE+1,JMAX,VCF,VCFE)
      T38=F38*TIM1
      SVCF(IM1)=T38*VCF
      SVCFE(IM1)=T38*VCFE
7     CONTINUE
C
      VALU2=0.0
      VALU2E=0.0
      DO 8 I=KTHP1,IF,3
      VALU2=VALU2+SVCF(I-1)+3.0*(SVCF(I)+SVCF(I+1))+SVCF(I+2)
      VALU2E=VALU2E+SVCFE(I-1)+3.0*(SVCFE(I)+SVCFE(I+1))+SVCFE(I+2)
8     CONTINUE
      VOLCF=TPI38*VALU2
      VOLCFE=TPI38*VALU2E
C
      PCTF=VOLCF/TVOL
      VOL1=TVOLE-VOLCFE
C
      X(30-N)=PCTF*100.0
      FVCF(N)=VOLCFE
      GV1(N)=VOL1
      GO TO (9,10), IPSWT
9     WRITE (61,21) NTHETA,VOLSSE,VOL1,VOLCFE,PCTF,N
10    CONTINUE
C
      X(1)=X(1)+1.0E-8
      X(2)=X(2)+5.0E-8
      X(3)=X(3)+10.0E-8
      DO 11 I=1,101
      U(I)=I-1
```

```
11    CONTINUE
      CALL INTRPL (61,31,X0,Y0,51,U,DEG)
      WRITE (61,22) (U(I),DEG(I),I=1,51)
      WRITE (61,23) MODE
      GV1(29)=GV1(29)+1.0E-8
      GV1(30)=GV1(30)+5.0E-8
      DO 12 I=1,31
      Y(I-1)=270.0-Y(I-1)
12    CONTINUE
      RK=1.0/1.44
      RKSQ=RK**2
      N1=N2=N3=0
      DO 16 I=1,51
      CALL INTRPL (61,31,Y0,V10,1,DEG(I),DGV1(I))
      CALL INTRPL (61,31,Y0,FVCF0,1,DEG(I),DFVCF(I))
      FI=I-1
      FM1=(RK*DFVCF(I)+DGV1(I))/VOL
      Y1(I)=SKFPGDC=SQRT(FM1)
      Y2(I)=RKFPGDC=SQRT(VOL/(1.44*DFVCF(I)+DGV1(I)))
      FM1SQ=FM1**2
      FM2=(RKSQ*DFVCF(I)+DGV1(I))/VOL
      QLB1=FM1-(FM2-FM1SQ)/((GAMA1**2-1.0)*FM1)
      FLB1=1.0E+50
      IF (QLB1.LT.0.0) GO TO 13
      N1=N1+1
      Y1LB1(I)=FLB1=SQRT(QLB1)
13    QLB2=FM1-(FM2-FM1SQ)/((GAMA2**2-1.0)*FM1)
      FLB2=1.0E+50
      IF (QLB2.LT.0.0) GO TO 14
      N2=N2+1
      Y1LB2(I)=FLB2=SQRT(QLB2)
14    QLB3=FM1-(FM2-FM1SQ)/((GAMA3**2-1.0)*FM1)
      FLB3=1.0E+50
      IF (QLB3.LT.0.0) GO TO 15
      N3=N3+1
      Y1LB3(I)=FLB3=SQRT(QLB3)
15    WRITE (61,24) FI,DFVCF(I),DGV1(I),SKFPGDC,RKFPGDC,FM2,FLB1,FLB2,FL
     1B3
16    CONTINUE
      WRITE (61,25) VOL
      WRITE (61,23) MODE
      DO 20 I=52,101
      FI=I-1
      XDGV1=VOL-DGV1(102-I)
      XDFVCF=VOL-DFVCF(102-I)
      FM1=(RK*XDFVCF+XDGV1)/VOL
      Y1(I)=SKFPGDC=SQRT(FM1)
      Y2(I)=RKFPGDC=SQRT(VOL/(1.44*XDFVCF+XDGV1))
      FM1SQ=FM1**2
      FM2=(RKSQ*XDFVCF+XDGV1)/VOL
      QLB1=FM1-(FM2-FM1SQ)/((GAMA1**2-1.0)*FM1)
      FLB1=1.0E+50
      IF (QLB1.LT.0.0) GO TO 17
      N1=N1+1
```

```
      Y1LB1(I)=FLB1=SQRT(QLB1)
17    QLB2=FM1-(FM2-FM1SQ)/((GAMA2**2-1.0)*FM1)
      FLB2=1.0E+50
      IF (QLB2.LT.0.0) GO TO 18
      N2=N2+1
      Y1LB2(I)=FLB2=SQRT(QLB2)
18    QLB3=FM1-(FM2-FM1SQ)/((GAMA3**2-1.0)*FM1)
      FLB3=1.0E+50
      IF (QLB3.LT.0.0) GO TO 19
      N3=N3+1
      Y1LB3(I)=FLB3=SQRT(QLB3)
19    WRITE (61,24) FI,XDFVCF,XDGV1,SKFPGDC,RKFPGDC,FM2,FLB1,FLB2,FLB3
20    CONTINUE
      WRITE (61,25) VOL
C
      XX=0.0
      CALL LINPT (XX,XX,XX,10.0,0.0,100.0,4,0.8,1.0,1,XX,XX)
      CALL LINPT (U,Y1,101,XX,XX,XX,XX,XX,XX,2,1,XX)
      CALL LINPT (U,Y2,101,XX,XX,XX,XX,XX,XX,2,1,XX)
      N1X=101-N1+1
      CALL LINPT (U(N1X),Y1LB1(N1X),N1,XX,XX,XX,XX,XX,XX,2,2,1R.)
      N2X=101-N2+1
      CALL LINPT (U(N2X),Y1LB2(N2X),N2,XX,XX,XX,XX,XX,XX,2,2,1R*)
      N3X=101-N3+1
      CALL LINPT (U(N3X),Y1LB3(N3X),N3,XX,XX,XX,XX,XX,XX,2,2,1R+)
      CALL LINPT (XX,XX,XX,XX,XX,XX,XX,XX,XX,3,XX,XX)
C
      RETURN
C
21    FORMAT (/I4,3F10.5,2PF8.2,I5)
22    FORMAT (F8.1,F8.2)
23    FORMAT (10H1TM MODE (,I2,1H)/3X,3HPCT,4X,6HF(VCF),5X,5HG(V1),3X,17
     1HSQRT((F/K + G)/C),3X,19HSQRT(C/(K*F + G)) *,12X,2HM2,9X,3HLB1,9X,
     23HLB2,9X,3HLB3/)
24    FORMAT (F6.1,F10.3,F10.3,2F16.6,8X,F17.6,3(4X,F8.6))
25    FORMAT (//9H * K=1.44/5H   C=,F9.5)
      END
      SUBROUTINE RINTGL (ISWT,I,JB,JE,SUM,SUME)
C
C        ROUTINE TO INTEGRATE ALONG THE RADIAL LINES, R, INVOLVED
C        IN A TWO DIMENSIONAL INTEGRAL TO SOLVE FOR (FUNCTIONS OF)
C        VOLUMES OF SPHERICAL SECTORS OR SEGMENTS
C
      DIMENSION RO(1), R(108), REO(1), RE(108)
C
      COMMON /DATA/ EMAGN(109,181),IRLAB(3),ICLAB(19),MODE,DELTAR,DELTAT
     1,NRINC,NTINC,NRIP1,NTIP1,PI,JJ(181),ESCALE
C
      GO TO (1,3,11,3), ISWT
C
1     DO 2 J=1,109
      JM1=J-1
      R(JM1)=((JM1*DELTAR)**2)*DELTAR
2     CONTINUE
```

```
      GO TO 11
C
3     SUM=0.0
      IF (JB-JE) 4,4,11
4     IJE=(JE/3)*3
      IJB=((JB+2)/3)*3-2
      IJBX=IJB
      IF ((JB-IJB)-1) 7,5,6
5     SUM=SUM+1.5*(R(IJB)+R(IJB+1))
6     SUM=SUM+1.5*R(IJB+1)+R(IJB+2)
      IJBX=IJB+3
      IF (IJE-IJBX) 11,11,7
7     DO 8 J=IJBX,IJE,3
      SUM=SUM+R(J-1)+3.0*(R(J)+R(J+1))+R(J+2)
8     CONTINUE
      IF ((JE-IJE)-1) 11,10,9
9     SUM=SUM+1.5*(R(IJE+2)+R(IJE+1))
10    SUM=SUM+1.5*R(IJE+1)+R(IJE)
C
C
11    SUME=0.0
      IF (JB-JE) 12,12,20
12    IJE=(JE/3)*3
      IJB=((JB+2)/3)*3-2
      IJBX=IJB
      DO 13 J=IJB,109
      JM1=J-1
      RE(JM1)=R(JM1)*EMAGN(J,I)
13    CONTINUE
      IF ((JB-IJB)-1) 16,14,15
14    SUME=SUME+1.5*(RE(IJB)+RE(IJB+1))
15    SUMF SUME+1.5*RE(IJB+1)+RE(IJB+2)
      IJBX=IJB+3
      IF (IJE-IJBX) 20,20,16
16    DO 17 J=IJBX,IJE,3
      SUME=SUME+RE(J-1)+3.0*(RE(J)+RE(J+1))+RE(J+2)
17    CONTINUE
      IF ((JE-IJE)-1) 20,18,19
18    SUME=SUME+1.5*(RE(IJE+2)+RE(IJE+1))
19    SUME=SUME+1.5*RE(IJE+1)+RE(IJE)
C
20    RETURN
      END
      SUBROUTINE LINPT(XI,YI,NPT,NXD,FMNX,FMXX,NYD,FMNY,FMXY,N,LS,ISYCH)
C
C
C        LINEAR PLOTTING ROUTINE
C
      COMMON /DD/ IN,IOR,IT,IS,IC,ICC,IX,IY
      COMMON /DDC/ LU,LUC,IFL
      COMMON /LABEL/ LABELX(5),LABELY(5),LSWTX,LSWTY
      COMMON /DATA/ EMAGN(109,181),IRLAB(3),ICLAB(19),MODE,DELTAR,DELTAT
     1,NRINC,NTINC,NRIP1,NTIP1,PI,JJ(181),ESCALE
      COMMON /INDEX/ INDEX,IFSWT,GAMA1,GAMA2,GAMA3
```

```
C
      DIMENSION XI(NPT), YI(NPT), ID(4)
C
      DATA (ID=32H RG PETERSON    X3184             )
      DATA (IXMIN=100),(IYMIN=100),(LSWTX=2),(LSWTY=2)
C     DATA (LABELX=5(8H          )),(LABELY=5(8H          ))
      DATA (LABELX=40H          PERCENT FULL (NORMAL GRAVITY)     )
      DATA (LABELY=40H               RESONANT FREQUENCY          )
C
      INTEGER EFSWT
C
      GO TO (1,10,21), N
C
1     IOR=0
      IN=0
      IC=0
      IF (EFSWT.EQ.3) CALL DDINIT (4,ID)
      IT=0
C        DRAW A BOX AROUND PLOTTING AREA
      CALL DDBOX (0,1023,0,1023)
C        SPECIAL LABEL PLOTTED
      IT=1
      IS=3
      IX=675
      IY=800
      LABEL=8HTM  MODE
      IF (INDEX.EQ.2) LABEL=8HTE  MODE
      CALL DDTAB
      CALL DDTABNA8 (1,LABEL,1)
      MODEX=1000+MODE
      ENCODE (8,23,LBMODE) MODEX
      IS=1
      IX=715
      IY=790
      CALL DDTAB
      CALL DDTABNA8 (1,LBMODE,1)
C
      NY=NYD+1
      LTYDIV=900/NYD
      IYMAX=IYMIN+LTYDIV*NYD
      NX=NXD+1
      LTXDIV=900/NXD
      IXMAX=IXMIN+LTXDIV*NXD
C
C        DRAW DIVISIONS OR TICKMARKS FOR X-AXIS
      IY=IYMAX
      IX=MINX=IXMIN
      CALL DDBP
      IY=IYMIN
      CALL DDVC
      DO 4 I=2,NX
      IY=IYMAX
      IXS=IX=IXMIN+(I-1)*LTXDIV
      CALL DDBP
```

```
      IYS=IY=IYMAX-8
      CALL DDVC
      IX=IXS
      IY=IYS
      IF (I.EQ.NX) GO TO 3
      GO TO (3,2), LSWTX
2     IY=IYMIN+8
      CALL DDBP
3     IY=IYMIN
      CALL DDVC
4     CONTINUE
C
C        DRAW DIVISIONS OR TICKMARKS FOR Y-AXIS
      IX=IXMAX
      IY=MINY=IYMIN
      CALL DDBP
      IX=IXMIN
      CALL DDVC
      DO 7 I=2,NY
      IX=IXMAX
      IYS=IY=IYMIN+(I-1)*LTYDIV
      CALL DDBP
      IXS=IX=IXMAX-8
      CALL DDVC
      IX=IXS
      IY=IYS
      IF (I.EQ.NY) GO TO 6
      GO TO (6,5), LSWTY
5     IX=IXMIN+8
      CALL DDBP
6     IX=IXMIN
      CALL DDVC
7     CONTINUE
C
C        NUMBER THE X-AXIS
      IS=1
      IT=0
      IOR=0
      FINCX=(FMXX-FMNX)/NXD
      DO 8 I=1,NX
      IYS=IY=IYMIN-15
      IM1=I-1
      IXS=IX=IXMAX-IM1*LTXDIV-32
      FNUMB=FMXX-IM1*FINCX
      ENCODE (8,24,FNUMBX) FNUMB
      CALL DDTAB
      CALL DDTABNA8 (1,FNUMBX,1)
8     CONTINUE
C        NUMBER THE Y AXIS
      IS=1
      IOR=0
      FINCY=(FMXY-FMNY)/NYD
      DO 9 I=1,NY
      IX=60
```

```
      IM1=I-1
      IY=IYMAX-IM1*LTYDIV
      FNUMB=FMXY-IM1*FINCY
      ENCODE (8,25,FNUMBY) FNUMB
      CALL DDTAB
      CALL DDTABNA8 (1,FNUMBY,1)
9     CONTINUE
C
C        LABEL X AND Y AXES
      IT=1
      IS=3
      IX=40
      IY=30
      CALL DDTAB
      CALL DDTABNA8 (5,LABELX(1),1)
      IX=30
      IY=40
      IOR=1
      CALL DDTAB
      CALL DDTABNA8 (5,LABELY(1),1)
C
      XMIN=FMNX
      XMAX=FMXX
      YMIN=FMNY
      YMAX=FMXY
      FMINX=IXMIN
      FMAXX=IXMAX
      FMINY=IYMIN
      FMAXY=IYMAX
      IS=0
      IT=0
      IOR=0
      GO TO 22
C
10    IXL=IYL=0
      JSWT=1
      GO TO (11,12), LS
C        PLOT VECTORS
11    CALL DDCONVEC
      GO TO 13
C        PLOT SYMBOLS OR CHARACTERS
12    ICC=ISYCH
      CALL DDSYMBOL
13    DO 20 I=1,NPT
      X=XI(I)
      Y=YI(I)
      IX=(X-XMIN)/(XMAX-XMIN)*(FMAXX-FMINX)+FMINX
      IY=(Y-YMIN)/(YMAX-YMIN)*(FMAXY-FMINY)+FMINY
      SLOPE=(IY-IYL)/(IX-IXL)
      IF (IX.GE.IXMIN) GO TO 14
      IY=SLOPE*(IXMIN-IXL)+IYL
      IX=IXMIN
      JSWT=2
      GO TO 15
```

```
14    IF (IX.LE.IXMAX) GO TO 15
      IY=SLOPE*(IXMAX-IXL)+IYL
      IX=IXMAX
      JSWT=2
15    IF (IY.GE.IYMIN) GO TO 16
      IY=IYMIN
      GO TO 17
16    IF (IY.LE.IYMAX) GO TO 18
      IY=IYMAX
17    IX=(IY-IYL)/SLOPE+IXL
      JSWT=2
18    IF (I.EQ.1.AND.JSWT.EQ.2) GO TO 19
      IF (IX.EQ.IXL.AND.IY.EQ.IYL) GO TO 20
      CALL DDXY
19    IXL=IX
      IYL=IY
20    CONTINUE
C
      CALL DDTAB
      GO TO 22
C
C        FRAME ADVANCE
21    CALL DDFR
C
22    RETURN
C
23    FORMAT (I3)
24    FORMAT (F4.0)
25    FORMAT (F4.2)
      END
      SUBROUTINE TMTEPLOT
C
C        SPECIAL PLOTTING ROUTINE TO PLOT MAGNITUDES OF ELECTRIC FIELDS
C
      COMMON /DD/ IN,IOR,IT,IS,IC,ICC,IX,IY
      COMMON /DDC/ LU,LUC,IFL
      COMMON /DATA/ EMAGN(109,181),IRLAB(3),ICLAB(19),MODE,DELTAR,DELTAT
     1,NRINC,NTINC,NRIP1,NTIP1,PI,JJ(181),ESCALE
      COMMON /INDEX/ INDEX,EFSWT,GAMA1,GAMA2,GAMA3
      COMMON /SUB/ IRR(181),IXS(181),IYS(181),PID2,PIDNTI,R,NP
C
      DIMENSION LABEL(5), IXN(10), RAD(36), ID(4)
C
      DATA (ID=32HRG PETERSON  X3184             ),(LABEL=40H R F MASS
     1GUAGING-PLOT OF  E , TM  MODE ),(RAD=20(475.0),477.0,478.0,480.0,4
     281.0,483.0,485.0,488.0,490.0,488.0,485.0,483.0,481.0,480.0,478.0,4
     377.0,475.0)
C
      IOR=0
      IC=0
      IT=0
      CALL DDINIT (4,ID)
C
C       DRAW A BOX AROUND PLOTTING AREA
```

```
      IN=1
      CALL DDBOX (0,1023,0,1023)
C
C      PLOT A CONTINUOUS CIRCLE CENTERED AT RASTER COOR. (512,562)
C      WITH RADIUS = 450 RASTER UNITS
      IS=0
      CALL DDCONVEC
      PIDNTI=PI/NTINC
      PID2=PI/2.0
      DO 1 I=1,NTIP1
      T=(I-1)*PIDNTI
      TT=PID2-T
      IX=COS(TT)*450.0+512.0
      IY=SIN(TT)*450.0+532.0
      IXS(NTIP1-I+1)=1024-IX
      IYS(NTIP1-I+1)=IY
      CALL DDXY
    1 CONTINUE
      DO 2 I=2,NTIP1
      IX=IXS(I)
      IY=IYS(I)
      CALL DDXY
    2 CONTINUE
C      NUMBER CIRCLE EVERY 10 DEGREES
      DO 3 I=1,36
      IDEG=(I-1)*10
      TT=PID2-IDEG*PIDNTI
      COSTT=COS(TT)
      SINTT=SIN(TT)
      CALL DDCONVEC
      IX=COSTT*450.0+512.0
      IY=SINTT*450.0+532.0
      CALL DDXY
      IX=COSTT*458.0+512.0
      IY=SINTT*458.0+532.0
      CALL DDXY
      IX=COSTT*RAD(I)+512.0
      IY=SINTT*RAD(I)+532.0
      IDEGX=1000+IDEG
      ENCODE (8,13,NV) IDEGX
      CALL DDTAB
      CALL DDTABNA8 (1,NV,1)
    3 CONTINUE
C
C      LABEL PLOTTED
      IT=1
      IS=3
      IX=10
      IY=25
      LABEL(5)=8HM  MODE
      IF (INDEX.EQ.2) LABEL(5)=8HE  MODE
      CALL DDTAB
      CALL DDTABNA8 (5,LABEL(1),1)
      MODEX=1000+MODE
```

```
      ENCODE (8,13,LBMODE) MODEX
      IS=1
      IX=794
      IY=15
      CALL DDTAB
      CALL DDTABNAB (1,LBMODE,1)
C
      IS=0
      NTID2=NTINC/2+1
C
C      SEARCH FOR CONTOURS
      DO 12 NC=1,10
      R=NC
C      ASSIGN BEGINNING INDICES, 2 FOR TM OR TE 11,21,31, AND 20 FOR 41
      DO 5 ITH=1,NTIP1
      IF (MODE.EQ.41) GO TO 4
      IRR(ITH)=2
      GO TO 5
4     IRR(ITH)=20
5     CONTINUE
C
      ITH=1
6     CALL RCTOUR
      ITHB=ITH
C
C      PLOT THE CONTOURS
      IF (NP.EQ.0) GO TO 10
      CALL DDCONVEC
      DO 7 I=1,NP
      IX=IXS(I)
      IY=IYS(I)
      CALL DDXY
7     CONTINUE
      IXR=1024-IXS(NP)
      IF (IXS(1).EQ.IXR) GO TO 8
      CALL DDBP
      CALL DDCONVEC
8     DO 9 I=1,NP
      NPMIP1=NP-I+1
      IX=1024-IXS(NPMIP1)
      IY=IYS(NPMIP1)
      CALL DDXY
9     CONTINUE
      CALL DDBP
C
10    DO 11 ITH=ITHB,NTIP1
      IF (IRR(ITH).LE.NRIP1) GO TO 6
11    CONTINUE
12    CONTINUE
C
C      FRAME ADVANCE AND RETURN
      CALL DDFR
C
      RETURN
```

```
C
13    FORMAT (I3)
      END
      SUBROUTINE RCTOUR
C
C        SPECIAL ROUTINE TO SEARCH FOR ALL VALUES BELONGING TO A CONTOUR
C
      COMMON /DATA/ EMAGN(109,181),IRLAB(3),ICLAB(19),MODE,DELTAR,DELTAT
     1,NRINC,NTINC,NRIP1,NTIP1,PI,JJ(181),ESCALE
      COMMON /SUB/ IRR(181),IXS(181),IYS(181),PID2,PIDNTI,R,NP
C
      NP=0
      DO 4 ITH=1,NTIP1
      IRB=IRR(ITH)
      IF (IRB.GT.NRIP1) GO TO 4
      EM1=EMAGN(IRB-1,ITH)
      DO 1 IR=IRB,NRIP1
      E=EMAGN(IR,ITH)
      IF (EM1.LE.R.AND.R.LE.E) GO TO 2
      IF (EM1.GE.R.AND.R.GE.E) GO TO 2
      EM1=E
1     CONTINUE
      RNUM=0.0
      GO TO 3
2     RNUM=EM1-R
      RDEN=EM1-E
      RINTP=(IR-2.0+RNUM/RDEN)*DELTAR
      RADIUS=RINTP*450.0
      TT=PID2-(ITH-1)*PIDNTI
      NP=NP+1
      IXS(NP)=COS(TT)*RADIUS+512.0
      IYS(NP)=SIN(TT)*RADIUS+532.0
3     IRR(ITH)=IR+1
      IF (RNUM.EQ.0.0.AND.NP.NE.0) GO TO 5
4     CONTINUE
C
5     RETURN
      END
      SUBROUTINE  INTRPL(IU,L,X,Y,N,U,V)
C INTERPOLATION OF A SINGLE-VALUED FUNCTION
C
C THIS SUBROUTINE INTERPOLATES, FROM VALUES OF THE FUNCTION
C GIVEN AS ORDINATES OF INPUT DATA POINTS IN AN X-Y PLANE
C AND FOR A GIVEN SET OF X VALUES (ABSCISSAS), THE VALUES OF
C A SINGLE-VALUED FUNCTION Y = Y(X).
C
C
C THE INPUT PARAMETERS ARE
C
C       IU = LOGICAL UNIT NUMBER OF STANDARD OUTPUT UNIT
C       L  = NUMBER OF INPUT DATA POINTS
C            (MUST BE 2 OR GREATER)
C       X  = ARRAY OF DIMENSION L STORING THE X VALUES
C            (ABSCISSAS) OF INPUT DATA POINTS
```

```
C           (IN ASCENDING ORDER)
C      Y  = ARRAY OF DIMENSION L STORING THE Y VALUES
C           (ORDINATES) OF INPUT DATA POINTS
C      N  = NUMBER OF POINTS AT WHICH INTERPOLATION OF THE
C           Y VALUE (ORDINATE) IS DESIRED
C           (MUST BE 1 OR GREATER)
C      U  = ARRAY OF DIMENSION N STORING THE X VALUES
C           (ABSCISSAS) OF DESIRED POINTS
C
C THE OUTPUT PARAMETER IS
C
C      V  = ARRAY OF DIMENSION N WHERE THE INTERPOLATED Y
C           VALUES (ORDINATES) ARE TO BE DISPLAYED
C
C
C DECLARATION STATEMENTS
C
      DIMENSION    X(1),Y(1),U(1),V(1)
      EQUIVALENCE  (P0,X3),(Q0,Y3),(Q1,T3),(UK,DX),(IMN,X2,A1,FM1),
     1 (IMX,X5,A5,FM5),(J,SW,SA),(Y2,W2,W4,Q2),(Y5,W3,Q3)
C
C PRELIMINARY PROCESSING
C
   10 L0=L
      LM1=L0-1
      LM2=LM1-1
      LP1=L0+1
      N0=N
      IF(LM2)90,100,100
  100 IF(N0)91,91,105
  105 DO 11  I=2,L0
        IF(X(I-1)-X(I))   11,95,96
   11   CONTINUE
      IPV=0
C
C MAIN DO-LOOP
C
      DO 80  K=1,N0
        UK=U(K)
C
C ROUTINE TO LOCATE THE DESIRED POINT
C
   20   IF(LM2)200,27,200
  200   IF(UK - X(L0))205,26,26
  205   IF(UK -  X(1))25,208,208
  208   IMN=2
        IMX=L0
   21   I=(IMN+IMX)/2
        IF(UK -  X(I))22,23,23
   22   IMX=I
        GO TO 24
   23   IMN=I+1
   24   IF(IMX -  IMN)240,240,21
  240   I=IMX
```

```
      GO TO 30
25    I=1
      GO TO 30
26    I=LP1
    GO TO 30
27  I=2
C
C CHECK IF I = IPV
C
30    IF(I -  IPV)300,70,300
300   IPV=I
C
C ROUTINES TO PICK UP NECESSARY X AND Y VALUES AND
C          TO ESTIMATE THEM IF NECESSARY
C
40  J=I
    IF(J-1)401,400,401
400 J=2
401 IF(J-LP1)403,402,403
402 J=L0
403   X3=X(J-1)
      Y3=Y(J-1)
      X4=X(J)
      Y4=Y(J)
      A3=X4-X3
      FM3=(Y4-Y3)/A3
      IF(LM2)404,43,404
404   IF(J -  2)405,41,405
405   X2=X(J-2)
      Y2=Y(J-2)
      A2=X3-X2
      FM2=(Y3-Y2)/A2
      IF(J -  L0)41,42,41
41    X5=X(J+1)
      Y5=Y(J+1)
      A4=X5-X4
      FM4=(Y5-Y4)/A4
      IF(J -  2)45,410,45
410    FM2=FM3+FM3-FM4
      GO TO 45
42    FM4=FM3+FM3-FM2
      GO TO 45
43    FM2=FM3
      FM4=FM3
45    IF(J -  3)46,46,450
450   A1=X2-X(J-3)
      FM1=(Y2-Y(J-3))/A1
      GO TO 47
46    FM1=FM2+FM2-FM3
47    IF(J -  LM1)470,48,48
470   A5=X(J+2)-X5
      FM5=(Y(J+2)-Y5)/A5
      GO TO 50
48    FM5=FM4+FM4-FM3
```

```
C
C NUMERICAL DIFFERENTIATION
C
   50 IF(I-LP1)500,52,500
  500    W2=ABS(FM4-FM3)
         W3=ABS(FM2-FM1)
         SW=W2+W3
         IF(SW)51,501,51
  501    W2=0.5
         W3=0.5
         SW=1.0
   51    T3=(W2*FM2+W3*FM3)/SW
      IF(I-1)52,54,52
   52    W3=ABS(FM5-FM4)
         W4=ABS(FM3-FM2)
         SW=W3+W4
         IF(SW)53,520,53
  520    W3=0.5
         W4=0.5
         SW=1.0
   53    T4=(W3*FM3+W4*FM4)/SW
      IF(I-LP1)60,530,60
  530 T3=T4
      SA=A2+A3
      T4=0.5*(FM4+FM5-A2*(A2-A3)*(FM2-FM3)/(SA*SA))
      X3=X4
      Y3=Y4
      A3=A2
      FM3=FM4
      GO TO 60
   54 T4=T3
      SA=A3+A4
      T3=0.5*(FM1+FM2-A4*(A3-A4)*(FM3-FM4)/(SA*SA))
      X3=X3-A4
      Y3=Y3-FM2*A4
      A3=A4
      FM3=FM2
C
C DETERMINATION OF THE COEFFICIENTS
C
   60    Q2=(2.0*(FM3-T3)+FM3-T4)/A3
         Q3=(-FM3-FM3+T3+T4)/(A3*A3)
C
C COMPUTATION OF THE POLYNOMIAL
C
   70    DX=UK-P0
   80    V(K)=Q0+DX*(Q1+DX*(Q2+DX*Q3))
      RETURN
C
C ERROR EXIT
C
   90 WRITE (IU,2090)
      GO TO 99
   91 WRITE (IU,2091)
```

```
      GO TO 99
   95 WRITE (IU,2095)
      GO TO 97
   96 WRITE (IU,2096)
   97 WRITE (IU,2097)  I,X(I)
   99 WRITE (IU,2099)  LO,NO
      RETURN
C
C FORMAT STATEMENTS
C
 2090 FORMAT(1X/22H  ***   L = 1 OR LESS./)
 2091 FORMAT(1X/22H  ***   N = 0 OR LESS./)
 2095 FORMAT(1X/27H  ***   IDENTICAL X VALUES./)
 2096 FORMAT(1X/33H  ***   X VALUES OUT OF SEQUENCE./)
 2097 FORMAT(6H   I =,I7,10X,6HX(I) =,E12.3/)
 2099 FORMAT(6H   L =,I7,10X,3HN =,I7/
     1       36H ERROR DETECTED IN ROUTINE    INTRPL/)
      END
      FUNCTION BJ(Z,N)
C
C        THIS ROUTINE COMPUTES THE SPHERICAL BESSEL FUNCTIONS
C        OF THE 1ST KIND JN(Z) FOR THE FIRST FIVE VALUES OF N
C
      NP1=N+1
      GO TO (10,20,30,19,19),NP1
C
C        J0(Z)
   10 IF(Z.NE.0.0)GO TO 11
      BJ=1.0
      GO TO 60
   11 BJ=SIN(Z)/Z
      GO TO 60
C
   19 ASSIGN 30 TO JNSWT
      GO TO 21
C        J1(Z)
   20 ASSIGN 60 TO JNSWT
   21 IF(Z.NE.0.0)GO TO 22
      BJ=0.0
      BJ1=0.0
      GO TO 23
   22 BJ=(SIN(Z)-Z*COS(Z))/Z**2
      BJ1=BJ
   23 GO TO JNSWT,(60,30)
C        J2(Z)
   30 BJ=((3.0-Z*Z)*SIN(Z)-3.0*Z*COS(Z))/Z**3
      BJ2=BJ
      IF(N-3)60,40,50
C
C        J3(Z)
   40 BJ=5.0/Z*BJ2-BJ1
      GO TO 60
C        J4(Z)
   50 BJ=7.0/Z*(5.0/Z*BJ2-BJ1)-BJ2
```

APPENDIX I

LIST OF FIGURES

FORM NBS-114A (1-71)

U.S. DEPT. OF COMM. BIBLIOGRAPHIC DATA SHEET	1. PUBLICATION OR REPORT NO. NBSIR 73-318	2. Gov't Accession No.	3. Recipient's Accession No.

4. TITLE AND SUBTITLE

Mass Quantity Gauging by RF Mode Analysis

5. Publication Date

6. Performing Organization Code

7. AUTHOR(S) R. S. Collier, Doyle Ellerbruch, J. E. Cruz, Robert W. Stokes, Philip E. Luft, Gordon Peterson & A. E. Hiester

8. Performing Organization

9. PERFORMING ORGANIZATION NAME AND ADDRESS

NATIONAL BUREAU OF STANDARDS, Boulder Labs.
DEPARTMENT OF COMMERCE
Boulder, Colorado 80302

10. Project/Task/Work Unit No. 2750563

11. Contract/Grant No. T-1738B

12. Sponsoring Organization Name and Address

National Aeronautics and Space Administration
Johnson Space Center
Houston, TX

13. Type of Report & Period Covered

14. Sponsoring Agency Code

15. SUPPLEMENTARY NOTES

16. ABSTRACT (A 200-word or less factual summary of most significant information. If document includes a significant bibliography or literature survey, mention it here.)

This is a summary report of work done to date or NASA (Johnson Space Center) purchase order T-1738B concerning Radio Frequency (RF) Mass Quantity Gauging. Experimental apparatus has been designed and tested which measures the resonant frequencies of a tank in the "time domain." These frequencies correspond to the total mass of fluid within the tank. Experimental results are discussed for nitrogen and hydrogen in normal gravity both in the supercritical state and also in the two phase (liquid-gas) region. Theoretical discussions for more general cases are given.

17. KEY WORDS (Alphabetical order, separated by semicolons)

Gauging; hydrogen; nitrogen; radio frequency; total mass

18. AVAILABILITY STATEMENT	19. SECURITY CLASS (THIS REPORT)	21. NO. OF PAGES
[X] UNLIMITED.	UNCLASSIFIED	
[ ] FOR OFFICIAL DISTRIBUTION. DO NOT RELEASE TO NTIS.	20. SECURITY CLASS (THIS PAGE) UNCLASSIFIED	22. Price